RWTH AACHEN UNIVERSITY

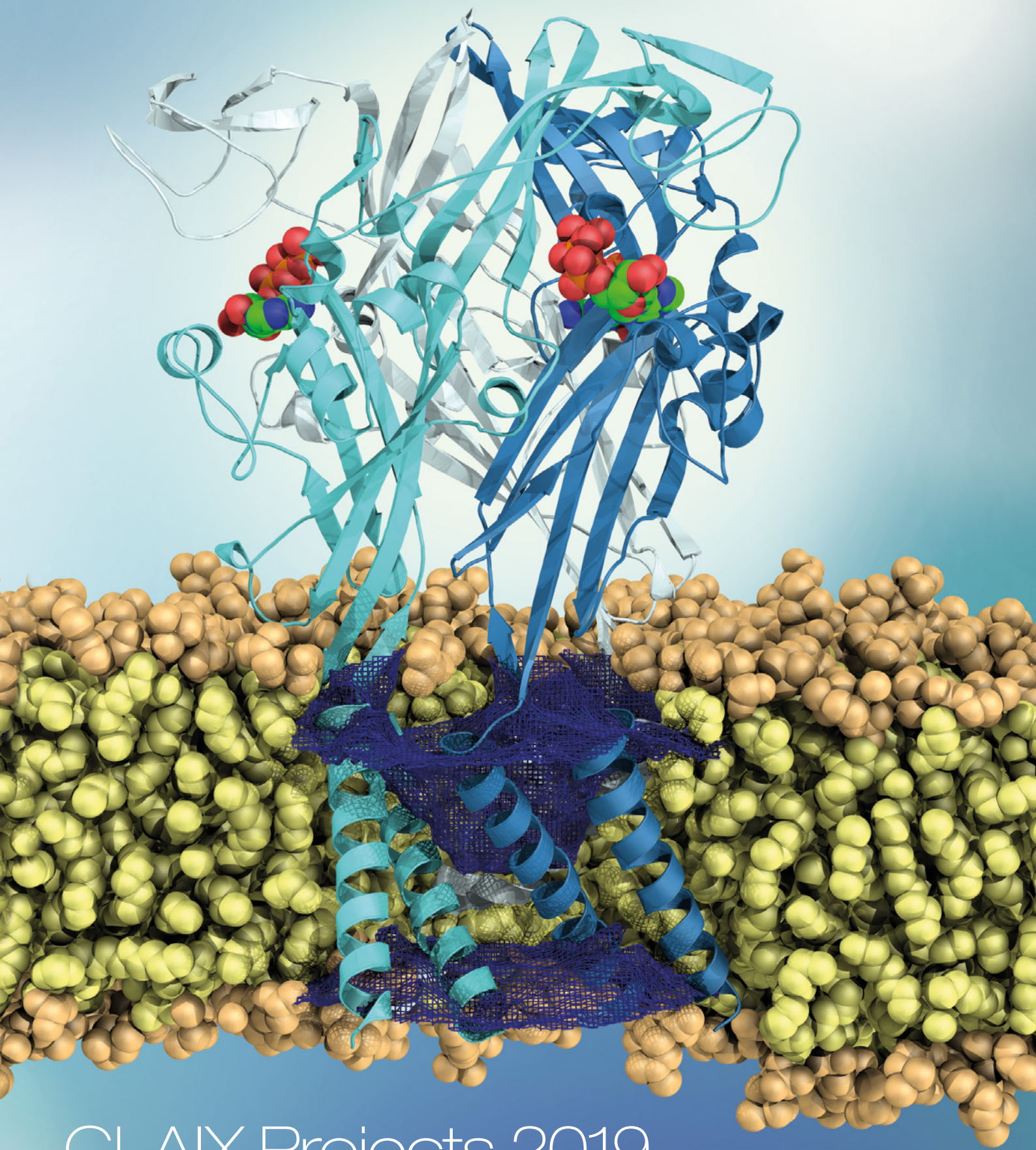

CLAIX Projects 2019

High Performance Computing at RWTH Aachen University

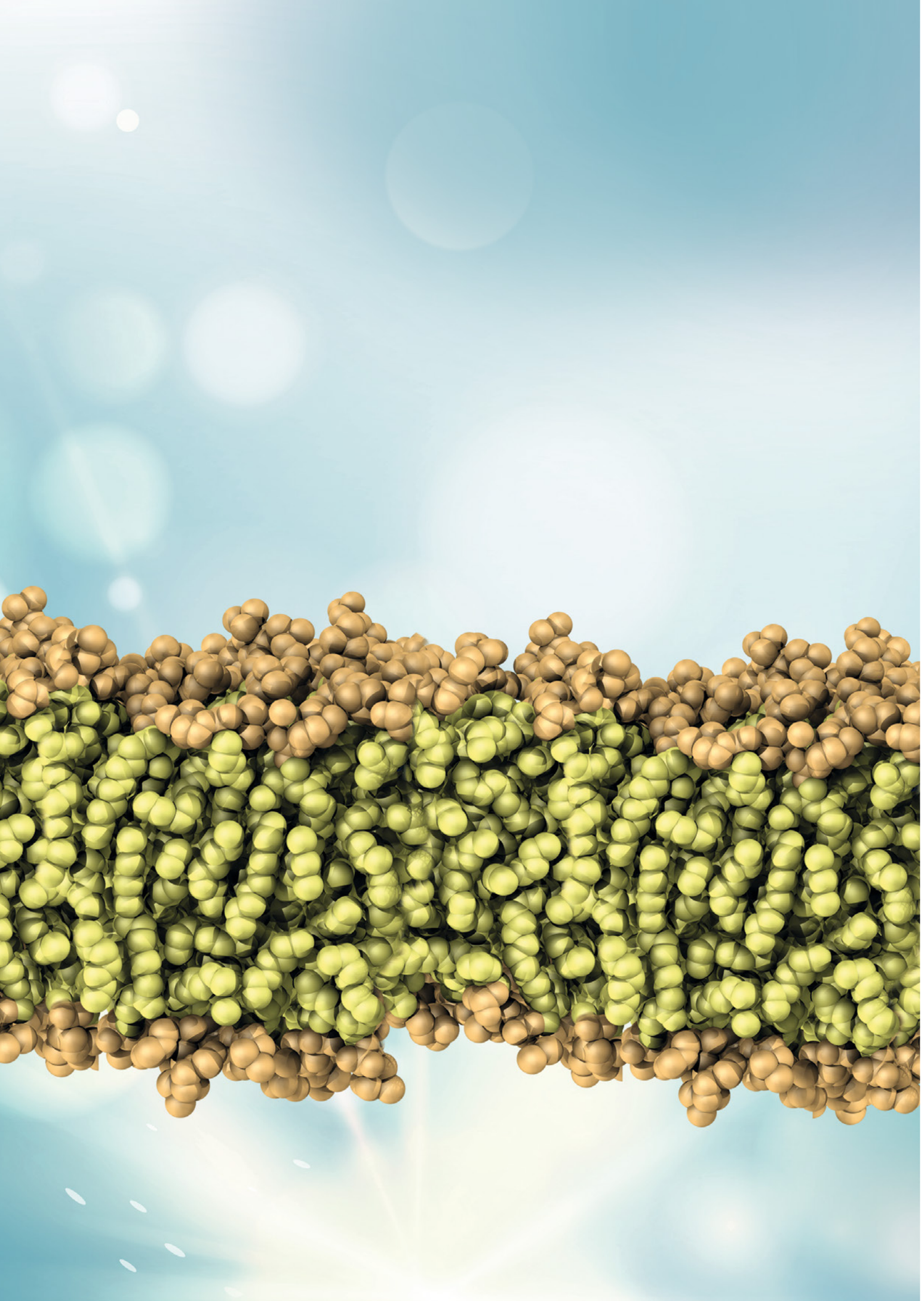

IT Center | RWTH AACHEN UNIVERSITY

CLAIX Projects 2019

High Performance Computing at RWTH Aachen University

Imprint

IT Center
RWTH Aachen University

Seffenter Weg 23
D-52074 Aachen

Phone: +49 241 80 24680
Fax: +49 241 80 22134

info@itc.rwth-aachen.de
www.itc.rwth-aachen.de

Editorial Design
HPC Offices, IT Center

Aachen, December 2020

Content

Picture: Alexander F. Müller

Preface

Dear reader,

Computer simulations have gained enormous importance in many different areas of our daily life as well as in most areas of scientific research. This insight has led to extensive investments in new and powerful high-performance computers such as the Cluster Aix-la-Chapelle (CLAIX) system at RWTH Aachen University.

In October 2019, CLAIX was officially inaugurated with a festive ceremony at the IT Center of RWTH Aachen University. The numerous top-class guests not only had the opportunity to learn about the importance of the computer for science, but were also invited to a guided tour of the new machine hall and CLAIX. Tim Berresheim, an internationally known artist who produces art with the help of computers, presented his artistic realization of the CLAIX lettering (see page 10).

In this report, we present a variety of exciting research projects using the CLAIX system in 2019.

The figure presented on the cover of this report is an example for the work of the Institute of Clinical Pharmacology of the Uniklinik RWTH Aachen and the Institute of Biological Information Processing at Forschungszentrum Jülich work together to study Molecular dynamics simulations of P2X receptors. P2X receptors represent promising drug targets because the seven mammalian family members of P2X are widespread across various cell types and are involved in important physiological processes including immune response, nociception, or muscle contraction (for more information, see page 20).

The study of Topological-chiral magnetic interactions driven by emergent orbital magnetism is another example for top-class science using CLAIX. Two hundred years ago, Ampère discovered that electric loops in which currents of electrons are generated by a penetrating magnetic field can mutually interact. This computing time project shows that Ampère's observation can be transferred to the quantum realm of interactions between triangular plaquettes of spins on a lattice, where the electrical currents at the atomic scale are associated with the orbital motion of electrons in response to the non-coplanarity of neighbouring spins playing the role of a magnetic field (see page 44).

Yours sincerely,

Matthias Müller

PROF. DR. MATTHIAS MÜLLER

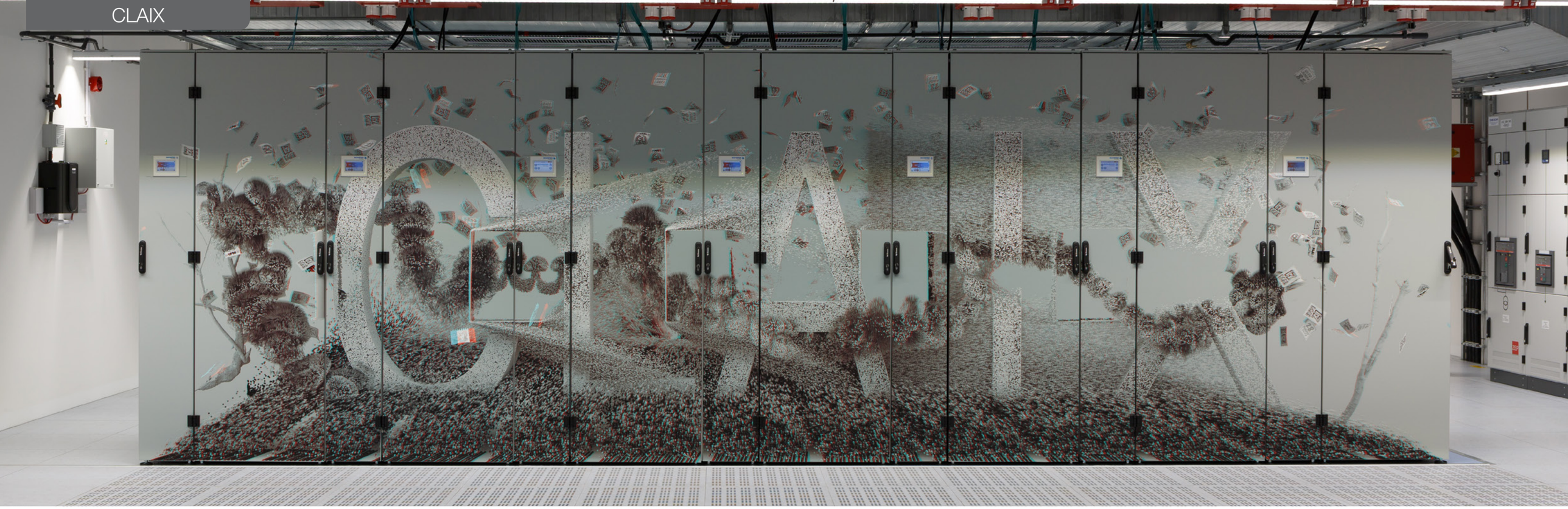

“CLAIX is a new flagship for Aachen as a high-performance computing location and we are proud of that.“

Parliamentary State Secretary Thomas Rachel MdB

“CLAIX is Germany’s fastest university high-performance computer in North Rhine-Westphalia. The new computer, which is operated jointly with Forschungszentrum Jülich, offers an outstanding research infrastructure and will make a decisive contribution to further expanding the leading position of RWTH Aachen and FZJ in the fields of simulation, data analysis and high-performance computing.“

Minister of Culture and Science Isabel Pfeiffer-Poensgen

The inauguration of CLAIX-2018

On October 02, 2019, the fastest university computer in Germany “Cluster Aix-la-Chapelle” (CLAIX) was officially inaugurated with a festive ceremony at the IT Center of RWTH Aachen University.

The ceremony was opened by Prof. Ulrich Rüdiger, Rector of RWTH Aachen University. He took this opportunity to introduce the new computer to numerous top-class guests. In attendance were for example Isabel Pfeiffer-Poensgen, Minister of Culture and Science of North Rhine-Westphalia, Thomas Rachel MdB, Parliamentary State Secretary in the Federal Ministry of Education and Research, Marcel Philipp, Lord Mayor of Aachen, Marcus Hermes, Managing Director of Bau- und Liegenschaftsbetrieb NRW, Yuichi Kojima, Managing Director of NEC Deutschland GmbH and Professor Matthias Müller, Head of the IT Centre at RWTH.

To quote Prof. Rüdiger, “the name CLAIX is actually the wrong name as we are not actually claixing here, but rather doing things in a big way. That’s why the computer should probably be called Klotz.”

The festive ceremony was followed by the symbolic handover of the key to the new machine hall and guests were given the opportunity to participate in a guided tour of CLAIX-2018. The internationally known artist Tim Berresheim presented his artistic realisation of the CLAIX lettering using an augmented reality app specially developed for this purpose.

The HPC system at RWTH Aachen University: CLAIX

The research projects in this report represent a selection of projects using the high-performance computing system CLAIX - Cluster Aix-la-Chapelle - at RWTH Aachen University in 2019. The system is operated by the IT Center and currently consists of three parts: the Tier-2 part from the procurement phases 2016 and 2018 and the Tier-3 part from the procurement phase 2018.

CLAIX-2016
The system consists of over 600 systems with 2x Intel Xeon Broadwell processors. Specialized node types with up to 144 cores at 1 Terabyte main memory or integrated GPGPUs or NVRAM complete the system for special tasks. All nodes as well as the parallel Lustre file system with a capacity of 3 petabytes are connected with an Intel Omni-Path network at 100-GigaBit/s speed. The overall system achieves a computing power of approx. 670 TeraFlop/s.

CLAIX-2016 started test operation in November 2016 and since December 2016 the system has been available without restriction for use by computing time projects.

CLAIX-2018
CLAIX-2018 consists of over 1000 computing nodes with 2x Intel Xeon Skylake processors, each with 24 cores and 192 GB RAM. In addition, there are 48 computing nodes of identical architecture, each equipped with two NVIDIA Volta V100 GPUs (incl. NVLink) as accelerators and available for special applications such as machine learning. A high-performance Lustre-based storage system offers a file system capacity of 10 petabytes and a bandwidth of 150 gigabytes/s (read and write). For interactive work with the system, CLAIX has eight additional dialog systems that are equipped with the same CPUs but have 384 GB more RAM. All nodes are connected to an Intel Omni-Path 100 Gigabit/s network.

The Tier-3 part consists of over 220 compute nodes with identical configuration (6 of those with GPUs) and are fully integrated into the overall cluster.

CLAIX-2018 started test operation in November 2018 and since January 2019 the system has been available without restriction for use by computing time projects.

Application for Compute Time
The allocation of compute time follows the recommendations of the Gauss Alliance for the establishment of nationally coordinated application and approval procedures. Depending on the amount of compute time request, independent national and international experts assess each proposal. According to regulations of the Deutsche Forschungsgemeinschaft (DFG), the Vergabegremium (VGG) of JARA-HPC or RWTH determines detailed scientific and technical criteria for the assessment of proposals for computing time. The VGG is also being supported by experts on operating supercomputers from both facilities.

Technical Summary

	CLAIX-2016	CLAIX-2018
# compute notes for projects	609 standard nodes + special nodes	1080 standard nodes + 221 Tier-3 std. nodes
Processor type	Intel Xeon E5-2650v4 (Broadwell-EP)	Intel Xeon Platinum 8160 (Skylake)
# cores per node	24	48
Main memory per node [GB]	192	128
Capacity of Lustre HPC filesystem	3 PB	10 PB
Bandwidth of Lustre HPC filesystem	45 GB/s	150 GB/s
Theoretical peak performance	0.53 Pflops	3.55 Pflops
LINPACK performance	0.51 PFlops	2.04 Pflops on 2014 nodes

Life Sciences

Life Sciences

Picture: Kjpargeter / Freepik

Life Sciences

Basic Biological and Medical Research | DFG 201

Molecular mechanism of proton-coupled metal ion transport in the SLC11/NRAMP family of transporters

Project ID: jara0178

EMILIANO IPPOLITI
Institute for Advanced Simulations and Institute for Neuroscience and Medicine (IAS-5/INM-9), FZ Jülich, Germany

MARIA LETIZIA MERLINI
PhD student, EPFL, Lausanne, Switzerland

ALESSANDRA MAGISTRATO
CNR-IOM and SISSA, Trieste, Italy

URSULA RÖTHLISBERGER
EPFL, Lausanne, Switzerland

PAOLO CARLONI
Institute for Advanced Simulations and Institute for Neuroscience and Medicine (IAS-5/INM-9), FZ Jülich, Germany

DANIELE NARZI
EPFL, Lausanne, Switzerland

Abstract

Metal ion transporters have gained increased attention due to their implication in the neurodegenerative diseases' onset. Among these the family of "solute carrier 11" (SLC11) or "natural resistance-associated macrophage proteins" (NRAMPs) are of intense interest since they function as secondary active transporters, regulating the influx of essential divalent transition-metal ions across cellular membranes [1-4]. DMT1 (divalent metal transporter 1), the best characterized member of this family, is widely expressed in different human tissues [5-6] and carries out coupled divalent transition-metal ions/H+ transport [7], exhibiting selectivity towards Mn^{2+}, Fe^{2+}, Co^{2+} and Cd^{2+}. Interestingly, mutations in DMT1 cause diseases (anemia) in humans and rodents [8].

Two X-ray structures, one of Staphylococcus capitis DMT1 (ScaDMT) [9], capturing an inward-facing conformation (IFC) of the transporter (i.e. the access route opens towards the cytoplasm) and another one from the bacterium Eremococcus coleocola (EcoDMT) with DMT1 in apo form and an outward facing conformation (OFC), revealed that DMT1 [10,11] work via an alternating access mechanism during which the protein is opened either towards the cytoplasm (IFC) or the extracellular matrix (OFC). In the first structure [9], a Mn2+ ion was identified coordinated by the carbonyl oxygen of A223, and the side chains of D49, N52 and M226. This structure also showed that the mutations identified in human patients with anemia are scattered in different parts of DMT1. The transport mechanism of this prokaryotic DMT1 is similar to the human one and depends on pH. Hence, DMT1 might actually couple Mn2+ transport with the symport of H+, although also uncoupled transport mechanisms have been detected [9,11]. In this project, we have used multiscale simulations to unravel the transport mechanism of metal ions in DMT1. This knowledge may be of key importance for therapeutic regulation of metal ion dys-homeostasis with potential applications in neurodegeneration.

Scientific work accomplished and results obtained

Figure 1: Mutations of DMT1 associated to human diseases' onset.

This system is extremely interesting to study as it is one of the few metal ions transporters for which an atomic level structure has been resolved. Since metal ion dys-homeostasis is increasingly implicated in major human diseases such as cancer and, in particular, neurodegeneration, in this project we tackle different important mechanistic traits, whose understanding may lead to novel regulatory strategies associated to metal ions transport dysfunctions.

To this end multiscale simulations (unbiased MD and enhanced-sampling QM/MM MD) have been employed to unravel the mechanism of transport of metal ions. Specifically, we have addressed specific points of the coupled H^+/Mn^{2+} transport mechanism and the origin of the specificity towards certain metals.

Sub-project A: The specific aims of this sub-project were: (i) understand the molecular mechanism of Mn2+ release towards the cytosol, starting from the IFC of ScaDMT; (ii) identify a stable binding site for Mn^{2+} in the OFC, starting from the X-ray structure of EcoDMT; (iii) unravel the pathway for H^+ transport across the transporter, identifying and characterizing the role of the residues crucially involved in this transport.

Sub-project B: This part of the project aims at (iv) elucidating the origin of metal ions selectivity of DMT1 towards specific divalent transition metal ions, and (v) finally, at understanding the impact of specific mutations associated to human disease on the structural dynamical and transport mechanism.

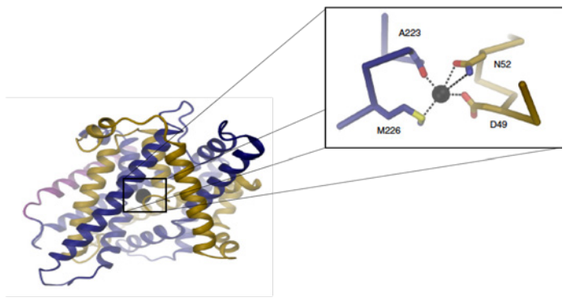

Figure 2: Cartoon of the ScaDMT protein structure; in the inset the Mn2+ binding site.

Realization of the project

To run the FF-based simulations of both wild type and mutated ScaDMT and EcoDMT we have used the GROMACS 2016.4 programs. The two systems have ~266,000 atoms, and scale very well up to 4 nodes (96 core) keeping a computational efficiency of 72.5%. Therefore, all the classical MD simulations in this project were performed with 96 cores. Simulations of the transport mechanism of Mn^{2+} and other metals (Zn^{2+}) required so far unbiased and biased Metadynamics-based QM/MM MD simulations by using CPMD 4.1 code. For this kind of simulations, we used 6 nodes (144 cores) on CLAIX-2016 (pure MPI) as this represented a good compromise between scaling performances and computational cost. The used codes were not modified during the execution of this project. The granted computing time was employed completely.

References

[1] RADISKY D, KAPLAN J, J. Biol. Chem., 1999, 274, (8), 4481-4484.
[2] NEVO Y, NELSON N, Biochim. Biophys. Acta, 2006, 1763, (7), 609-620.
[3] MONTALBETTI N, SIMONIN A, KOVACS G, HEDIGER MA, Mol. Aspects Med., 2013, 34, 270-287.
[4] CELLIER MF, BERGEVIN I, BOYER E, RICHER E, Trends Genet., 2001, 17, (7), 365-370.
[5] GUNSHIN H, MACKENZIE B, BERGER UV, GUNSHIN Y, ROMERO MF, BORON WF, NUSSBERGER S, GOLLAN JL, HEDIGER, MA, Nature, 1997, 388, (6641), 482-488.
[6] Shawki A, Knight PB, Maliken BD, Niespodzany EJ, Mackenzie B, Curr. Top. Membr., 2012, 70, 169-214.
[7] Mackenzie B, Ujwal ML, Chang MH, Romero MF, Hediger MA, Pfugers. Arch., 2006, 451, (4), 544-558.
[8] IOLASCON A, D'APOLITO M, SERVEDIO V, CIMMINO F, PIGA A, CAMASCHELLA C, Blood, 2006, 107, (1), 349-354.
[9] EHRNSTORFER IA, GEERSTMA ER, PARDON E, STEYAERT J, DUTZLER R, Nat. Struct. Mol. Biol., 2014, 21, (11), 990-996.
[10] YAMASHITA A, SINGH SK, KAWATE T, JIN Y, GOUAUX E, Nature, 2005, 437, (7056), 215-223.
[11] EHRNSTORFER IA, MANATSCHAL C, ARNOLD FM, LAEDERACH J, DUTZLER R, Nature Commun., 2017,8.
[12] http://biophysics.cs.vt.edu/
[13] LINDORFF-LARSEN K, PIANA S, PALMO K, MARAGAKIS P, KLEPEIS JL, DROR RO, SHAW DE Proteins: Structure, Function, and Bioinformatics, 2010, 78, (8), 1950-1958.

Life Sciences

Molecular dynamics of the SLC26 family of ion channels and transporters

Project ID: jara0177

JAN-PHILIPP MACHTENS
Institute of Biological Information Processing (IBI-1), Forschungszentrum Jülich, Germany and Institute of Clinical Pharmacology, Uniklinik RWTH Aachen, Germany

PIERSILVIO LONGO
Institute of Biological Information Processing (IBI-1), Forschungszentrum Jülich, Germany

Project Report

The Solute Carrier family 26 (SLC26) of membrane proteins includes secondary active anion exchangers, isoforms that mediate channel-like anion conduction transport, as well as the voltage-driven motor protein prestin (SLC26A5). SLC26 transporters have essential roles in the ion homeostasis of many organs, and human mutations and animal models of SLC26 dysfunction are associated with multiple disease conditions.

Owing to their physiological importance, SLC26 transporters represent important, yet unexplored, drug targets for various diseases, including cystic fibrosis. Recently, the first high-resolution structure of a mammalian SLC26 transporter (murine Slc26a9) has been determined using cryo-electron microscopy. This transporter mediates uncoupled Cl- transport across the membrane, and human SLC26A9 is an important disease modifier of cystic fibrosis. However, its transport mechanism is still unclear. For example, it is unknown whether SLC26A9 mediates channel-like conductive Cl- transport or uses an alternating-access transport mechanism.

So far, experimental structures of SLC26 transporters have been obtained only for inward-facing conformations, leaving the transport mechanisms elusive. We employed extensive all-atom molecular dynamics (MD) simulations to obtain first insights into the transport mechanisms of SLC26 transporters. The Accelerated Weight Histogram (AWH) method is an efficient extended ensemble sampling technique which adaptively biases the simulation to promote efficient exploration of multi-dimensional free-energy landscapes. Starting from the inward-facing conformation of Slc26a9, we developed a protocol using AWH simulations to rigorously explore the conformational landscape of transmembrane translocation.

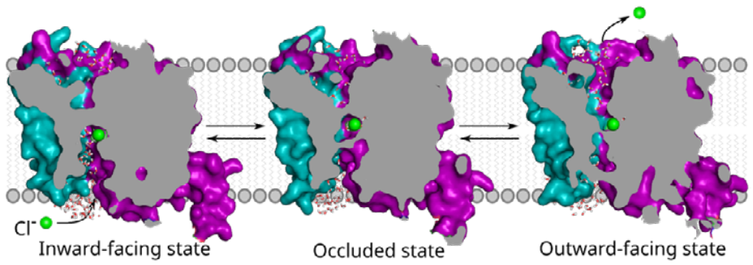

Figure 1: Proposed elevator transport mechanism based on MD simulations of Slc26a9.
AWH simulations have been used to sample the translocation pathway starting from the inward-facing conformation (PDB ID: 6RTC). Analysis of water accessibility of the Cl^--binding site indicates an elevator alternating-access mechanism for Cl^- transport.
Left, the Cl^--binding pocket is accessible only from the intracellular side (inward-facing state).
Middle, Cl^--binding pocket is occluded (intermediate state).
Right, the Cl^--binding pocket is accessible only from the extracellular side (outward-facing state).

Using AWH simulations, we have been able to reproducibly simulate transmembrane translocation on the microsecond timescale, and we identified hitherto unknown intermediate and outward-facing states. Since Cl- ions bound and unbound spontaneously during our simulations, these simulations captured complete Cl^--transport events. Our simulations revealed rotational-translational rigid-body motions of the core domain relative to the static gate domain that alternatively expose the Cl^--binding site to either the intracellular or the extracellular side. These simulations thereby established an alternating-access transport mechanism for the SLC26A9 transporter and provide a foundation for further experiments and simulations to obtain a complete understanding of the transport cycle at atomic resolution.

Selected honors, prizes, awards

This project is part of the DFG Research Unit FOR 5046 Integrated analysis of epithelial SLC26 anion transporters - from molecular structure to pathophysiology. This consortium, including the PI's project on molecular simulations of SLC26 transporters, was established in April 2020, and both have successfully evaluated for a four-years funding period by an international review board.

Selected national and international cooperations

- Dominik Oliver, Institute of Physiology and Pathophysiology, Philipps-University Marburg, Germany
- Eric Geertsma, Institute of Biochemistry, Goethe-University Frankfurt, Germany

Selected publications

[1] KORTZAK D, ALLEVA C, WEYAND I, EWERS D, ZIMMERMANN MI, FRANZEN A, MACHTENS JP, FAHLKE C
(2019) Allosteric gate modulation confers K+ coupling in glutamate transporters.
EMBO J: e101468

Life Sciences

Molecular dynamics simulations of P2X receptors

Project ID: jara0180

JAN-PHILIPP MACHTENS
Institute of Clinical Pharmacology, Uniklinik RWTH Aachen, Germany and Institute of Biological Information Processing (IBI-1), Forschungszentrum Jülich, Germany

SASKIA CÖNEN
Institute of Clinical Pharmacology, Uniklinik RWTH Aachen, Germany and Institute of Biological Information Processing (IBI-1), Forschungszentrum Jülich, Germany

RALF HAUSMANN
Institute of Clinical Pharmacology, Uniklinik RWTH Aachen, Germany

LINHAN CHENG
Institute of Clinical Pharmacology, Uniklinik RWTH Aachen, Germany

Project Report

The P2X family of membrane proteins encompasses ligand-gated ion channels that are activated by extracellular ATP. The subtypes named P2X1 to P2X7 assemble in homo- or heterotrimeric complexes and are permeable to mono- or divalent cations. The seven mammalian family members of P2X are widespread across various cell types and are involved in important physiological processes including immune response, nociception, or muscle contraction. Therefore, P2X receptors represent promising drug targets.

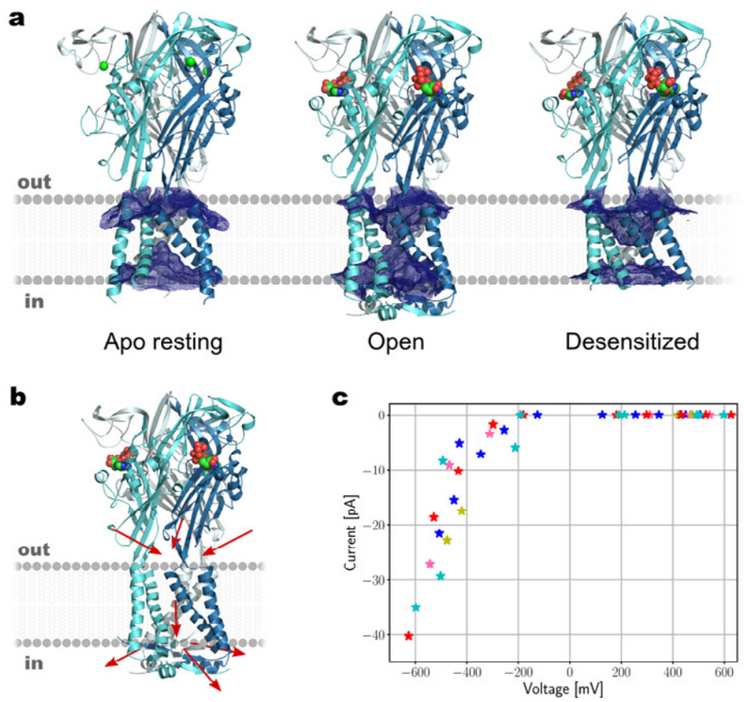

Figure 1: MD simulations of the human P2X3 receptor.
(a) Averaged water densities (contoured at 0.015σ) in unbiased 1-µs MD simulation of hP2X3 in the apo, open, and desensitized states. Continuous water density along the pore is found in the open state.
(b) Illustration of the permeation pathway observed in computational electrophysiology simulations with applied transmembrane voltages and spontaneous cation permeations. Cations enter the pore through three extracellular fenestrations and enter the cytoplasmic side through lateral fenestrations.
(c) Multiple replicas of computational electrophysiology simulations in the open state hP2X3 were carried out with various transmembrane voltages between -600 and 600 mV. The resulting current–voltage curve closely resembles experimental data.

To establish a basis for rational drug development, it is essential to understand the receptor and channel function at the molecular level. Electrophysiological experiments established that upon binding of ATP, the receptor leaves the apo (resting) state and enters the open (ion conductive) state, while under sustained presence of ATP most P2X isoforms subsequently enter the (non-conductive) desensitized state. Recently, the first high-resolution X-ray crystal structures of a functional P2X3 receptor were determined in three different conformations, presumably representing the open, desensitized, and apo resting states. Using extensive all-atom molecular dynamics (MD) simulations, we obtained a functional annotation of these structures. We found the ion pore to be permeable for cations in the open state, whereas ion access was restricted in both apo and desensitized states.

In the open state, the intracellular domains of hP2X3 form a complex structure called the cytoplasmic cap, which is assumed to dynamically fold during receptor activation. MD simulations of hP2X3 were used to investigate conformational changes and pore closure during receptor desensitization. The results demonstrate that the cytoplasmic cap markedly stabilizes the transmembrane domains in the open state, thereby preventing pore closure.

Using extensive microsecond-long computational electrophysiology simulations with applied transmembrane voltages, we directly simulated ion conduction in open-state hP2X3. These simulations defined the unusual ion permeation pathway: Na+ ions enter the pore through three extracellular fenestrations, permeates through the pore and leaves into the intracellular space through lateral cytoplasmic fenestrations. The headgroups from lipids of the surrounding membrane protrude into the pore center and thereby influence the rate of cation permeation. These simulations permitted us to directly calculate ion currents, resulting in a current–voltage curve that closely resembles experimental recordings with a strong inward rectification.

Selected conference participations

- Saskia Cönen, Molecular dynamics study of hP2X3 receptor desensitization, Symposium of Young Physiologists and Pharmacologists, Nuremberg, March 14-15, 2019

Selected national and international cooperations

- Fritz Markwardt, Julius-Bernstein-Institut für Physiologie, Martin-Luther-Universität Halle-Wittenberg, Halle, Germany

Selected publications

[1] BRATANOV D, KOVALEV K, MACHTENS JP, ASTASHKIN R, CHIZHOV I, SOLOVIOV D, VOLKOV D, POLOVINKIN V, ZABELSKII D, MAGER T, GUSHCHIN I, ROKITSKAYA T, ANTONENKO Y, ALEKSEEV A, SHEVCHENKO V, YUTIN N, ROSSELLI R, BAEKEN C, BORSHCHEVSKIY V, BOURENKOV G ET AL.
(2019) Unique structure and function of viral rhodopsins.
Nat Commun 10: 4939

Natural Sciences

Picture: Katemangostar / Freepik

Natural Sciences

Molecular Chemistry | DFG 301

Computational elucidation of mechanistic aspects of water oxidation with manganese based homogeneous catalysts

Project ID: rwth0317
MARKUS HÖLSCHER
Institute of Technical and Macromolecular Chemistry
RWTH Aachen University

MARTIN SCHWARZER
RWTH Aachen University

Project Report

The aim of this project was to elucidate mechanistic aspects of the water oxidation reaction, specifically the oxygen evolution, to understand the behaviour of manganese complexes synthesised by our group with specifically designed ligands: a pentadentate system dpaq, and a tetradentate system ppqma.

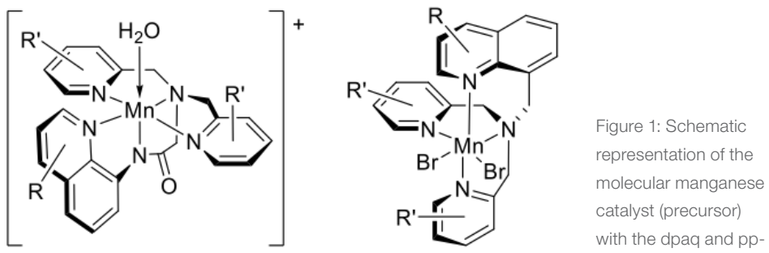

Figure 1: Schematic representation of the molecular manganese catalyst (precursor) with the dpaq and ppqma ligand systems.

We used quantum chemical calculations based on Density Functional Theory (DFT) to gain insight into the reaction pathways of these systems, and elucidated the relative stabilities of reactant, intermediate, and product complexes (local minima) based on postulated reaction pathways (Figure 2).

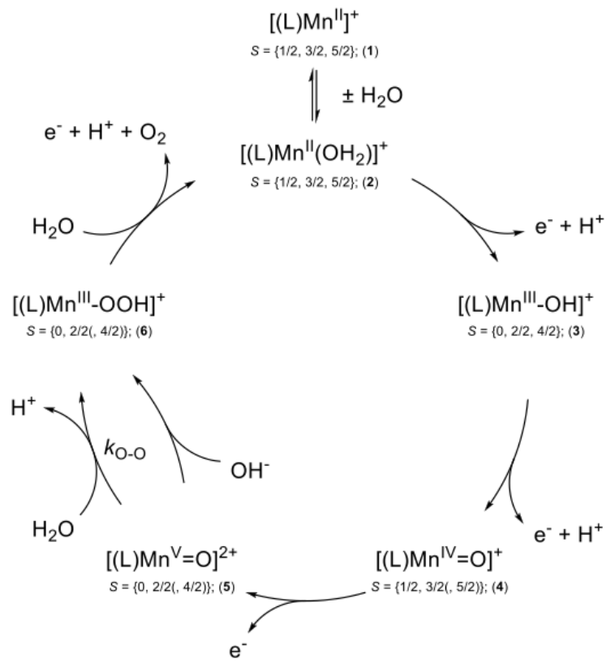

Figure 2: Postulated reaction mechanism for the catalyst system with the dpaq ligand.

We gained valuable insight as we were able to determine which spin state is the ground state and further on deduce which reaction pathways are most feasible (excerpt of the results in Table 1).

During our investigations we had to realise that DFT-based calculations are incapable of describing the mechanistic aspects behind the reactions of these molecular catalyst systems; proton transfers can only be described insufficiently as points on a potential energy surface. A more dynamic approach has to be explored albeit at the loss of chemical accuracy.

Complex	Low-Spin	High-Spin	
[(dpaq)MnII(OH2)]$^+$	136.3 (d)	90.7 (q)	0.0 (sx)
[(dpaq)MnIII-OH]$^+$	188.5 (s)	73.8 (t)	0.0 (qi)
[(dpaq)MnV=O]$^+$	13.5 (s)	0.0 (t)*	40.1 (qi)**
[(dpaq)MnIII-OOH]$^+$	117.5 (s)	68.1 (t)	0.0 (qi)

s: singlet; d: doublet; t: triplet; q: quartet; qi: quintet; sx: sextett; *high-spin state; **excited state

Table 1: Relative Gibbs energies ΔG/ kJ mol^{-1} of the calculated complexes in reference to its determined ground state at the DF-B97D3/def2-SVP lvel of theory including thermal corrections at 25 °C and 1 atm.

1 dpaq: (2-[bis(pyridin-2-ylmethyl)]amino-N-quinolin-8-yl-acetamidate); ppqma: (1-(pyridin-2-yl)-N-(pyridin-2-ylmethyl)-N-(quinolin-8-ylmethyl)methanamine)

2 Quantum chemical computations of the various structures were performed with the Gaussian 16 program package on various levels of theory. Density functional approximations (DFA) provide a reasonable trade-off between accuracy and performance. Among those DFA were B97D3, BP86, TPSS, M06, MN15, PBE0, B3LYP, and other variations thereof in conjunction with the def2-SVP and def2-TZVPP basis sets. Density fitting was applied where possible. Solvent corrections have been considered either as implemented polarisable continuum models, or explicitly, where necessary and feasible. Normal coordinate analyses have been performed to verify and characterise the calculated states, as well as to include thermal corrections

Natural Sciences

Molecular Chemistry | DFG 301

DFT-based investigation of DMSO-hydrogenation to methanol with a ruthenium pincer complex

Project ID: rwth0332
MARKUS HÖLSCHER
Institute of Technical
and Macromolecular Chemistry
RWTH Aachen University

MERIA RONGE
RWTH Aachen University

Project Report

Dimethyl sulfoxide (DMSO), a by-product of the wood pulping industry is a commonly applied solvent in organic chemistry and is furthermore widely utilized in industrial processes. The development of DMSO-based reaction pathways and the respective elucidation of mechanistic details have been focal points of a variety of research projects and publications.[1,2,3] Understanding the various reactive pathways originating from DMSO might open up interesting new opportunities in industrial chemistry and is thus highly desirable. [4] Recently, we have discovered the homogeneously catalyzed hydrogenation and rearrangement of DMSO to yield methanol in very good turnover numbers (Figure 1).

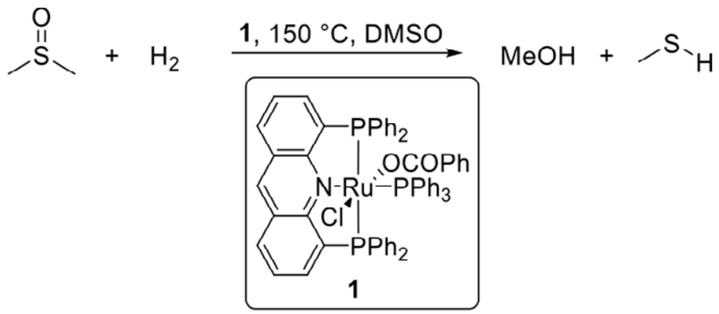

Figure 1: The net reaction equation of the hydrogenation of DMSO to methanol and methylmercaptane with pincer complexes 1.

Already early on, it was possible to rule out many of the previously suggested mechanistic pathways of the reaction and propose a straightforward route to the desired product methanol. In a thermal decomposition of DMSO, the intermediate formaldehyde is generated, which constitutes a highly reactive substrate for the formation of methanol under the reductive conditions in the reaction vessel in presence of catalyst 1 (Figure 2).

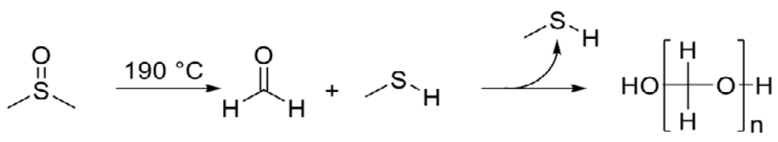

Figure 2: Formation of formaldehyde under thermal treatment.[5]

Having elucidated the reaction mechanism of methanol from DMSO, the same catalyst system was further investigated for the hydrogenation of CO2 to formic acid, which involves similar reactivities like the ones observed in the hydrogenation of DMSO to methanol. We therefore screened computational four derivatives of catalyst 1 to optimize the catalytic system both sterically and electronically and tailor it to the specific requirements of the hydrogenation of CO2 to methanol.

The DFT calculations carried out in this project helped to elucidate details of the reaction mechanism and suggested a variety of variations of the catalyst structure to improve the catalytic performance.

References

[1] a) SCHÖNHERR H, CERNAK T. Angew. Chem. 2013, 12480–12492.
b) KAWAI K, LI YS, SONG MF, KASAI H. Bioorg. & med. chem. lett. 2010, 260–265.
c) RUSSELL GA, WEINER SA.
d) GARCÍA N, RUBIO-PRESA R, GARCÍA-GARCÍA P, FERNÁNDEZ-RODRÍGUEZ MA, PEDROSA MR, ARNÁIZ FJ, SANZ R. Green Chem. 2016, 2335–2340.
e) SUN K, LV Y, ZHU Z, ZHANG L, WU H, LIU L, JIANG Y, XIAO B, WANG X. RSC Adv. 2015, 3094–3097.
f) LV Y, LI Y, XIONG T, PU W, ZHANG H, SUN K, LIU Q, ZHANG Q. Chem. Commun. 2013, 6439–6441.
g) PAN X, LIU Q, CHANG L, YUAN G. RSC Adv. 2015, 51183–51187.
h) WANG F, SHEN J, CHENG G, CUI X. RSC Adv. 2015, 73180–73183.
i) DEVARI S, KUMAR A, DESHIDI R, SHAH BA. Chemical communications (Cambridge, England) 2015, 5013–5016.
j) ZHANG J, GAO X, ZHANG C, ZHANG C, LUAN J, ZHAO D. Syn. Commun. 2010, 1794–1801.
[2] QIAN J, ZHANG Z, LIU Q, LIU T, ZHANG G.
Adv. Synth. Catal. 2014, 3119–3124.
[3] LIANG YF, WU K, SONG S, LI X, HUANG X, JIAO N.
Organic letters 2015, 876–879.
[4] WU XF, NATTE K.
Adv. Synth. Catal. 2016, 336–352.
[5] TRAYNELIS VJ, HERGENROTHER WL.
J. Org. Chem. 1964, 221–222.

Computational studies of reactivities in organic and organometallic transformations

Project ID: jara0091
FRANZISKA SCHOENEBECK
Institute of Organic Chemistry,
RWTH Aachen University

AJOY KAPAT
MAOPING PU
THERESA SPERGER
ERDEM SENOL
CHRISTOPH FRICKE
CLAUDIA DIEHL
GUILLAUME MAGNIN
BHASKAR MONDAL
ABDURRAHMAN TURKSOY
SAMIR BOUAYAD-GERVAIS
WILLIAM REID
FILIP OPINCAL
SARAH MICHAEL
TATJANA KREISEL
IGNACIO FUNES-ARDOIZ
DANIEL HUPPERICH
SEBASTIAN WELLIG
Institute of Organic Chemistry,
RWTH Aachen University

Project Report

The general aim of our research is the investigation of reactivity phenomena. By gaining a thorough understanding of reaction mechanisms, novel catalysts and transformations are designed. In particular, we intend to use the added benefits of the synergistic use of combining computational and experimental approaches. More specifically, we have investigated the distinct mechanistic features of dinuclear Pd(I) compared to mononuclear Pd(0) catalysis in the context of the reactivity of aryl fluorosulfates [1], the formation of aryl phosphorothioates [2], in selenolation reactions [3] and dispersion effects during oxidative addition [4]. We have also studied purely organic reactivity in the case of tetramethylammonium fluoride and its use as a methylating agent [5].Lastly, we have made further advances in our ongoing studies on transmetalation at palladium by employing Born-Oppenheimer molecular dynamics calculations. The latter was also used to uncover dynamic effects in the context of copper catalyzed oxidations and high-energy intermediates in cobalt catalyzed C-H activation. In the following three projects are highlighted.

(1) Effects of Dispersion on Oxidative Addition: Traditionally, steric hindrance in the ortho position of a haloarene has been considered a drawback for many catalytic reactions due to the arguably high reaction barriers caused by detrimental steric interactions. However, some bulky groups, such as adamantyl, can display increased dispersion interactions with the catalyst, therefore lowering the expected high barriers. We have explored the oxidative addition of different aryl bromides, including bulky adamantyl derivatives, to a bisligated Pd-phosphine catalyst[4]. The controlling dispersion interaction was showcased by enabling/disabling empirical dispersion corrections. To validate the employed methodology, an extensive benchmark was carried out, including high-level DLPNO-CCSD(T) calculations in addition to different DFT functionals, basis sets, solvation and empirical dispersion methods. We have also assessed the reactivity of monophosphine Pd(0) towards different C-OSO2R electrophiles. In order to compare the reactivity of triflates, nonaflates, mesylates, tosylates and fluorosulfates, their barriers towards oxidative addition were calculated. Almost identical barriers were found for these functionalities in the favored 5-membered transition state geometry. Following this computational assessment, the fluorosulfate moiety was experimentally demonstrated as a lower cost surrogate for the more expensive triflates[1].

(2) Reactivity trends of C(sp2)-X bonds towards Pd(0) vs. dinuclear Pd(I): In continuation of our earlier work on dinuclear Pd(I)-catalysis we have computationally explored the mechanism of our novel protocol on the selenolation of aryl iodides and bromides.[3] In line with our previously proposed mechanism we located a dinuclear pathway proceeding via oxidative addition to form a dinuclear Pd(II) dimer and successive reductive elimination to yield the aryl selenol product. The process was shown to be thermodynamically driven with a ΔG of -13.8 kcal/mol. A dinuclear Pd(I) reaction pathway was also studied for the C-SP(=O)(OR)2 coupling.[2] Notably, the calculations showed that the corresponding mononuclear Pd(0)/Pd(II) pathway is not a viable alternative, since reductive elimination has a high barrier (>30 kcal/mol) and is endergonic. On the other hand, the dinuclear Pd(I) pathway circumvents this problem by altering the thermodynamic driving force, while activation barriers remained feasible and were in line with our previous studies on Pd(I) dimers.

(3) Selective Methylation: The selective methylation of amides by tetramethylammonium fluoride was explored by DFT calculations. In our previous studies we have demonstrated that a direct methyl cation transfer can occur from the tetramethylammonium cation. However, in the context of this study a direct methyl cation transfer showed a prohibitively high barrier (>45 kcal/mol). Instead, we found that a concerted deprotonation and methyl transfer occurs with a lower activation barrier. Moreover, the tautomerization of the amide to the imidic acid allowed for an energetically more favorable transition state than the corresponding direct reaction of the amide, despite the energetic drawback arising from forming the less stable imidic acid. The experimentally observed chemoselectivity of amides over anilines is in line with the found concerted mechanism as the corresponding transition state for anilines was found to be more than 8 kcal/mol higher [5].

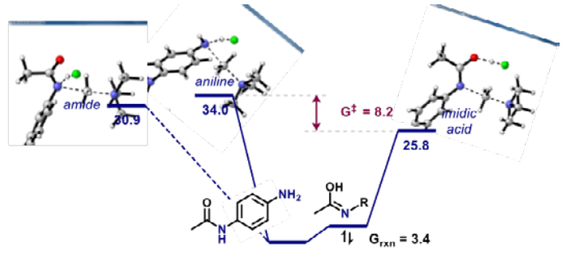

Figure 1: Competing transition states and selectivities of selective methylation of amides over anilines.

References

[1] MENDEL M, KALVET I, HUPPERICH D, MAGNIN G, SCHOENEBECK F. Angew. Chem. Int. Ed. 2020, 59, 2115-2119.
[2] CHEN XY, PU M, CHENG HG, SPERGER T, SCHOENEBECK F. Angew. Chem. Int. Ed. 2019, 58, 11395-11399.
[3] SENOL E, SCATTOLIN T, SCHOENEBECK F. Chem. Eur. J. 2019, 25, 9419-9422.
[4] KALVET I, DECKERS K, FUNES-ARDOIZ I, MAGNIN G, SPERGER T, KREMER M, SCHOENEBECK F. Angew. Chem. Int. Ed. 2020, 59, 7721-7725.
[5] CHENG HG, PU M, KUNDU G, SCHOENEBECK F. Org. Lett. 2020, 22, 331-334.

Selected honors, prizes, awards

- Merck Lecturer at Boston College, 2019
- Boehringer-Ingelheim-MIT Lecturer, 2019
- ERC Consolidator Grant

Selected conference participations

see report rwth0350, page 31

National and international cooperations

see report rwth0350, page 31

Selected publications

[1] CHEN XY, PU M, CHENG HG, SPERGER T, SCHOENEBECK F. Arylation of Axially Chiral Phosphorothioate Salts by Dinuclear PdI Catalysis, Angew. Chem. Int. Ed. 2019, 58, 11395-11399.
[2] SENOL E, SCATTOLIN T, SCHOENEBECK F. Selenolation of Aryl Iodides and Bromides Enabled by a Bench-Stable PdI Dimer, Chem. Eur. J. 2019, 25, 9419-9422.
[3] AGASTI S, MONDAL B, ACHAR TK, SINHA SK, SARALA SUSEELAN A, SZABO KJ, SCHOENEBECK F, MAITI D.
Orthogonal Selectivity in C–H Olefination: Synthesis of Branched Vinylarene with Unactivated Aliphatic Substitution, ACS Catal. 2019, 9, 9606-9613.
[4] CHENG HG, PU M, KUNDU G, SCHOENEBECK F.
Selective Methylation of Amides, N-Heterocycles, Thiols, and Alcohols with Tetramethylammonium Fluoride, Org. Lett. 2020, 22, 331-334. (most read publication in Org. Lett. in Dec 2019/Jan 2020)

New vistas in metal-based homogeneous and biocatalysis – from analysis to design

Project ID: rwth0350
FRANZISKA SCHOENEBECK
Institute of Organic Chemistry,
RWTH Aachen University

CHRISTOPH FRICKE
CLAUDIA DIEHL
GUILLAUME MAGNIN
BHASKAR MONDAL
WILLIAM REID
FILIP OPINCAL
IGNACIO FUNES-ARDOIZ
Institute of Organic Chemistry,
RWTH Aachen University

Project Report

As part of our ongoing research program on alternative mechanisms in cross-coupling and C-X functionalization reactions, we have explored dimeric Pd(I) catalysts and their intriguing reactivity. The possibility of two or more metals taking part in key steps of catalysis enables a plethora of reactivity. Similar to Nature's enzymes small metal clusters can have synergistic effects on reactivity and allow for reactions that are not possible or inefficient using just one metal center. In the following two sub-projects of our ongoing work in this area are highlighted: (i) the reactivity of trimeric Pd complexes as well as small Pd clusters in the form of nanoparticles, (ii) the reactivity of so far underexplored organogermanes and their transmetalation to Au complexes.

(1) Trimeric palladium catalysis: Building on our previous work with Pd(I) dimers and their intriguing reactivity, we embarked on exploring the reactivity of trimeric Pd species.[1] While key mechanistic steps are well-studied for monomeric and also dimeric Pd complexes, multiple pathways had to be evaluated in the case of Pd trimers. Our experiments showed reactivity towards aryl halides and hence we were prompted to study this activation in detail by means of DFT calculations. Initially, the electronic structure of the trimer was explored and suggested that the complex is aromatic and a singlet, closed-shell species. Multiple mechanistic alternatives for the activation of aryl halides were then investigated, such as halogen abstraction, electrophilic activation, oxidative addition-type mechanisms. The latter was found to be favoured and the three-membered concerted oxidative addition transition states were located for iodobenzene, as well as the analogous bromide and chloride (Figure 1A). The higher activation barriers for Br and Cl were in line with the experimentally observed exclusive reactivity of aryl iodides.

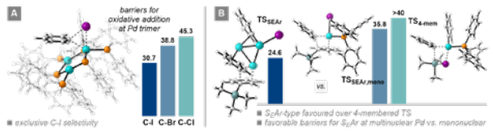

Figure 1: Reactivity of multinuclear Pd: (A) activation of aryl iodides by a Pd trimer, (B) transmetallation of organogermanes at Pd clusters.

Next, we also studied the reactivity of small Pd clusters, i.e. nanoparticles, and their reactivity with organogermanes.[2] Notably, we observed a reversal of selectivity using Pd nanoparticles compared to traditional homogeneous Pd(0)/Pd(II) catalysis: organogermaniums were unreactive under these conditions, but were exclusively activated by Pd nanoparticles. Our computational study shed light on this intriguing selectivity and indicated that an electrophilic aromatic substitution is favoured over the commonly proposed 4-membered transmetalation at Pd(II) (Figure 1B, right). As a consequence, the nucleophilic organogermanes are rather activated by electron-deficient metal clusters than by the more electron-rich phosphine-ligated Pd(II) species. To further explore their reactivity with small Pd clusters, a phosphine-free Pd trimer was used as a model catalyst. The computational data suggests that an initial activation of the trimer via oxidative addition of aryl iodide takes place. The formed cationic cluster is then highly reactive towards the organogermane and transmetallation occurs in an electrophilic aromatic substitution-type mechanism (Figure 1B). Although a Pd trimer was used as a representative model for nanoparticles, our computational studies indicate that the reactivity trends also remain for larger Pd clusters.

(2) Transmetalation to gold: Intrigued by the unusual reactivity of organogermanes we further set out to explore their reactivity with electrophilic gold complexes.[3] Our computational studies showed the initial formation of a Wheland-type intermediate with Au(III), followed by C-Ge bond scission. A distortion/interaction analysis was performed and showed that the activation barrier is mainly dictated by the distortion of the organogermane rather than that of the Au complex (Figure 2, left). As distortion is commonly related to bond dissociation energies, this is in line with the observed superior reactivity of germanes compared to the corresponding silanes as their BDE is roughly 10 kcal/mol lower. Moreover, aryl germanes were also found to be reactive towards Au(I) (Figure 2, right), exhibiting an 8.8 kcal/mol lower activation barrier than the corresponding silanes, which were found unreactive.

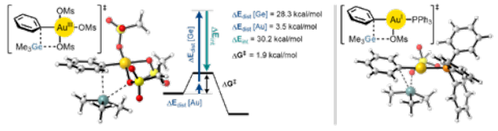

Figure 2: Transmetalation of aryl germanes at Au(III) (left) and Au(I) (right).

References

[1] DIEHL CJ, SCATTOLIN T, ENGLERT U, SCHOENEBECK F. Angew. Chem. Int. Ed. 2019, 58, 211-215.
[2] FRICKE C, SHERBORNE GJ, FUNES-ARDOIZ I, SENOL E, GUVEN S, SCHOENEBECK F. Angew. Chem. Int. Ed. 2019, 58, 17788-17795.
[3] FRICKE C, DAHIYA A, REID WB, SCHOENEBECK F. ACS Catal. 2019, 9, 9231-9236.

Selected honors, prizes, awards

- Merck Lecturer at Boston College
- Boehringer-Ingelheim-MIT Lecturer
- ERC Consolidator Grant

Selected conference participations

- Lecture at LMU Munich, Germany, January 2019
- Lecture at Boehringer Ingelheim, Biberach, Germany, March 2019
- Lecture at ETH Zürich, Switzerland, May 2019
- Lecture at GlaxoSmithKline (GSK), Stevenage, UK, June 2019
- Keynote speaker 9th Pacific Symposium on Radical Chemistry, USA, June 2019
- Keynote speaker 26th International Symposium on Synthesis in Organic Chemistry, Cambridge, UK, July 2019
- Lecture at Columbia University, USA, October 2019
- Keynote speaker Journées de Chimie Organique, Palaiseau, France, October 2019
- Lecture at Massachusetts Institute of Technology, USA, October 2019
- Lecture at Boehringer Ingelheim, USA, October 2019
- Keynote speaker Merck Symposium in Organic Chemistry at Boston College, USA, October 2019
- Keynote speaker 'New Frontiers in Synthetic Chemistry' RSC Symposium, UK, November 2019

National and international cooperations

- Prof. Rovis, Columbia University, New York, USA
- Prof. Carreira, ETH Zürich, Zürich, Switzerland
- Prof. John Murphy, Univ. of Strathclyde, Glasgow, UK

Selected publications

[1] DIEHL CJ, SCATTOLIN T, ENGLERT U, SCHOENEBECK F.
C-I Selective Cross-Coupling Enabled by a Cationic Pd Trimer,
Angew. Chem. Int. Ed. 2019, 58, 211-215.
[2] FRICKE C, SHERBORNE GJ, FUNES-ARDOIZ I, SENOL E, GUVEN S, SCHOENEBECK F.
Orthogonal Nanoparticle Catalysis with Organogermanes,
Angew. Chem. Int. Ed. 2019, 58, 17788-17795
[2] FRICKE C, DAHIYA A, REID WB, SCHOENEBECK F.
Gold-Catalyzed C–H Functionalization with Aryl Germanes,
ACS Catal. 2019, 9, 9231-9236.

Natural Sciences

Chemical Solid State and Surface Research | DFG 302

Atomistic modeling of radionuclide-bearing materials for safe management of high level nuclear waste

Project ID: jara0037

PIOTR KOWALSKI
Institute of Energy and Climate Research: Nuclear Waste Management and Reactor Safety and Theory and Computation of Energy Materials (IEK-6 /IEK-13), Forschungszentrum Jülich, Germany

MENGLI SUN
Institute of Energy and Climate Research: Nuclear Waste Management and Reactor Safety and Theory and Computation of Energy Materials (IEK-6 /IEK-13), Forschungszentrum Jülich, Germany and Lanzhou University, China

MILAN PSENICKA
Charles University
Prague, Czech Republic

BART VERLINDEN
SCK CEN, Belgium

VICTOR VINOGRAD
EVGENY ALEKSEEV
GABRIEL MURPHY
DIRK BOSBACH
Institute of Energy and Climate Research: Nuclear Waste Management and Reactor Safety (IEK-6), Forschungszentrum Jülich, Germany

SAMUEL EDWARDS
ROBERT BAKER
Trinity College Dublin, Ireland

EUGENIA KUO
ZHAOMING ZHANG
ANSTO, AUSTRALIA
GREG LUMPKIN
ANSTO, Australia

BRENDAN KENNEDY
University of Sydney, Australia

DAVID SIMEONE
CEA, France

Project Report

Understanding the behavior and safe management of radionuclide-bearing materials such as nuclear fuel and waste, building blocks of reactors and nuclear waste storage containers requires a solid scientific basis. Spent nuclear fuels contain actinides and long-lived fission and activation products, which can remain radioactive for hundreds of thousands of years. The limited understanding of the processes associated with the interaction of radionuclides with different materials and disposal environment limits the availability of materials for safe storage of nuclear waste. The aim of our research is to investigate the ability of different materials (e.g. waste forms, engineered barriers, buffer materials, secondary phases, spent fuel (UO2 -based materials), etc...) to incorporate and immobilize radionuclides, to understand the radiolytical degradation of the organic compounds used in the liquid-liquid extraction technology and to characterize further the parameters of different nuclear waste form, including ceramics and borosilicate glasses, to name but a few.

In 2019 we investigated new processes and materials such as, for instance, reaction paths for radiolysis, radionuclide immobilization capability of cement phases (e.g. derivatives of AFM phases) and disordering tendencies in various functional materials applied in energy production and storage. Among others, the investigation involves calculations of the structural and thermodynamic parameters of incorporation of radionuclides into different solid phases, with focus on solid phases/aqueous solutions interphases, and on the characterization of the behavior of radioactive fission products in UO2 spent fuel matrix.

We have demonstrated that the experimental research can benefit from the molecular level simulations, which not only provide a unique insight into the investigated processes on the atomic-scale, but also help in the prediction of materials properties under conditions that are difficult to achieve in experiments. The performed up to date systematic simulations of various materials properties, together with the relevant experimental effort of our collaborators, have helped to set up models that provide improved description of properties of various materials. These models are used in characterization of nuclear waste forms, including assessment of their long-term stability. The long-term goal of the joint experimental and computational research aims at the development of new, advanced materials and techniques for energy materials, including these for safe nuclear waste management and disposal.

Selected honors, prizes, awards

- Ms. Mengli Sun received Best Poster Presentation Award at the Fall Meeting of the European Materials Research Society
- Dr. Gabriel Murphy received the Australia Institute of Nuclear Science and Engineering (AINSE) Gold Medal for research excellence as a result of the research outcomes of his PhD work that was highly supported by the JARA-HPC project

Selected conference participations

- Materials for disposal of radioactive waste learning from nature and computer simulations, Steinmann-Institut für Geologie, Mineralogie und Paläontologie, Rheinische Friedrich-Wilhems-Universität Bonn, Germany, June 19, 2019
- How challenging is it to compute actinides? atomistic modeling of nuclear materials relevant for nuclear waste management,
  Department of Physics, Universiteit Antwerpen, Belgium, July 04, 2019
- Properties of nuclear waste materials from atomistic simulations: what have we learned?
  EMRS Fall Meeting, Warsaw, Poland, September 16, 2019
- Nuclear waste materials from atomistic simulations,
  Institute of Nuclear Chemistry and Technology, Warsaw, Poland, September 18, 2019
- Modeling of Nuclear Waste Forms: State-of-the-Art and Perspectives,
  Scientific Basis for Nuclear Waste Management, MRS meeting,
  IAEA Headquoter, Vienna, Austria, October 24, 2019

Selected national and international cooperations

- Brendan Kennedy, Gabriel Murphy, Zhaoming Zhang, Eugenia Kuo, Greg Lumpkin, ANSTO/ University of Sydney, Australia
- Mengli Sun, Tieshan Wang, Lanzhou University, China
- Milan Psenicka, Charles University, Prague, Czech Republic
- Bart Verlinden, SCK CEN, Belgium
- Samuel Edwards, Robert Baker, Trinity College Dublin, Ireland

Selected publications

[1] LELET MI, BORODULINA ML, KOWALSKI PM, SULEIMANOV EV, GEIGER CA, ALEKSEEV EV.
Experimental and Computational Study of Thermodynamic Properties of Cs4[(UO2)4(WO5)(W2O8)O2] and Cs4[(UO2)7(WO5)3O3].
Journal of Chemical Thermodynamics. 2019;139:105873.

[2] BISWAS S, EDWARDS SJ, WANG Z, SI H, VINTRÓ LL, TWAMLEY B, KOWALSKI PM, BAKER RJ.
Americium incorporation into studtite: a theoretical and experimental study.
Dalton Trans. 2019;48:13057-13063.

[3] MURPHY G, WANG CHH, ZHANG Z, KOWALSKI PM, BERIDZE G, AVDEEV M, MURANSKY O, BRAND H, GU Q, KENNEDY B.
Controlling Oxygen Defect Formation and its Effect on Reversible Symmetry Lowering and Disorder-to-Order Phase Transformations in Non-Stoichiometric Ternary Uranium Oxides.
Inorganic Chemistry. 2019;58:6143-6154.

[4] JI Y, MARKS NA, BOSBACH D, KOWALSKI PM.
Elastic and thermal parameters of lanthanide-orthophosphate (LnPO4) ceramics from atomistic simulations.
Journal of European Ceramic Society. 2019;39:4264.

[5] DANIELS N, FRANZEN C, MURPHY GL, KVASHNINA K, PETROV V, TORAPAVA N, BUKAEMSKIY A, KOWALSKI PM, SI H, JI Y, HÖLZER A, WALTHER C.
exit. Applied Clay Science. 2019;176:1.

[6] WILDEN A, KOWALSKI PM, KLASS L, KRAUS B, KREFT F, MODOLO G, LI Y, ROTHE J, DARDENNE K, GEIST A, LEONCINI A, HUSKENS J, VERBOOM W.
Unique Difference and Unprecedented Inversion of Selectivity in the Complexation of Trivalent f-Elements by Different Diastereomers of a Modified Diglycolamide.
Chemistry-European Journal. 2019;25:5507.

[7] JI Y, KOWALSKI PM, KEGLER P, HUITTINEN N, MARKS N, VINOGRAD VL, ARINICHEVA Y, NEUMEIER S, BOSBACH D.
Rare-Earth orthophosphates from atomistic simulations.
Frontiers in Chemistry. 2019;7:197.

Natural Sciences

Ab-initio study of structure, conductivity and thermodynamics of doped and non-stoichiometric ceria

Project ID: jara0035

JULIUS KÖTTGEN
Institute of Physical Chemistry,
RWTH Aachen University

STEFFEN GRIESHAMMER
Helmholtz-Institut Münster,
Forschungszentrum Jülich, Germany

JOHN ARNOLD
Institute of Physical Chemistry,
RWTH Aachen University

Project Report

In this project, we studied the structure, the conductivity, and the thermodynamics of doped and non-stoichiometric ceria with ab-initio methods. In the recent application period, we focused on the influence of strain and localized electron (polaron) transport on the conductivity and the comparison with experimental results.

The migration of polarons in ceria was investigated with respect to the adiabaticity, the applicability of Marcus-Theory for polaron transport, and the impact of the lattice constant on the migration barriers. To achieve these goals, we applied DFT+U calculations and used the nudged elastic band (NEB) approach.

In Marcus-Theory, two parabolic potentials are used to describe the energy profile. If the theory applies to polaron hopping in ceria, the migration path should be described by these potentials. We find that the difference between the mean distance of cerium and oxygen in the nearest-neighbor position at the initial and final polaron position is a suitable migration coordinate. Energies were obtained from NEB calculations and the corresponding Density of States (DOS). Our results show that the Marcus-Model can be used as a good description of our results. We determined the adiabatic migration barrier to be 0.25 eV and the electronic coupling constant to be 0.033 eV. This means that the polaronic migration in the ceria system is between the strict adiabatic and diabatic case.

With a similar methodology, we analyzed the dependence of the activation energy and adiabaticity on the lattice constant. We find that with an increasing lattice constant the energy barrier rises. This is probably due to a longer cerium-cerium distance, which in terms of Marcus-Theory would mean a greater distance between the two potential curves. However, in comparison with the oxygen migration, determined in previous calculations, the effect is small. With a lattice change of 0.1Å the migration energy changes by about 30 meV. Interestingly, compressive and tensile strain have a contrary effect on the migration of polarons and oxygen ions. At the same time, the adiabaticity is nearly unaffected by a changing lattice constant.

In the second sub-project, we investigated the influence of biaxial strain on the migration energies and the ionic conductivity of pure and doped ceria. Application of biaxial strain in the a/b-plane leads to two different modes of interaction and migration, one in-plane and one out-of-plane. The migration barriers across the migration edge and defect interactions were calculated for three types of dopants with different radii (Lu, Gd, La) and three strain states ($\varepsilon = \frac{a-a_0}{a_0}$ = -1%,0%,+1%).

The interaction between dopant ion and oxygen vacancy becomes stronger for compressive strain and weaker for tensile strain in nearest-neighbor (1NN) position, whereas the interaction in second nearest-neighbor (2NN) position is barely influenced. During the migration to an adjacent vacancy, the oxygen ion has to pass through an edge formed by two cations. For each dopant, there are three possible edge configurations (Ce-Ce, RE-Ce, RE-RE). The edge barriers were calculated in-plane and out-of-plane for the different edge configurations and for the different strain states. The results can be described by a critical radius model $r_{crit} = \frac{d_{AB}-(r_A+r_B)}{2}$, where d_{AB} is the distance between the edge cations and r_A, r_B are their ionic radii. In general, tensile strain and smaller dopant ions lead to a decrease of the migration barrier.

Based on the calculated energies, Kinetic Monte Carlo simulations were performed to predict the influence of strain on the ionic conductivity for different dopants and temperatures. From the results, the following conclusions can be drawn: Lu-doped ceria shows a considerably lower conductivity than Gd-doped and La-doped ceria. The ionic conductivity increases for tensile strain and decreases for compressive strain. Out-of-plane conductivity is more susceptible to the strain effect than in-plane conductivity.

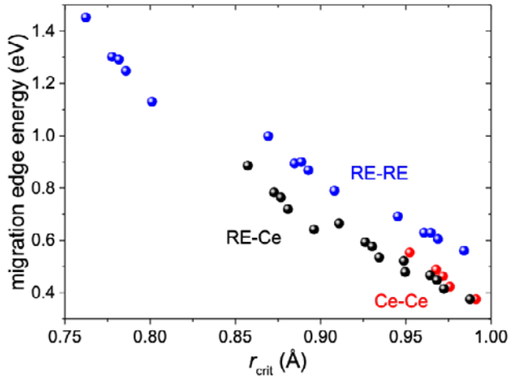

Figure 1: The migration barrier for different strain and dopant depending on the critical radius

Finally, we investigated impurities in experimental samples. It is well known that pure ceria samples in experiments always contain small impurity amounts. Though often in literature no defect interactions for small dopant concentrations are expected, experiments show a significant influence of the impurity level. Thus, impurities and their interaction with mobile oxygen vacancies can affect the ionic conductivity and can hamper the correct analysis of experimental data. We found a significant influence of Zr impurities on the ionic conductivities in Sm- and Gd-doped ceria. Zr is well known to be mixed with ceria and is therefore a typical impurity in this material. In addition, Zr can diffuse into doped ceria in ceria/zirconia heterostructures as applied in solid oxide fuel cells. Even for impurities of a few percent, a drastic drop in conductivity can be found. This is in agreement with experimental findings based on impedance spectroscopy.

Selected conference participations

- STEFFEN GRIESHAMMER
  Structure-conductivity relation in oxygen ion conductors: Doped ceria and La-melilites,
  Non-stoichiometric compounds VII, Miyazaki, Japan, March 10-14, 2019

Selected publications

[1] ARJMANDI HR, GRIESHAMMER S.
Defect formation and migration in Nasicon Li1+xAlxTi2-x(PO4)3.
Phys. Chem. Chem. Phys. 2019;21:24232.

[2] KOETTGEN J, MARTIN M.
Coordination Numbers in Sm-Doped Ceria Using X-ray Absorption Spectroscopy.
The Journal of Physical Chemistry C. 2019;123:6333-6339.

[3] KOETTGEN J, MARTIN M.
The Effect of Jump Attempt Frequencies on the Ionic Conductivity of Doped Ceria.
The Journal of Physical Chemistry C. 2019;123:19437-19446.

Natural Sciences

Proton and oxygen ion conductivity of doped $BaZrO_3$: A DFT and Kinetic Monte Carlo study

Project ID: jara0141

MANFRED MARTIN
Institute of Physical Chemistry,
RWTH Aachen University

FABIAN DRABER
Institute of Physical Chemistry,
RWTH Aachen University

Project Report

Main challenges of today's economy are related to energy problems: The usage of renewable energies, the energy storage in batteries, e.g. in electric cars, or the enhancement of solid oxide fuel cells require high-tech materials for high performance devices. Therefore, a major task for the scientific society is the investigation of these materials.

Proton conducting materials for application in solid oxide fuel cells are of special interest in this field. Barium zirconate doped with acceptors is a favorable proton conducting oxide for many applications, e.g. fuel cells, electrolysers, or methane conversion cells [1-3]. Although there are many theoretical and experimental investigations, there is only limited understanding how to connect the complex microscopic proton motion and the macroscopic proton conductivity for the full range of acceptor levels, ranging from diluted acceptors to concentrated solid solutions. Using a combination of density functional theory (DFT) calculations and kinetic Monte Carlo (KMC) simulations we accomplished this connection. At low dopant concentrations, acceptors trap protons, resulting in a decrease of the average proton mobility. With increasing concentration acceptors form, however, nanoscale percolation pathways with low proton migration energies, leading to a strong increase of the proton mobility and conductivity (see Figure). A comparison of our simulated proton conductivities with experimental values for yttrium-doped barium zirconate yields excellent agreement. We then predict that ordered dopant structures would not only enhance the proton conductivities strongly but would also enable one- or two-dimensional proton conduction in barium zirconate. [4].

Using the above methods, we include also the investigation of different dopant ions, the interplay between protons and oxygen vacancies as mobile species and the influence of the dopant distribution in the material with special interest in dopant superstructures. We are able to comprehend the experimental procedure and gain deeper insight into occurring phenomena like trapping zones, nanoscale percolation pathways and increased proton mobility and conductivity.

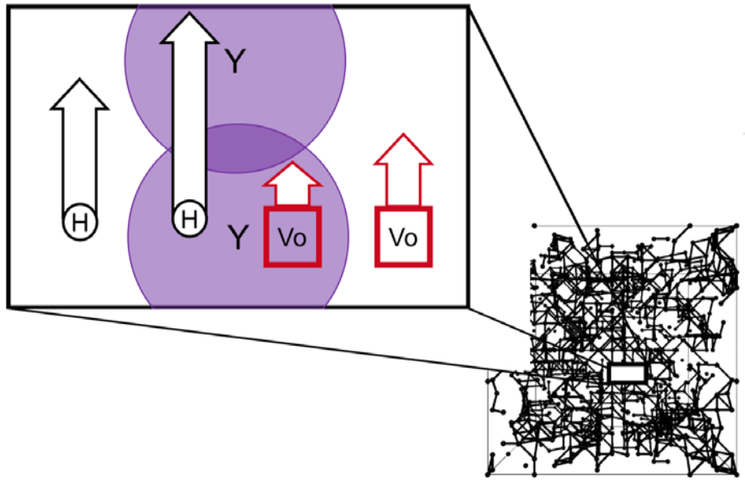

Figure 1: Zoom into a 16x16x16 simulation cell with a dopant fraction of x = 0.25.
Right: Every black dot represents an yttrium dopant and two connected dots stand for overlapping trapping zones.
Left: Schematic display of two overlapping yttrium trapping zones building one (part of) a percolation pathway. The arrows represent mobilities. The proton mobility is higher inside of the pathway than outside. For oxygen vacancies the opposite is the case.

References

[1] BI L, BOULFRAD S, TRAVERSA E. Chemical Society reviews. 2014;43:8255–8270.
[2] BAE K ET AL. Nature communications. 2017;8:14553.
[3] MALERØD-FJELD H ET AL. Nature Energy. 2017;2:923–931.
[4] DRABER FM, ADER C, ARNOLD JP, EISELE S, GRIESHAMMER S, YAMAGUCHI S, MARTIN M. Nature Materials. 2020;19:338-346. Published online: 23.12.2019.

Selected conference participations

- DRABER FM, SOMMERFELD IK, EISELE S, ARNOLD JP, MARTIN M.
  Kinetic Monte Carlo simulations on proton and oxygen conductivity in doped BaZrO3
  Presentation at the 118th General Assembly of the German Bunsen Society for Physical Chemistry, Jena, Germany, May 30-June 01, 2019
- MARTIN M.
  Plenary talk. Solid State Ionics: A brief history, unresolved problems, and plenty of room…. 22nd International Conference on Solid State Ionics, PyeongChang, Korea, June 16-21, 2019
- DRABER FM, MARTIN M.
  Predicting the perfect dopant superstructure for maximum ionic conductivity in acceptor doped BaZrO3. Poster at 22nd International Conference on Solid State Ionics (SSI-22), PyeongChang , South Korea, June 16-21, 2019
- DRABER FM, MARTIN M.
  KMC Simulations on Proton and Oxygen Vacancy Conductivity in Doped BaZrO3.
  Presentation at the Konferenz über aktuelle Fragestellungen der physikalischen Festkörperchemie, Kall, Germany, August 05-09, 2019
- DRABER FM, MARTI M.
  Ionic conductivity in acceptor-doped BaZrO3. Presentation at the 11th Petite Workshop, Sommaroy, Norway, October 19-22, 2019

Selected national and international cooperations

- SHU YAMAGUCHI
  National Institute for Accreditation of Degrees and Quality Enhancement of Higher Education (NIAD-QE), Tokyo, Japan
- STEFFEN GRIESHAMMER
  Helmholtz-Institut Münster (IEK-12) and Forschungszentrum Jülich GmbH, Münster, Germany

Selected publications

- DRABER FM, ADER C, ARNOLD JP, EISELE S, GRIESHAMMER S, YAMAGUCHI S, MARTIN M.
  Nanoscale percolation in doped BaZrO3 for high proton mobility.
  Nature Materials. 2020;19:338–346. Published online: December 23, 2019.

Natural Sciences

Ab-initio study of composition, structure and conductivity in interstitial oxygen conductors

Project ID: jara0156

STEFFEN NEITZEL-GRIESHAMMER
Forschungszentrum Jülich, Germany

TIM SCHULTZE
Forschungszentrum Jülich, Germany

MANFRED MARTIN
Institute of Physical Chemistry
RWTH Aachen University

Project Report

Two types of oxygen interstitial conducting oxides, namely apatites of composition $La_{10-x}B_xSi_6O_{26\pm\delta}$ and melilites of composition $La_{1+x}Sr_{1-x}Ga_3O7_{+x/2}$, were investigated by means of density functional theory. These materials are promising as ion conductors for electrolytes in solid oxide fuel cells or oxide batteries.

Melilites are composed of alternating layers of La/Sr cations and anionic GaO4 tetrahedrons that are interconnected to form pentagonal rings. The variation of the La/Sr ratio leads to the introduction of oxygen defects into the structure. An increase of the Sr content results in formation of oxygen vacancies whereas additional La results in formation of oxygen interstitials. The vacancies are part of the gallium tetrahedral network. The calculations show that due to the strong Ga-O bonding, the migration barriers for the vacancy mechanism are high with values around 0.7 eV. In contrast, the calculated barriers for the migration of oxygen interstitials between adjacent rings are between 0.15 and 0.35 eV. The calculations furthermore show that interstitial migration follows an interstitialcy mechanism.

However, the individual migration barrier for each jump and consequently the ionic conductivity also depends on the local environment of the respective defect. Therefore, supercells of compositions $La_{1.5}Sr_{0.5}Ga_3O_{7.25}$, $La_{1.25}Sr_{0.75}Ga_3O_{7.25}$ and $La_{1.125}Sr_{0.875}Ga_3O_{7.25}$ were calculated with different arrangements of cations and interstitial defects.

The energy for different distributions of cations and oxygen interstitials varies in a range of about 0.5 eV. The energetically favorable configurations feature a maximal distance between Sr-ion and oxygen interstitial due to electrostatic interactions. The calculated energies were applied to create an energy model that describes the local energy of each interstitial position depending on the number of neighboring Sr-ions up to 5 Å and oxygen interstitials up to 7 Å.

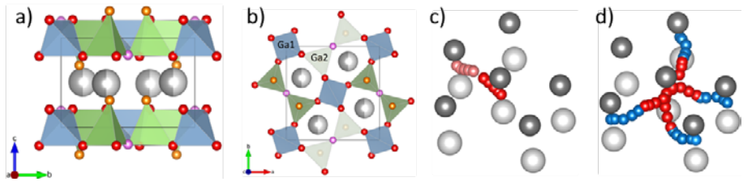

Figure 1: Side (a) and top (b) view of the melilite structure. Migration paths of the interstitialcy mechanismen with energy barrieres of 0.15 eV (c) and 0.35 eV (d).

Lanthanum apatites crystallize in a hexagonal structure ($P6_3/m$). Cations form a hexagonal tunnel with oxygen ions where additional oxygen interstitials can be accommodated and migration along the c-axis is possible.

We considered three compositions as basic materials for investigations, specifically $La_{9.33}Si_6O_{26}$, $La_8B_2Si_6O_{26}$ (B = Mg, Ca, Sr, Ba) and $La_{10}Si_6O_{27}$. Energies of anti-Frenkel and Schottky disorder were calculated for $La_{9.33}Si_6O_{26}$ and $La_8B_2Si_6O_{26}$ showing that oxygen interstitial and vacancy formation by intrinsic disorder is unlikely.

Calculations for the supercell of $La_{9.33}Si_6O_{26}$ show that there are three different nonequivalent distances between oxide ions along the c-axis which we regard as individual sections, respectively. Within each section there are two layers that contain stable interstitial positions. Every layer itself has again three equivalent sites within the a/b-plane. Our calculations of the migration path show that the oxide interstitials move via these sites while migrating by an interstitialcy mechanism. The migration path through the whole cell consists of three sections with two layers each. The migration barrier for $La_{9.33}Si_6O_{26}$ has a total height of 0.3 eV.

For $La_8B_2Si_6O_{26}$ compositions with different alkaline earth metals as B-atoms were calculated. Analogous to the cation deficient apatite, two non-equivalent sections with two layers each were found in $La_8B_2Si_6O_{26}$ that participate in an interstitialcy migration mechanism. Consequently, there are only four different configurations that need to be considered for the migration through the whole cell. The migration is analogous to the migration in $La_{9.33}Si_6O_{26}$. The total height of the migration barrier along the c-axis depends on the dopant and is between 0.1 eV for Sr and 0.2 eV for Ba.

The interstitialcy migration in the a/b-plane has been analyzed for $La_8Sr_2Si_6O_{26}$. The migration along the ab-plane consists of three steps. The first step is for the interstitial to leave channel and to migrate to an adjacent SiO_4 tetrahedron, forming a SiO_5 polyhedron. The second step is the jump of one oxide ion to an adjacent SiO_4 polyhedron. The third step is the re-entry of the oxygen ion into the La tunnel onto an interstitial site. The energy barrier of this migration path is approx. 0.5 eV depending on the surrounding cation distribution.

In the third basic composition $La_{10}Si_6O_{27}$ the lanthanum excess is compensated by interstitial oxygen ions. As a consequence, this composition contains one intrinsic oxygen interstitial per unit cell. Our calculations suggest two positions for this oxygen interstitial, one in the lanthanum tunnel and one outside of the tunnel forming a SiO_5 polyhedron. Placing two interstitials at SiO_5 polyhedrons the remaining interstitial can migrate analogous to the compositions described above with a total migration barrier of 0.62 eV.

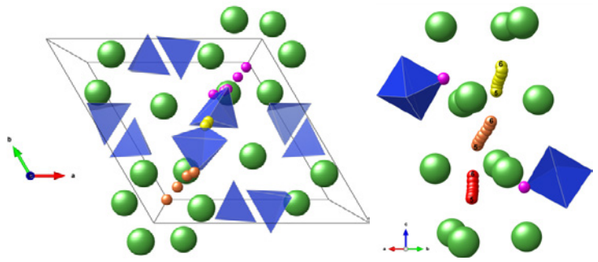

Figure 2: Visualization of the a/b-plane of the apatite structure and the migration between two channels (Left). Migration in the channel of $La_{10}Si_6O_{27}$ with two interstitial ions at SiO_5 polyhedra (Right).

Selected conference participations

- STEFFEN GRIESHAMMER
  Structure-conductivity relation in oxygen ion conductors: Doped ceria and La-melilites, Non-stoichiometric compounds VII, Miyazaki, Japan, March 10-14, 2019

Selected publications

- SCHULTZE T, ARNOLD JP, GRIESHAMMER S.
  Ab Initio Investigation of Migration Mechanisms in La Apatites.
  Appl. Energ. Mater. 2019;2:4708-4717. 10.1021/acsaem.9b00226

Natural Sciences

Kinetic Monte Carlo Simulation of Polaron and Oxygen Ion Transport in Solids

Project ID: rwth0329

JOHN ARNOLD
Institute of Physical Chemistry,
RWTH Aachen University

MANFRED MARTIN
Institute of Physical Chemistry,
RWTH Aachen University

Project Report

Reduced ceria ($CeO_{2-\delta}$) has been the subject of many studies due to its promising applications within environmental and energy technologies. [1] This can be explained by its high ionic (i) and electronic (e) conductivities at medium temperatures. By removing oxygen from the structure via reduction, oxygen vacancies as well as polarons are created, which leads to the aforementioned conductive behaviour. Understanding the migration behavior on an atomic level is crucial to the adjustment of material properties. For this reason, we conducted Kinetic Monte Carlo (KMC) simulations with interaction and migration energies that were obtained by density functional theory calculations. [2] Within our simulations oxygen vacancies as well as polarons are able to move. By applying an external electrical field to the simulation cell and measuring the displacement of the defects, it is possible to calculate the ionic and electronic conductivities. Our finding that the electronic conductivity is two orders of magnitute larger than the ionic conductivity is in good agreement with experiments. [3] In addition, the total conductivity of around 1 S/cm from our simulations also matches experimental results (see Figure). [4-7]

One study found that the migrations of oxygen ions and polarons are not independent. The effective charge of the oxygen vacancy is therefore not equal to its ideal value but expressed by 2-αi. [3] αi is called the transport charge. We were interested whether our model could reproduce this effect. In order to calculate α_i it is neccecary to determin the Onsager transport coefficients L_{kk} (k = i, e) and $L_{ie} = L_{ei}$. These describe the defect fluxes due to their own electrochemical potential gradient and due to that of their corresponding counter defect, respectively. The oxygen vacancy transport charge is equal to L_{ie}/L_{ii}.

For these simulations we applied an external potential gradient which only affected either the polarons ∇Ee or the vacancies ∇E_i. The Onsager coefficients are then accessable from the following expressions: [3]

$$L_{ii} = (\Delta x_i/(Vt\ \nabla E_i))_{\nabla E_e=0} \qquad L_{ie} = (\Delta x_i/(Vt\ \nabla E_e))_{\nabla E_i=0}$$

$$L_{ei} = (\Delta x_e/(Vt\ \nabla E_i))_{\nabla E_e=0} \qquad L_{ee} = (\Delta x_e/(Vt\ \nabla E_e))_{\nabla E_i=0}$$

Here Δx_k (k = i,e) is the ensemble defect displacement in the direction of the potential gratient, V is the volume of the simulation cell, and t is the time. Even though only one defect species is pulled by the gradient, both exhibit a shift in the gradients direction. This can be explained by the drag acting from the pulled species upon the unaffected one.

We found that at 1273 K α_i takes a value between 0.15 and 0.23 depending on the degree of ceria reduction. This value differs from the experimental value of 0.4 to 1.3. We expect that with better parameters for the KMC simulation, we will obtain better agreement with experiments. In the present model, vacancies and polarons always jump as individual particles. We are currently working on migration mechanisms in which concerted jumps take place. Still, we are able to qualitativley reproduce the experimental findings with simple pair interactions and migration energies. We also find, that α_i increases with decreasing temperature, suggesting that defect pairs are more easily separated at higher temperatures. For the effective charge of the polaron, we found a value that is close to its ideal value of -1. This is in good agreement with experiments. [3]

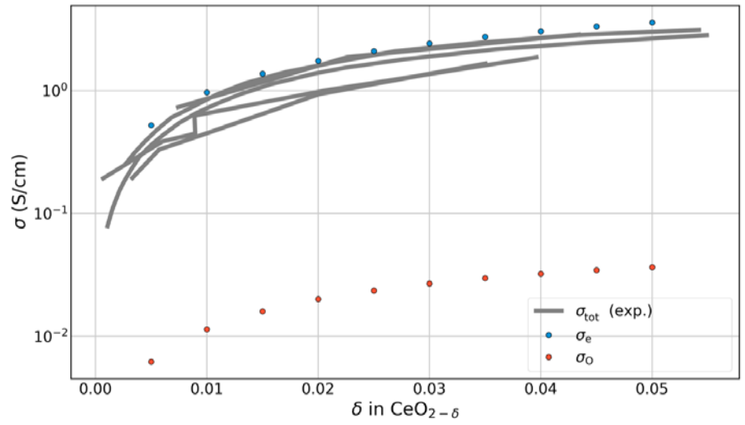

Figure 1: Simulated electronic (blue) and ionic (red) conductivities and experimental total conductivity (grey) in dependence of the non-stoichiometry δ of ceria at 1273 K. Experimental values are taken from [3-7].

References

[1] KHARTON VV ET AL. J. MATER. Sci. 2001;36:1105 - 1117.
[2] GRIESHAMMER S, NAKAYAMA M, MARTIN M. Phys. Chem. Chem. Phys. 2016;18:3804–3811.
[3] PARK WS, YANG I, YOO HI. ECS Trans. 2008;26:327–336.
[4] BLUMENTHAL RN, LEE PW, PANLENER RJ. J. Electrochem. Soc. 1971;118:123–129.
[5] NAIK IK, TIEN TY. J. Phys. Chem. Solids. 1978;39:331–315.
[6] TULLER HL, NOWICK AS. J. Phys. Chem. Solids. 1977;38:859–867.
[7] BLUMENTHAL RN, SHARMA RK. J. Solid State Chem. 1975;13:360–364.

Selected honors, prizes, awards

- JOHN ARNOLD
  Best Poster Award,
  22nd International Conference on Solid State Ionics, PyeongChang, Korea

Selected conference participations

- MANFRED MARTIN
  Plenary talk, Solid State Ionics: A brief history,
  unresolved problems, and plenty of room …,
  22nd International Conference on Solid State Ionics,
  PyeongChang, Korea, June 16-21, 2019
- JOHN ARNOLD
  KMC Simulations of the Onsager Transport Coefficients of reduced Ceria,
  22nd International Conference on Solid State Ionics,
  PyeongChang, Korea, June 16-21, 2019

Five selected national and international cooperations

- P.C SCHMIDT, TU Darmstadt, Germany
- MASANOBU NAKAYAMA, Nagoya Institute of Technology, Japan

Natural Sciences

Physical and Theoretical Chemistry | DFG 303

Full Wave Function Optimization of Transition Metal Compounds using Quantum Monte Carlo Methods

Project ID: jara0194

ARNE LÜCHOW
Institute of Physical Chemistry,
RWTH Aachen University

JIL LUDOVICY
Institute of Physical Chemistry,
RWTH Aachen University

Project Report

The theoretical investigation of transition metal compounds is a highly interesting field of re-search, since the accurate description of those systems is of crucial importance when it comes to elucidating catalytic processes. The large non-dynamic correlation of transition metal com-pounds still poses a great challenge for high-level theoretical methods. While DFT is often inaccurate, traditional wave function methods can yield accurate results. They however usually suffer from an unfavorable scaling with respect to the number of electrons and the number of CPUs and their accuracy strongly depends on the zeroth order wave function. The quantum Monte Carlo (QMC) approach offers an elegant way to tackle these problems due to its highly parallel regime.

The variational (VMC) and diffusion (DMC) Monte Carlo methods are the most commonly used stochastic approaches when an accuracy beyond mean field theory is required. Wave function-based approaches, such as multi-reference CI (MRCI) and multi-reference perturbation theory (CASPT2) account for the non-dynamic correlation through an expansion in determinants. This technique is adopted in QMC, meaning that a linear combination of Slater determinants is employed together with a Jastrow correlation function in order to determine the properties of transition metal compounds.

All calculations were performed using effective core potentials (ECPs) in order to reduce the computational extent of the calculations and to include scalar relativistic effects. ECPs are well suited for these kind of calculations, since they do not treat the core electrons explicitly. The removal of the core electrons is judged to have a negligible impact on the dissociation energy, since the latter is a property that is mainly described through the valence electrons.

In this project, we computed the dissociation energies of CoH and NiSi. For both systems, we computed the potential energy curve at multi-reference DMC (MR-DMC) level with fully optimized wave functions for a given time step. The calculations were repeated for the equilibrium bond distance and the MR-DMC energies were extrapolated to a zero time step. For CoH, our dissociation energy is in good agreement with the coupled cluster (CC) results from Truhlar and coworkers [1].

For NiSi, our spin-orbit corrected MR-DMC dissociation energy - without core-valence (CV) correlation contribution - corresponds to 2.91(2) eV. We determined the CV correlation contribution which adds up to 1.88 eV by means of multi-reference perturbation theory (MR-MP2). By adding this quantity to our dissociation energy, the latter increases to 4.80(2), which substantially overestimates the experimental dissociation energy of 3.324(3) eV from Morse and coworkers [2]. We judge the use of an ECP for Si to be mainly responsible for this large discrepancy. By using an ECP for Si, only four electrons are treated explicitly, namely the 3s and 3p electrons. We assume that the 2nd period electrons have a large impact on the valence electrons, which would explain the large CV correlation contribution. In order to solve this problem, we are going to repeat the calculations for NiSi in a future project with the correlation consistent ECPs of Mitas and coworkers [3], for which an explicit treatment of the CV correlation contribution will not be necessary.

In addition, we performed wave function optimizations for NiB. We only used an ECP for the Ni species, the boron atom was described by an all-electron basis. The substantial amount of parameters that needed to be optimized with VMC proved rather challenging. The configuration interaction (CI) coefficients corresponded by far to the largest number of parameters for the optimization, being one to two orders of magnitude larger than the other sets of parameters. In order to reduce the number of CSFs and thus the number of CI coefficients that need to be optimized, we performed preliminary calculations using a selected CI approach, based on the linear optimization method from Toulouse et al. [4] The second-order perturbation theory criterion that determines whether a CSF is added to the initial wave function is the same as the one used in the CIPSI algorithm, developed by Malrieu and coworkers [5]. The goal is to obtain more compact wave functions without forfeiting the accuracy. The calculations were performed for C2. The criterion that is used to choose the CSFs exhibits rather large fluctuations. We are currently trying to resolve this issue by working with larger sample sizes and using correlated sampling.

Nonetheless, we have proven for various systems in previous work, that our method is able to yield accurate dissociation energies within chemical accuracy when fully optimized MR-DMC guide functions are used. We analyzed NiSi and NiB in this project, which proved rather challenging due to large amount of parameters, that needed to be optimized. We are however confident that by generating more compact wave functions through a selected CI approach, we will be able to achieve a substantial improvement of our results and tackle the optimization of larger systems.

References

[1] XU X, ZHANG W, TANG M, TRUHLAR DG.
Do practical stan-dard coupled cluster calculations agree better than Kohn-Sham calculations with currently available functionals when compared to the best available experimental data for dissocia-tion energies of bonds to 3d transition metals?, J. Chem. Theory Comput., 11, 2036–2052, 2015.

[2] SEVY A, TIEU E, MORSE MD.
Bond dissociation energies of FeSi, RuSi, OsSi, CoSi, RhSi, IrSi, NiSi, and PtSi, J. Chem. Phys., 149, 174307, 2018.

[3] Bennett MC, Wang G, Annaberdiyev A, Melton CA, Shulenburger L, Mitas L.
A new generation of effective core potentials from corre-lated calculations: 2nd row elements, J. Chem. Phys., 149, 104108, 2018.

[4] TOULOUSE J, UMRIGAR CJ.
Optimization of quantum Monte Carlo wave functions by energy minimization, J. Chem. Phys., 126, 084102, 2007.

[5] EVANGELISTI S, DAUDEY JP, MALRIEU JP.
Convergence of an im-proved CIPSI algorithm, Chem. Phys., 75, 91–102, 1983.

Selected conference participations

- JIL LUDOVICY
  Full Wave Function Optimization of Transition Metal Compounds using Quantum Monte Carlo
  10th Triennial Congress of the International Society for Theoretical Chemical Physics, Tromso, Norway, July 11-17, 2019

Natural Sciences

Condensed Matter Physics | DFG 307

Magnetic Skyrmions from first-principles

Project ID: jara0161
STEFAN BLÜGEL
ULIANA ALEKSEEVA
SERGII GRYTSIUK
HONGYING JIA
VIKAS KASHID
BERND ZIMMERMANN
Peter Grünberg Institute (PGI-1)
and Institute for Advanced
Simulation (IAS-1),
Forschungszentrum Jülich, Germany

Project Report

Topological-chiral magnetic interactions driven by emergent orbital magnetism

Two hundred years ago, Ampère discovered that electric loops in which currents of electrons are generated by a penetrating magnetic field can mutually interact. Here we show that Ampère's observation can be transferred to the quantum realm of interactions between triangular plaquettes of spins on a lattice, where the electrical currents at the atomic scale are associated with the orbital motion of electrons in response to the non-coplanarity of neighbouring spins playing the role of a magnetic field.

The resulting topological orbital moment underlies the relation of the orbital dynamics with the topology of the spin structure. We demonstrate that the interactions of the topological orbital moments with each other and with the spins form a new class of magnetic interactions –– topological–chiral interactions –– which can dominate over the Dzyaloshinskii–Moriya interaction, thus opening a path for realizing new classes of chiral magnetic materials with three-dimensional magnetization textures such as hopfions.

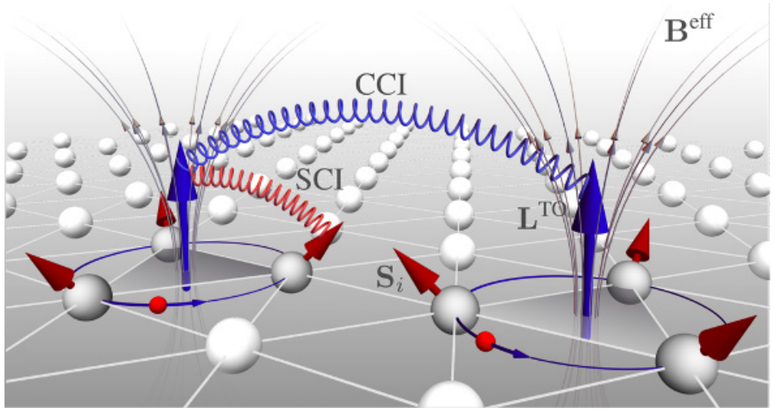

Figure 1: Formation of topological orbital moments L^TO(large blue arrows) as a result of circular currents (thin blue arrows) flowing through groups of three atoms in a crystal lattice with a specific spin structure S_i(red arrows). The magnetic fields B^eff (black arrows) induced by such orbital currents, mediate interactions of the TOMs with each other (blue strings, CCI) and with the magnetic moments of neighbouring atoms (red strings, SCI).

Opening several exciting vistas in the field of chiral magnetism, our findings raise a number of important fundamental questions. Above all, they call for a review of the relevance of the chiral-chiral and spin-chiral coupling, uncovered in this study, for the ground state of existing materials that exhibit diverse magnetic orders. This also concerns the systems in which emerging homochiral magnetic structures were previously thought to be the result of the Dzyaloshinskii–Moriya interaction (DMI). In contrast, topological–chiral interactions offer fundamentally different opportunities for imprinting chiral magnetism, as they manifest in the scalar chirality of spin arrangements on triangular plaquettes, as opposed to the vector chirality between pairs of spins in the case of DMI.

In the continuum limit, the spin-chirality relates to the curvature of the magnetization field and the chiral-chiral interaction reverts to the Faddeev model. Thus, magnets with topological-chiral magnetic interactions offer the first experimental realization of this model with hopfions as the emergent 3D magnetic particles. It could be speculated that the unique 3D magnetic order of MnGe explained in this article by the occurrence of the topological–chiral interaction is a precursor state. Another important aspect to be explored is the influence of the discovered interactions on the dynamical properties of ferromagnetic, chiral, and antiferromagnetic systems. As we show in Supplementary Note 7, the corresponding modifications to the phenomenological model for the free energy of antiferromagnets, brought about by topological–chiral interactions, enable a direct interpretation of magnetic phase transitions at high pressure and finite temperature. This provides a foundation for studying antiferromagnetic dynamics in materials that exhibit the proposed chiral-chiral and spin-chiral interactions.

Figure 2: Representation of the magnetic structures of a doughnut-shaped hopfion, together with a

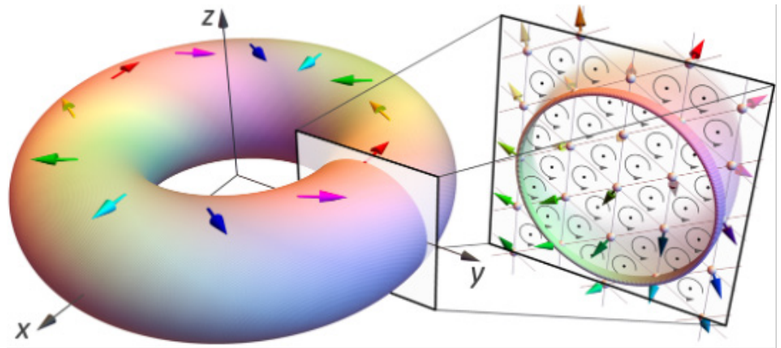

hopfion cross section. Coloured arrows represent the in-plane orientations of the magnetic moments. The cross-section shows the circular currents (grey arrows) formed by the spin arrangement within each triplet giving rise to TOM and associated non-zero CCI.

Selected conference participations

- BLÜGEL S. Topological Magnetization Solitons: From Fundamentals to Technology. Joint Annual Meeting of SPS and ÖPG 2019. Zürich, Switzerland, August 26-30, 2019
- BLÜGEL S. Magnetization textures beyond skyrmions: Bobbers, Quanco balls and Hopfions. Annual Conference on Magnetism and Magnetic Materials. Las Vegas, USA, November 04-08, 2019
- BLÜGEL S. Topological-Chiral Interactions for 3D Textures. CEMS Symposium on Emergent Quantum Materials. Tokyo, Japan, May 22-24, 2019

Selected national and international cooperations

- Olena Gomonay, Institute of Physics, Johannes Gutenberg University Mainz, Germany

Selected publications

- GRYTSIUK S, HOFFMANN M, HANKE JP, MAVROPOULOS P, MOKROUSOV Y, BIHLMAYER G, BLÜGEL S.
  Ab initio analysis of magnetic properties of the prototype B20 chiral magnet FeGe.
  Phys. Rev. B. 2019;100:214406.

- ZIMMERMANN B, BIHLMAYER G, BÖTTCHER M, BOUHASSOUNE M, LOUNIS S, SINOVA J, HEINZE S, BLÜGEL S, DUPÉ B.
  Comparison of first-principles methods to extract magnetic parameters in ultrathin films: Co/Pt(111). Phys. Rev. B. 2019;99:214426.

Natural Sciences

Systematic investigation of magnetic thin films and multi-layers - towards sub-10nm skyrmions for future data storage devices

Project ID: jara0197
STEFAN BLÜGEL
BERND ZIMMERMANN
MARKUS HOFFMANN
HONGYING JIA
VASILY TSEPLYAEV
Peter Grünberg Institute (PGI-1)
and Institute for Advanced
Simulation (IAS-1),
Forschungszentrum Jülich, Germany

Project Report

Comparison of first-principles methods to extract magnetic parameters in ultrathin films: Co/Pt(111)

We compare three distinct computational approaches based on first-principles calculations within density functional theory to explore the magnetic exchange and the Dzyaloshinskii-Moriya interactions (DMI) of a Co monolayer on Pt(111), namely, (i) the method of infinitesimal rotations of magnetic moments based on the Korringa-Kohn-Rostoker (KKR) Green function method, (ii) the generalized Bloch theorem applied to spiraling magnetic structures and (iii) supercell calculations with noncollinear magnetic moments, the latter two being based on the full-potential linearized augmented plane wave (FLAPW) method. In particular, we show that the magnetic interaction parameters entering micromagnetic models describing the long-wavelength deviations from the ferromagnetic state might be different from those calculated for fast rotating magnetic structures, as they are obtained by using (necessarily rather small) supercell or large spin-spiral wave vectors. In the micromagnetic limit, which we motivate to use by an analysis of the Fourier components of the domain-wall profile, we obtain consistent results for the spin stiffness and DMI spiralization using methods (i) and (ii). The calculated spin stiffness and Curie temperature determined by subsequent Monte Carlo simulations are considerably higher than estimated from the bulk properties of Co, a consequence of a significantly increased nearest-neighbor exchange interaction in the Co monolayer (+50%). The calculated results are carefully compared with the literature.

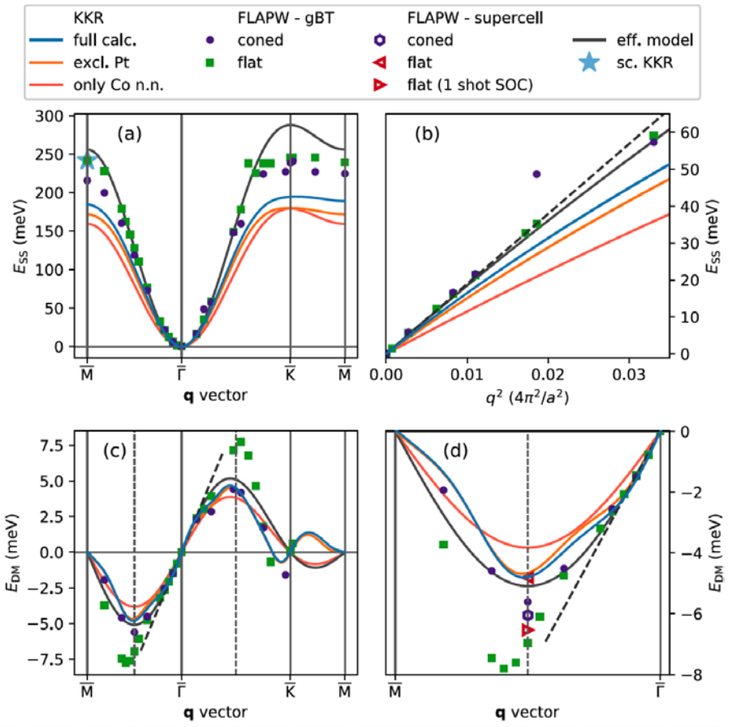

Figure 1: Energy dispersion of spin spirals for a monolayer Co(fcc) on Pt(111).
(a) Nonrelativistic dispersion curves E_{SS} (**q**) along the high-symmetry path of the first Brillouin zone.
(b) Zoom into the parabolic region of (a) around the $\bar{\Gamma}$ point to obtain the spin stiffness.
(c) Spin-orbit induced antisymmetric corrections E_{DM} (**q**) to the energies along the high-symmetry path and
(d) zoom onto the ($\bar{\Gamma}\bar{M}$) direction. Full lines represent KKR-derived spin-spiral energies including all relevant interactions constants J_{ij} (full calc.), exclude interactions between Co and Pt (excl. Pt) or consider only the nearest-neighbor Co interactions (only Co n.n.).
Dashed lines indicate the slopes in the limit q→0 and represent the (b) spin stiffness and [(c) and (d)] DMI spiralization. gBT = generalized Bloch theorem.

We have determined the magnetic interaction parameters for a Co monolayer on Pt(111) by three distinct approaches, (i) performing infinitesimal rotations, (ii) using spin spirals employing the generalized Bloch theorem for various q vec- tors, (iii) and constraining spin spirals into a rather small su- percell. We obtain consistent results for the spin stiffness and the Dzyaloshinskii-Moriya interaction in the long-wavelength (micromagnetic) limit around the ferromagnetic state using methods (i) and (ii). When going to higher spin-spiral q vec- tors, deviations through differences in the electronic structure play a role for flat spin spirals. In order to still realize the long- wavelength limit in the supercell approach, we propose to use a coned spiraling structure with a small cone angle, which leaves, e.g., the magnetic moments unchanged as a function of the spin-spiral q vector (being inversely proportional to the supercell size). We found that the micromagnetic DMI spiralization might not be accurately inferred by extrapolating from one data point obtained for a large q vector (i.e., small supercell).

Selected conference participations

- BLÜGEL S.
  Chiral Magnetic Skyrmions For Information Technology.
  CEMS Symposium on Emergent Quantum Materials. Tokyo, Japan, May 22-24, 2019
- BLÜGEL S.
  Ab-initio inspired design of magnetic multilayers for skyrmionics.
  10th International Symposium on Metallic Multilayers (MML 2019).
  Madrid, Spain, June 17-21, 2019

Five seleceted national and international cooperations

- Olivier Boulle, CNRS, Spintec, Grenoble, France
- Gong Chen, University of California, Davis, USA
- Vincent Cros, CNRS, Thales, Univ. Paris-Sud, France
- Bertrand Dupé, Johannes Gutenberg-Universität, Mainz, Germany

Selected publications

- ZIMMERMANN B ET AL.
  Comparison of first-principles methods to extract magnetic parameters in ultrathin films: Co/Pt(111). Phys. Rev. B. 2019;99:214426.

Natural Sciences

Properties of magnetic materials calculated using a high throughput framework for ab-initio Korringa-Kohn-Rostoker Green function method

Project ID: jara0182

ROMAN KOVÁČIK
Peter Grünberg Institute (PGI-1)
and Institute for Advanced
Simulation (IAS-1),
Forschungszentrum Jülich, Germany

Project Report

The project aims were: a) to analyze the predictive power of the local density (LDA) and generalized gradient (GGA) approximations in connection with the classical Heisenberg model to determine the critical temperature of the magnetic phase transition for a large set of about 200 Heusler alloys; b) to screen the experimentally known materials, in which the magnetic skyrmions, the technologically promising candidates for data storage solutions and other spintronics devices, could be stabilized. The computational approach is based on the combination of the ab-initio Korringa-Kohn-Rostoker Green function (KKR-GF) method and the Monte Carlo simulations. A high throughput workflow is implemented by using the AiiDA framework: www.aiida.net.

The results of the project a) are about to be submitted for a publication. To summarize, we calculated the self-consistent potential for about 300 experimentally known Heusler alloys containing 3d magnetic elements, in both, LDA and GGA. The convergence success rate using the automatic high-throughput workflow was 99% and 90% for LDA and GGA, respectively.

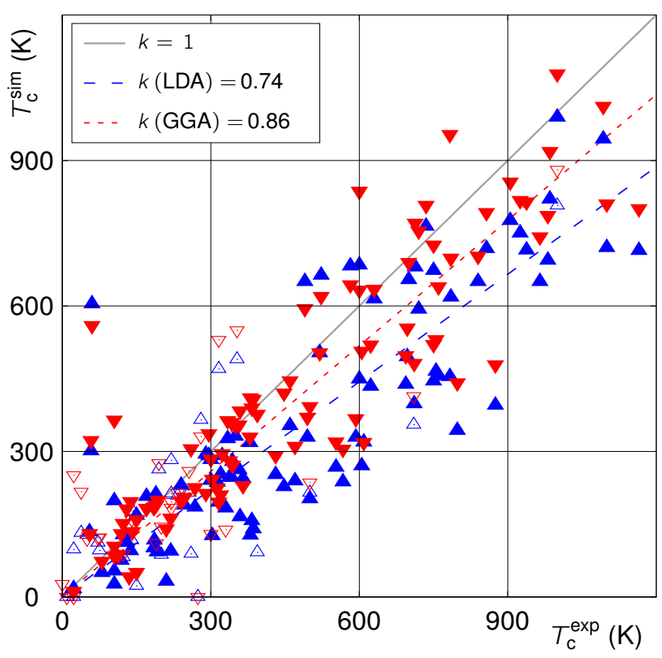

Figure 1: Correlation between the calculated and experimental critical temperature for the known magnetic Heusler alloys using LDA (blue) and GGA (red).

The systems which failed to converge were treated by using a different and computationally much more expensive solver with which we were able to converge all considered systems. About 200 alloys turned out to have a sizable magnetic moment. For these alloys, the exchange interaction parameters were evaluated with a large interaction cluster size corresponding to the radius cut-off 5.5 times the lattice constant which was necessary to achieve a good convergence of the critical temperature for many of the Heusler alloys but the majority of alloys required much smaller cut-off. An economical usage of computational time in the MC simulations was achieved by on-the-fly control of the number of simulation steps, proportional to the normalized fluctuation amplitude of the magnetization.

The project b) is currently in progress in the extension granting period 2020/05 – 2021/04. The project started with the detailed analysis of the crystal structures available in the Inorganic Crystal Structure Database (ICSD): icsd.products.fiz-karlsruhe.de. There are about 10000 existing inorganic compounds lacking inversion symmetry which contain magnetic elements. We target compounds which: (i) do not contain rare earth elements, (ii) contain at least 20% of magnetic atoms and (iii) are stoichiometric. In ICSD, we find 966 of such compounds. Further analysis of the ICSD shows that the majority of the compounds (656) contain up to 30 atoms in the unit cell. We do not consider, at least for now, compounds with very large unit cells having more than 80 atoms, which yields 901 compounds to be investigated.

Selected conference participations

- DR. ROMAN KOVÁČIK
  Critical temperature and effective magnetic moment of magnetic Heusler alloys from first principles.
  DPG spring meeting 2019.
  Regensburg, Germany, March 31 - April 05, 2019

Five selected national and international cooperations

- PROF. PHIVOS MAVROPOULOS, University Athens, Greece
- DR. MARJANA LEZAIC, Forschungszentrum Jülich, Germany
- DR. IVETTA SLIPUKHINA, Forschungszentrum Jülich, Germany

Natural Sciences

Ab initio study of the electronic and kinetic properties of clean and Scandium-alloyed Sb_2Te_3

Project ID: jara0183
MATTHIAS WUTTIG
PETER CHRISTIAN SCHMITZ
VALENTIN EVANG
IDER RONNEBERGER
Solid State Physics,
RWTH Aachen University

Project Report

Two main projects were carried out using the computational resources from JARA0183. Both projects deal with phase-change materials (PCMs), a technologically important family of materials employed in rewritable Blu-Ray discs and in non-volatile phase-change memories. These devices exploit the ability of PCMs to undergo fast and reversible transitions between a crystalline and an amorphous state at high temperatures. Since both phases are very stable at room temperature and exhibit strong optical and electronic contrast, they can be used to store bits of information. Phase-change memories are the most promising candidates for storage-class-memory devices. Such memories are very suitable for applications – such as data mining - that require fast access to huge amounts of data.

In subproject 1, we performed ab initio molecular dynamics (AIMD) simulations based on density functional theory (DFT) to investigate the structural changes that happen during the fast melt-quench process in two prototypical PCMs, namely Ag,In-doped Sb_2Te (AIST) and Ge15Sb85. The main goal of the analysis was to elucidate femtosecond X-ray diffraction experiments carried out at the SLAC National Accelerator Laboratory (USA). In these experiments, X-ray measurements were performed during the melting and subsequent quenching of selected PCMs to study atomic changes during the switching (amorphization) process. The experiments indicated that, when the liquid state generated by the laser heat pulse is cooled down well below the melting temperature, it undergoes a structural transition to a different liquid phase. Furthermore, comparison with previous experimental results on the viscosity of AIST suggested that the two liquid phases have different kinetic properties. Our AIMD simulations enabled us to obtain detailed information about the local structural motifs during the quenching process and thereby resolve the microscopic mechanisms responsible for the liquid- liquid transition. The statistical analysis of the AIMD trajectories showed a clear separation of inter-atomic distances into two distinct groups of three short and three long average distances. The calculation of the angular limited bond correlation, a structural quantity yielding the correlations between almost aligned triplets of atoms, confirmed that the separation between short and long bonds originates from a so-called Peierls-like distortion, which is the dominant mechanism inducing the liquid-liquid transition and is directly connected to the change in kinetic properties.

The Peierls distortion implies an increased bond stability preventing spontaneous crystallization from the glassy state at low temperatures. As observed in experiments, the liquid at high temperature shows high atomic mobility that enables fast crystallization, whereas in the low-temperature amorphous state chemical bonds are stronger, resulting in reduced mobility and a stable glass. Therefore, the liquid-liquid transition driven by the onset of Peierls distortion explains a crucial property of PCMs that puzzled researchers for decades, namely the huge change in mobility occurring in a narrow temperature range, which leads to a stable amorphous state at temperatures near room T.

The main goal of subproject 2 was to investigate the electronic and switching properties of ScSbTe (SST) alloys by DFT-based AIMD. The project was motivated by recent work carried out in my group in collaboration with two Chinese groups, which led to the design of a new, ultrafast PCM - $Sc_{0.2}Sb_2Te_3$ - allowing subnanosecond writing speeds, comparable to those of SRAM. Sb2Te3 was used as parent compound to avoid the complexity of tetrahedral motifs found in amorphous GeSbTe. Sb_2Te_3 forms a metastable rocksalt-like phase upon fast crystallization from the melt. To improve the switching speed by alloying, a systematic materials screening based on DFT calculations was carried out. The search was restricted to transition-metal alloys, and was based on the following criterion: the alloy was requested to promote and stabilize the crystalline precursors in amorphous Sb_2Te_3. Such precursors consist of 4-membered Sb-Te-Sb-Te rings and the cubes made of such rings. Scandium was found to best fulfil these requirements. Experiments on PCM cells containing Sc0.2Sb2Te3 confirmed that this alloy increases the writing speed by an order of magnitude as compared to GeSbTe.

In the current project, we performed AIMD simulations to generate amorphous models of the two parent phases, namely Sc_2Te_3 and Sb_2Te_3. Our structural analyses revealed good geometrical compatibility between the two compounds, although amorphous Sc2Te3 (a-Sc-2Te3) has a better-defined local geometry. Furthermore, homopolar bonds are absent in a-Sc_2Te_3, indicating a high energy penalty for such bonds. We attributed this property to the relatively strong charge transfer between Sc and Te and the more ionic character of bonding in a-Sc_2Te_3 as compared to amorphous Sb_2Te_3 (a-Sb_2Te_3). We also carried out a chemical bonding analysis based on the crystal orbital Hamilton population method, which showed that a-Sc_2Te_3 exhibits high chemical stability. Nevertheless, the AIMD simulations indicate that too large Sc concentration in the ScSbTe alloy needs to be avoided, as the increased medium-range order brought by a-Sc_2Te_3 drives the amorphous structure away from the local order in the crystalline counterparts, increasing structural complexity that impedes rapid nucleation. In contrast, by alloying a small amount of Sc_2Te_3 into Sb_2Te_3, one obtains better-defined and chemically more robust ABAB squares and cubes that enable enhanced nucleation in the resulting SST material and, thus, subnanosecond memory operations. These findings shed light on why SST alloys with moderate Sc content such as Sc0.2Sb2Te3 are most suitable for phase-change memory devices.

Selected conference participations

[1] MAZZARELLO R.
Ab initio guided design of an ultrafast phase-change material. Invited talk given at the 9th International Workshop on Characterization and Modeling of Memory devices. Milan, Italy. September 27 - 28, 2018

[2] MAZZARELLO R.
Ab initio simulations of phase-change materials. Invited talk given at the 2018 Glass and Optical Materials Division (GOMD) Meeting. San Antonio; USA. May 20 - 24, 2018

Seleceted national and international cooperations

- DR. PETER ZALDEN, European XFEL, Schenefeld, Germany
- PROF. KLAUS SOKOLOWSKI-TINTEN, Duisburg University, Germany
- DR. VOLKER DERINGER, University of Cambridge, UK
- PROF. WEI ZHANG, Xi'an Jiaotong University, Xi'an, China
- DR. IVAN KABAN, IFW Dresden, Institute for Complex Materials, Dresden, Germany

Selected publications

[1] ZHANG W, MAZZARELLO R, WUTTIG M, MA E.
Designing crystallization in phase-change materials for universal memory and neuro-inspired computing. Nat. Rev. Mater. 2019;4:150.

[2] ZALDEN P, QUIRIN F, SCHUMACHER M, SIEGEL J, WEI S, KOC A, NICOUL M, TRIGO M, ANDREASSON P, ENQUIST H, SHU M, PARDINI T, CHOLLET M, ZHU D, LEMKE H, RONNEBERGER I, LARSSON J, LINDENBERG AM, FISCHER HE, HAU-RIEGE S, REIS DA, MAZZARELLO R, WUTTIG M, SOKOLOWSKI-TINTEN K.
Femtosecond X-ray diffraction reveals a liquid-liquid phase transition in phase-change material. Science. 2019;364:162.

[3] ZEWDIE GM, ZHOU Y, SUN L, RAO F, DERINGER VL, MAZZARELLO R, ZHANG W.
Chemical design principles for cache-type Sc-Sb-Te phase-change memory materials. Chem. Mater. 2019;31:4008.

Natural Sciences

Topological transport in real materials from ab initio

Project ID: jara0062
JAN-PHILIPP HANKE
FABIAN LUX
WANXIANG FENG
MATTHIAS REDIES
MAXIMILIAN MERTE
FRANK FREIMUTH
LICHUAN ZHANG
Peter Grünberg Institute (PGI-1)
and Institute for Advanced
Simulation (IAS-1),
Forschungszentrum Jülich, Germany

Project Report

The potential of spintronics for applications and new emergent technologies is highest in decades. The discovery of the spin-orbit interaction as the source behind novel topological phases of matter, transverse spin-currents, spin-orbit torques and formation of chiral magnetic textures, heralds the beginning of a new era hinging on topological concepts for spin-orbit driven transport phenomena. This marks a novel paradigm, according to which relativistic effects taking place in materials can be utilized both for spin transport and magnetization control simultaneously. Our project made use of the highly-predictive microscopic and ab-initio tools to study, design, understand and discover novel relativistic effects which (i) couple electrical currents to the magnetization at interfaces by the effect of spin-torques; (ii) result in novel and efficient means of generation of spin currents at magnetic surfaces and interfaces; (iii) advance our ability to manipulate and engineer the dynamics of chiral magnetic textures such as skyrmions; and (iv) study in depth the properties of topologically non-trivial systems such as topological insulators or quantum anomalous Hall insulators.

In the research that was performed during the period of 2019 within our project, we highlight the following studies.

(i) In the past year, by referring to ab-initio and model calculations in the context of our project we demonstrated the emergence of zero-dimensional and one-dimensional semimetallic topological states, which arise at the boundary between distinct topological phases when the direction of the magnetization θ in a 2D magnet is varied. We showed that by including the direction of the magnetization into the topological analysis, one arrives at a natural classification of such mixed Weyl and nodal-line semimetallic phases, which paves the way to scrutinizing their stability with respect to perturbations. We uncovered that the appearance of semimetallic phases is typically enforced by the drastic variation of the orbital band character upon changing the magnetization direction, which arises commonly in 2D ferromagnets, and we predicted that emergent semimetals can be experimentally detected by measuring the current-induced orbital response, e.g., via XMCD.

(ii) We considered the effect of anisotropy in spin-orbit torques (SOTs) on the dynamics of skyrmions. These torques contain two qualitatively distinct contributions, namely, a field-like term T_{FL} and an anti-damping term T_{AD}, both of which root in relativistic spin-orbit effects in systems that lack spatial inversion symmetry. It is known that owing to their nontrivial topology in two-dimensional real space, under the influence of SOTs skyrmions move under an angle θ_{sk} with respect to the line of the applied current. In our work, we demonstrated that this widely accepted picture needs to be extended owing to the nontrivial form of SOTs in magnetic multilayers. Using first-principles calculations we showed the strong anisotropy of antidamping and field-like torques in Ir/Co/Pt and Au/Co/Pt trilayers, see Fig. 3. Moreover, we uncovered that the coupling of magnetic textures to field-like torques which are higher order in the local magnetization can manifest in large corrections to the skyrmion Hall effect. Based on first-principles calculations and symmetry arguments, we quantified the relevance of these modifications for the dynamical properties of skyrmions and antiskyrmions in layered magnetic films of Ir/Co/Pt and Au/Co/Pt.

(iii) Magneto-optical effects, such as Kerr or Faraday effects, referring to changes in the polarization state of light upon interacting with magnetic matter, are some of the most basic phenomena in solid-state physics, which are widely used spectroscopic tools used to, e.g., visualize magnetic domains, detect and manipulate magnetic order, and measure ferromagnetism in two-dimensional (2D) systems. The microscopic origin of the described magneto-optical effects has long been deemed to be the interplay between band exchange splitting (BES) and spin–orbit coupling (SOC). With our latest work we have revisited this common belief. By using model arguments and first-principles calculations, we demonstrated that topological magneto-optical (TMO) effects, which arise without any reference to BES or SOC, can be prominent in fully compensated noncoplanar antiferromagnets. We showedthat the spectral integral of magneto-optical conductivity as well as the ones of Kerr and Faraday rotation angles, being spectroscopic fingerprints, identify the TMO effects essentially from their conventional cousins. Moreover, the quantum versions of these topological light-matter interactions, termed quantum TMO effects, can be realized in insulating non-collinear AFMs with nontrivial topology in momentum space, for which the Kerr rotational angle is quantized to a certain value close to 90 degrees and the Faraday rotation angle amounts to the product of Chern number and fine structure constant.

Selected conference participations

- Electrical and optical manifestations of emergent monopoles in complex magnets. 686. Wilhelm und Else Heraeus-Seminar on Spin-Based Information Processing. Bad-Honnef, Germany, January 2019
- Ab-Initio Antiferromagnetic Spintronics: from exotic interactions to novel transport effects. Magnetism 2019. University of Leeds, UK, April 2019
- Chiral electric transport effects in topological solitons. META 2019: 10th International Conference on Metamaterials, Photonic Crystals and Plasmonics. Lisbon, Portugal, July 2019
- Topology for spin interactions and the other way around. Skyrmionics Workshop for Young Researcher. Mainz, Germany, September 2019
- Spin “Chirotronics”: From antiferromagnets to 3D chiral particles. 17th RIEC International Workshop on Spintronics. Sendai, Japan, December 2019
- Skyrmions, quantum Hall effect and non-commutative geometry. British-German WE-Heraeus Seminar on Skyrmions in Magnetic Materials. Bad-Honnef, Germany, December 2019

Selected publications

[1] NIU C, HANKE JP, BUHL PM, ZHANG H, PLUCINSKI L, WORTMANN D, BLÜGEL S, BIHLMAYER G, MOKROUSOV Y. Mixed topological semimetals driven by orbital complexity in two-dimensional ferromagnets. Nature Communications. 2019;10;3179.

[2] REDIES M, LUX F, HANKE JP, BUHL PM, MÜLLER GP, KISELEV NS, BLÜGEL S, MOKROUSOV Y. Distinct magneto-transport and orbital fingerprints of chiral bobbers. Phys. Rev. B. 2019;99:140407(R).

[3] HANKE JP, FREIMUTH F, DUPE B, SINOVA J, KLÄUI M, MOKROUSOV Y. Engineering the dynamics of topological spin textures by anisotropic spin-orbit torques. Phys. Rev. B. 2020;101:014428.

[4] FENG W, HANKE JP, ZHOU X, GUO GY, BLÜGEL S, MOKROUSOV Y, YAO Y. Topological magneto-optical effects and their quantization in non-coplanar antiferromagents. Nature Communications. 2020;11:118.

[5] HAN DS, LEE K, HANKE JP, MOKROUSOV Y ET AL. Long-range chiral exchange interaction in synthetic antiferromagnets. Nature Materials. 2019;18:703.

Natural Sciences

Screening the impurity effects on transport properties in topological materials

Project ID: jara0191

PHILIPP RÜSSMANN
Peter Grünberg Institute (PGI-1)
and Institute for Advanced
Simulation (IAS-1),
Forschungszentrum Jülich, Germany

PHIVOS MAVROPOULOS
Physics Department,
National and Kapodistrian
University of Athens, Greece

Project Report

Topological materials have been a hot topic in solid state research in the recent years especially due to their intriguing transport properties. With our project “Screening the impurity effects on transport properties in topological materials” we investigated topological semimetals and magnetically doped topological insulators (TI) where the long-sought quantum anomalous Hall (QAH) effect can be realized. With a special emphasis on the implications of impurities on the transport properties in these materials, we analyzed their electronic structure as well as magnetic properties. Additionally, we started investigating the effect of co-doping with multiple defects on impurity properties which we will continue in the future.

Our computational approach is based on density functional theory which give our calculations the predictive power needed to be able to guide future experiments towards the realisation of topological material-based technology. We developed and used a high-throughput scheme (the AiiDA-KKR python package) to embed a large number of different impurities into topological materials. This resulted in the Jülich Database of impurities embedded into a Topological insulator (JuDiT for short). This database is now openly available and can be explored from a web interface which may help designing material’s properties in topological insulators based on doping.

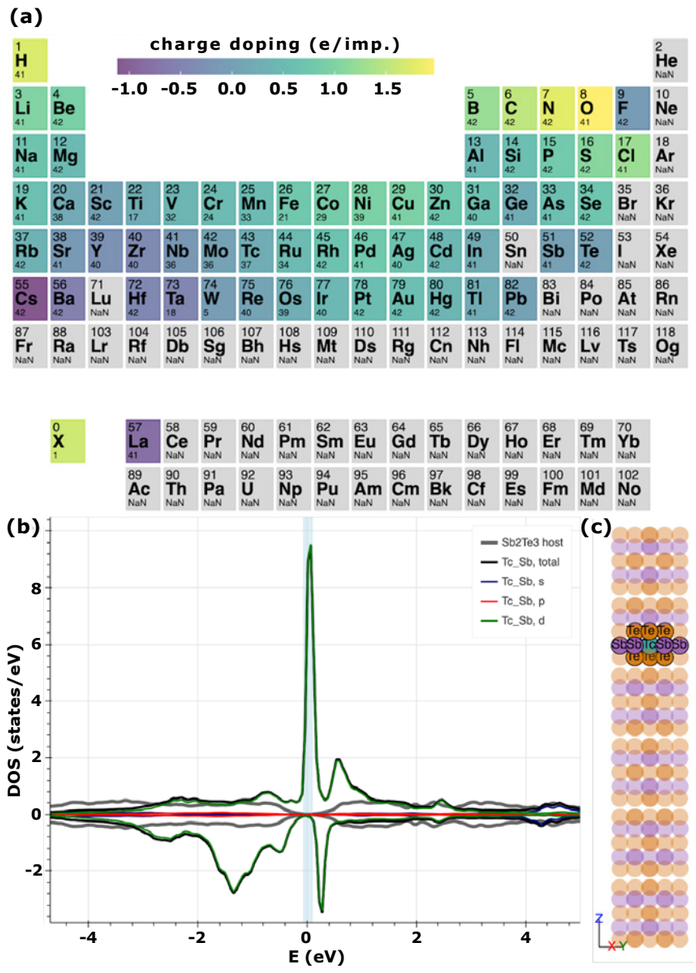

Figure 1: JuDiT database of impurity properties in a topological insulator

During the course of the project we contributed to the field of topological materials science in two ways: (i) through the investigation of magnetically doped TIs and (ii) by calculating a large number of substitutional defects in a thin film of the topological insulator Sb2Te3 (i.e. the JuDiT database). We studied the V and Cr doped TIs Sb2Te3 and Bi2Te3 and investigated doping with the rare earth element Europium. Our calculation of the exchange interactions between V and Cr impurities in TIs finally clarified the mechanism of the exchange interaction in these prototypical QAH systems. Magnetism in Europium comes from its partially occupied f orbitals which are strongly localized around the atom. Investigating this system from density functional theory required the need to include the effect of correlations using the LDA+U method. We improved our AiiDA-KKR package to be enable this and calculate dimers of impurities at different distance. Using these calculations and in collaboration with experiments we were able to show that Eu:Bi2Te3 has a high spin moment but shows short-ranged antiferromagnetism and only very weak hybridization with the TI host system.

Another focus was the study of topological semimetals where we started collaborations with the momentum microscopy group at PGI-6 (FZ Jülich). Here we studied the dichroism of the Weyl points in the type-II Weyl semimetal MoTe2 and found a good agreement between the experiments and our calculations of the orbital and spin resolved band structures. Furthermore, our joint experimental and theoretical investigations turned to the similar structure NiTe2, which is a type-II Dirac semimetal. Measurements of the Fermi surface and our calculations of the spin and orbital resolved band structure agree and we find the Dirac in close proximity to the Fermi level which makes this material a compelling candidate for further investigations.

Apart from applications of already existing features of the JuKKR code package, we succeeded in implementing the Bogoliubov de Genne (BdG) formalism in our density functional theory method. The BdG method allows to calculate inhomogeneous superconductors and in particular also study the band structures at interfaces of superconductors to non-superconductors. This is a vital ingredient in our future investigations in the field of Majorana Fermion based quantum computing.

Five selected bitonal and international cooperations

- THIAGO PEIXOTO, HENDRIK BENTMANN, University of Würzburg, Germany
- ABDUL-VAKHAB TCAKAEV, VLADIMIR HINKOV, University of Würzburg, Germany
- KENTA HAGIWARA, CHRISTIAN TUSCHE, PGI-6, FZ Jülich, Germany

Selected publications

[1] Master thesis by FABIAN BERTOLDO, Master of Science (Physics). High-Throughput Investigation of the Effect of Impurities on the Transport Properties of Topological Insulators. HHU Düsseldorf (2019).

Exploring Unconventional Magnetism by Quantum Monte Carlo Methods

Project ID: jara0190
STEFAN WESSEL
Institute for Theoretical Solid State Physics, RWTH Aachen University

Project Report

Quantum spin liquids are non-magnetic states of quantum matter in which interacting magnetic moment do not develop any sort of long-range order and do not break any symmetry even in the ground state. These systems exhibit topological order and fractionalized excitation.

One of he goals of current research is to provide quantitative spectral probes that can be used to identify such phases using, e.g., inelastic neutron scattering. Several compound have been identified as quantum spin liquid candidates, e.g., based on geometric frustration from their two-dimensional kagome lattice structure. In one of our sub-projects, we examined the quantum spin dynamics of a spin-1/2 quantum spin system on the kagome lattice, which in addition to a ferromagnetic transverse spin exchange interaction also exhibits transverse four-site ring exchange terms.

This system has been proposed to realize a quantum spin liquid ground state within an extended parameter space. Based on large-scale quantum Monte Carlo simulations using a sign-problem free simulation scheme, we obtained the dynamical spin structure factor of this spin system and studied its evolution from the ferromagnetic regime into the anticipated quantum spin liquid regime.

Depending on the scattering channel, distinct spectral features are observed, which can be linked to the vison excitations of a quantum spin liquid phase for the longitudinal channel, while characteristic differences to the spinon continuum in related quantum spin liquid regimes were observed in the transverse channel.

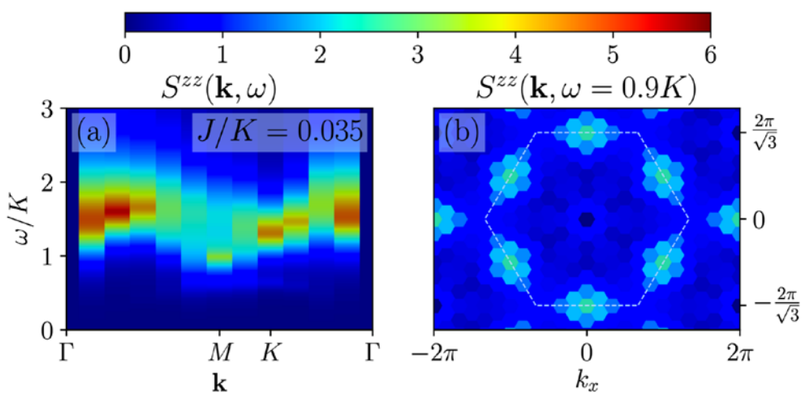

Figure 1: Quantum Monte Carlo results after a stochastic analytical continuation of the longitudinal dynamical spin structure factor of the ring-exchange model inside the non-magnetic regime, with characteristic features of momentum-fractionalization of the vison excitations.
(a) Cut along a high-symmetry cut in through momentum space.
(b) Cut at a fixed target scattering energy.

Selected conference participations

- STEFAN WESSEL. Boundary and Bulk Criticality 2019
  Würzburg, Germany, October 01-04, 2019

Five selected national and international cooperations

- F. MILA, EPFL Lausanne, Switzerland
- A. HONECKER, Universite Cergy Paris, France

Selected publications

- HESSELMANN S, HONERKAMP C, WESSEL S, LANG TC.
  Quantifying the fragility of unprotected quadratic band crossing points.
  Phys. Rev. B. 2020;101:075128.

- BECKER J, WESSEL S.
  Spin dynamics of the planar kagome lattice ferromagnet with four-site ring exchange processes.
  Phys. Rev. B. 2019;100:241113(R).

- HESSELMANN S, LANG TC, SCHULER M, WESSEL S, LÄUCHLI A.
  Comment on “The role of electron-electron interactions in two-dimensional Dirac fermions”.
  Science 10.1126/science.aav6869 (2019).

- WIETEK A, CORBOZ P, WESSEL S, NORMAND B, MILA F, HONECKER A.
  Thermodynamic properties of the Shastry-Sutherland model throughout the dimer-product phase.
  Phys. Rev. Research. 2019;1:033038.

- WEBER L, WESSEL S.
  Nonordinary criticality at the edges of planar spin-1 Heisenberg antiferromagnets.
  Phys. Rev. B. 2019;100:054437.

- YING T, SCHMIDT KP, WESSEL S.
  Higgs mode of Planar Coupled Spin Ladders and its Observation in $C_9H_{18}N_2CuBr_4$.
  Phys. Rev. Lett. 2019;122:127201.

Natural Sciences

Particles, Nuclei and Fields | DFG 309

Dark Simulations: understanding the dark side of particle physics and cosmology

Project ID: jara0184
JULIEN LESGOURGUES
Institute of Theoretical Particle Physics and Cosmology (TTK), RWTH Aachen University

FELIX KAHLHÖFER
MARIA ARCHIDIACONO
CHRISTIAN FIDLER
JESUS TORRADO
THEJS BRINCKMANN
DEANNA HOOPER
PATRICK STÖCKER
NILS SCHÖNEBERG
SAMUEL BRIEDEN
ALEXANDER KLEINJOHANN
CHRISTIAN PARTMANN
Institute of Theoretical Particle Physics and Cosmology (TTK), RWTH Aachen University

Project Report

Our primary use of the JARA cluster consists in comparing theoretical cosmological models to actual cosmological data. To do that, we compute theoretical predictions for millions of models in the cosmological parameter space, and compare it to data to finally infer the most likely models.

The Planck satellite (ESA) has recently provided new maps of the CMB anisotropies. We applied our method to produce some of the official derived constraints for cosmology. We further focused on the synergy between the Planck results and new data inferred from quasar spectra. First we derived new bounds on the total mass of neutrinos and on the mass of a dark matter candidate called Warm Dark matter (Palanque-Delabrouille et al.). Then we derived bounds on Dark Radiation and on the interaction cross-section that could exist between it and Dark Matter (Archidiacono et al.). Our bound on the summed mass of the three neutrino families, m1+m2+m3<0.11 eV, is currently the most stringent upper limit (Palanque-Delabrouille et al.).

Over the last years, a few discrepancies between the minimal cosmological model and various data sets have emerged. They are called “cosmological tensions” and hint at missing model ingredients, motivating many extensions of the minimal model. In Schöneberg et al., we have been able to exclude several categories of such extensions: we proved that even if we discard any CMB information from the Planck satellite, a combination of other robust data sets is sufficient for excluding any extension with extra relativistic degrees of freedom, which were suggested as a possible solution to the ``Hubble tension''. In Fidler et al., we further proved that the ``CMB lensing anomaly'' cannot be explained by second-order effects that are usually neglected in the minimal cosmological model.

We applied a similar methodology to predict the sensitivity of future cosmological surveys to several parameters related to the dark matter problem, such as the neutrino mass, a possible dark matter lifetime or its annihilation cross-section. We studied in particular the sensitivity of the Euclid satellite, to be launched by ESA in 2022 (Brinckmann et al., Sprenger et al.); and of future experiments that will measure the departure of the CMB from a pure black body spectrum (Lucca et al., Bolliet et al.). For each of these cases, we released our results together with some sophisticated numerical packages that we developed.

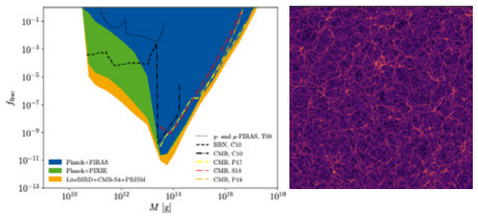

Figure 1: Left: Primordial Black Holes (PBHs) could make up a fraction f_{frac} of the total dark matter density in our Universe. In Lucca et al. we derived some new exclusion bounds on the mass M and fraction f_{frac} of such PBHs using CMB data from FIRAS and Planck. We further showed how these bonds are likely to evolve with future CMB experiments like PIXIE, LiteBIRD, CMB-S4 and PRISM. Right: results of an N-body simulation for the formation of dark matter filaments and halos with the effect of neutrino masses taken into account using the new method of Fidler et al.

In parallel, we used the JARA cluster for a second line of research. To model the evolution of the ingredients of the universe at late times and small scales, one needs to run sophisticated simulation tools called “N-body codes”. These codes usually neglect some effects that would make them much slower: general relativistic corrections, and massive neutrinos. A few years ago, we proposed a method to account for these effects without significantly increasing the computing time (C. Fidler). Indeed, the relevant effects can be incorporated by applying a special coordinate transformation to the original results. We used the JARA cluster to further test, improve and validate this revolutionary method. Our results have been published in four papers by Fidler et al.
There are two other topics we have used the JARA resources for that are not mentioned in the previous paragraphs: “Global fits of non-standard Dark Matter models'' and “Machine-Learning sampling algorithms for cosmology”. After obtaining results that go beyond our expectations, these two sub-projects have significantly expanded in scope and are therefore still ongoing.
For the first topic, we published new results and released a vast numerical software package in September 2020. For the second topic, we plan to publish a paper in late 2020 or early 2021.

Selected honors, prizes, awards

- 2019 Cocconi Prize of the European Physical Society, awarded to all members of the Planck satellite collaboration, including J. Lesgourgues

Selected conference participations

- Massive Neutrinos, Bad Honnef, Germany, July 08-11, 2019
- Understanding Cosmological Observations, Benasque, Spain, July 28-Sep. 09, 2019
- Cosyne: Cosmological Synergies in the upcoming decade, IAP, Paris, France, Dec. 9-12, 2019

Selected national and international cooperations

- Jens Chluba, Jodrell Bank Centre for Astrophysics, Manchester, UK
- Nathalie Palanque-Delabrouille, IRFU, CEA, Saclay, France
- Matteo Viel, SISSA, Trieste, Italy
- Christophe Ringeval, University of Louvain-la-Neuve, Belgium
- Oliver Hahn, Observatory of Cote d’Azur, Nice, France

Selected publications

1. PALANQUE-DELABROUILLE N, YECHE C, SCHÖNEBERG N, LESGOURGUES J, WALTER M. Hints, neutrinos bounds and WDM constraints from SDSS DR14 Lyman-alpha and Planck full-survey data, e-print 1911.09073, JCAP 04 (2020) 038.
2. LUCCA M, SCHÖNEBERG N, HOOPER D, LESGOURGUES J, CHLUBA J. The synergy between CMB spectral distorsions and anisotropies, e-print 1910.04619, JCAP 02 (2020) 026.
3. BOLLIET B, BRINCKMANN T, CHLUBA J, LESGOURGUES J. Including massive neutrinos in thermal Sunyaev-Zeldovitvh power spectrum and cluster counts analyses, e-print 1906.10359, MNRAS 497 (2020) 1332.
4. SCHÖNEBERG N, LESGOURGUES J, HOOPER D. The BAO+BBN take on the Hubble tension, e-print 1907.11594, JCAP 10 (2019) 029.
5. ARCHIDIACONO M, HOOPER D, MURGIA R, BOHR S, LESGOURGUES J, VIEL M. Constraining Dark Matter-Dark Radiation interactions with CMB, BAO and Lyman-alpha, e-print 1907.01496, JCAP 10 (2019) 055.
6. FIDLER C, LESGOURGUES J, RINGEVAL C. Lensing anomalies from the epoch of reionisation, e-print 1906.05042, JCAP 10 (2019) 042.
7. BRINCKMANN T, HOOPER D, ARCHIDIACONO M, LESGOURGUES J, SRPINGER T. The promising future of a robust cosmological neutrino mass measurement, e-print 1808.05955, JCAP 01 (2019) 059.
8. SPRENGER T, ARCHIDIACONO M, BRINCKMANN T, CLESSE S, LESGOURGUES J. Cosmology in the era of Euclid and the Square Kilometer Array, e-print 1801.08331, JCAP 02 (2019) 047.
9 . FIDLER C, KLEINJOHANN A. Suitable initial conditions for Newtonian simulations with massive neutrinos, e-print 18010.12019, JCAP 06 (2019) 018.
10. FIDLER C, KLEINJOHANN A, TRAM T, RAMPF C, KOYAMA K. A new approach to cosmological structure formation with massive neutrinos, e-print 1807.03701, JCAP 01 (2019) 025.

Natural Sciences

Statistical Physics, Soft Matter, Biological Physics, Nonlinear Dynamics | DFG 310

Dissecting the functional dynamics of HypA: an HPC-based molecular simulation approach

Project ID: rwth0365

PAOLO CARLONI
Institute for Advanced Simulation and Institute of Neuroscience and Medicine (IAS-5 /INM-9), Computational Biomedicine, Forschungszentrum Jülich, Germany

FRANCESCO MUSIANI
STEFANO CIURLI
University of Bologna, Bologna, Italy

EMILIANO IPPOLITI
Institute for Advanced Simulation and Institute of Neuroscience and Medicine (IAS-5 /INM-9), Computational Biomedicine, Forschungszentrum Jülich, Germany

Project Report

Proteins are involved in a huge number of tasks inside the cells. Among others, they can catalyze reactions, recognize ligands, propagate information across the cell and transform energy into work. These duties are often accomplished through conformational changes and rearrangements that can involve small regions of the protein or even the motion of entire domains. These motions are accessible to the protein even before protein-protein/ligand interactions and are fundamental for proteins function. The dynamics and the conformational changes occurring in different protein conditions or in the presence of specific cofactors and ligands have been widely studied but are still object of debate.

A paradigmatic case-study is represented by the bacterial accessory protein HypA, deputed to the transport of nickel ions required for the maturation of two enzymes: urease and [Ni,Fe]-hydrogenase. Both enzymes are essential for the survival of several often-deadly pathogenic bacteria, such as Helicobacter pylori (Hp). In the specific case of Hp, urease neutralizes the gastric microenvironment and buffers the bacterial periplasm and cytoplasm by catalyzing the conversion of urea into ammonia and carbon dioxide. HypA contains an N-terminal Ni(II)-binding domain and a Zn(II)-binding domain. The coordination of both Ni(II) and Zn(II) ions within HypA is known to be critical for urease maturation and activity. In particular, even if the structure of nickel bound HypA has not been solved yet, indirect studies show that HypA binds one Ni(II) to Met1, His2, Glu3 and Asp40 and another backbone amide. The tetrahedral Zn(II) binding is associated with two conserved CXXC sequences.

HpHypA has an elongated structure formed by two domains (Figure 1): the Zn(II)-binding domain well-separated from the Ni(II)-binding domain containing the Met1-His2-Glu3 motif associated with the Ni(II)-binding site at the N-terminal, thus providing no evidence as to how the two metal sites might be cooperating in nickel delivery.

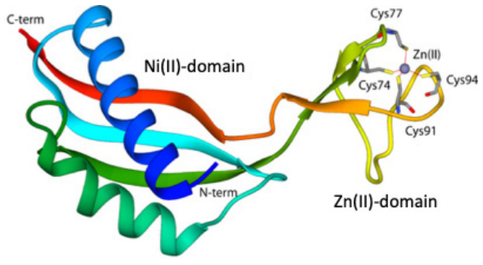

Figure 1: Ribbon of the wild type HpHypA structure determined through NMR spectroscopy.

Previous atomistic Molecular Dynamics (MD) calculations highlighted the mobility of the Ni(II)-binding domain with respect to the Zn(II) binding domain. Starting from these evidences, during this project we used accelerated sampling MD simulation methods to investigate the large-scale motions of Zn(II) bound HpHypA at different acidic conditions. In particular, we used the Replica Exchange with Solute Tempering (REST2) protocol to explore domain motions with the aim to link them to the functional role of HpHypA. This technique consists of running several – 24 in our case – MD simulations of the same systems (called replicas) at different effective temperatures. At given time intervals, replicas with similar temperature can exchange their coordinates and, in this way, an accelerated sampling of the potential energy surface (PES) is achieved. The present project granted 961,000 CPU hours on the supercomputer CLAIX2018. We run four REST2 simulations – two at pH 7.2 and two at pH 6.3 – starting from the same geometry reported in Figure 1 but using different initial velocities in order to further enhance the PES sampling. For each system we run 35 ns of simulation per replica, for a total of 3.36 µs of simulation time.

The analyses conducted on the REST2 trajectories show that the general fold of Zn-HpHypA is stable during all the simulations and that the protein can be roughly divided in two domains (corresponding to the Ni- and Zn-domain) that move independently. The angle formed by the axes described by the Ni-domain and Zn-domain (Ω hereafter) was calculated. The results show the conformational space sampled by MD simulations implemented with REST2 was larger if compared with that of the NMR ensemble previously obtained. Notably, at physiological pH the protein seems to reach conformations characterized by an interdomain angle of ca. 72°, leading to a “close” structure (Figure 2). In the other hand, at acidic conditions Zn-HpHypA reaches conformations characterized by an interdomain angle of ca. 153°, leading to a “wide open” structure (Figure 2). The presence of such different populations was also corroborated by the identification of at least three different distributions of Cartesian component of the gyration radii (Figure 3), confirming a different shape assumed by the protein in different acidic conditions.

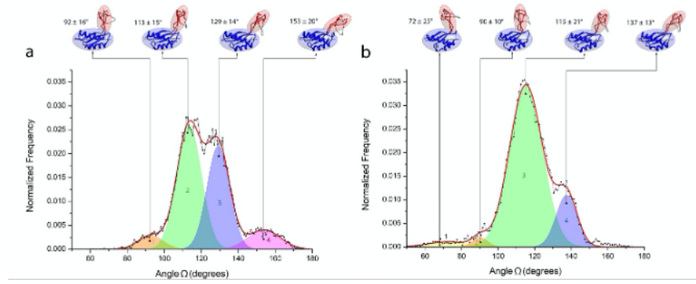

Figure 2: Distribution of the angle Ω measured between the axes defined by the Cα atoms of the Ni-domain (in blue) and those of the residues Zn-domain (in red) measured at physiological (7.2, a) and acidic (6.3, b) pH. The ellipsoids inscribing the domains are also represented.

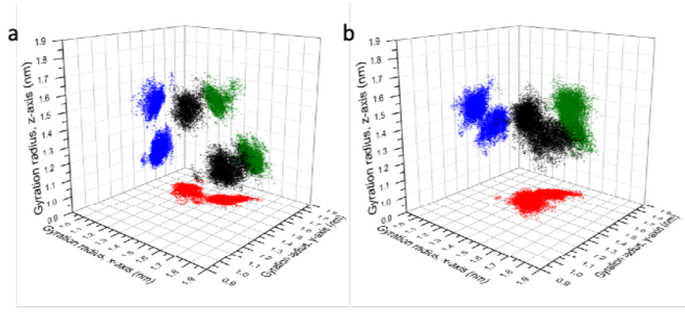

Figure 3. Cartesian components of the gyration radius of HpHypA at physiological (7.2, a) and acidic (6.3, b).

Selected conference participations

- FRANCESCO MUSIANI, A computational approach to nickel trafficking and utilization in pathogenic bacteria, Forschungszentrum Jülich, Jülich, Germany, February 25, 2019
- FRANCESCO MUSIANI, How pathogenic bacteria handle poisonous nickel ions: a computational approach, Second training course and international workshop on multi-scale simulation”, Hanoi, Vietnam, September 27, 2019

Natural Sciences

Molecular Dynamics Simulations of TRAP1 in Complex with Novel Modulators: Toward Linking Predictive Modeling to Function and Pharmacology

Project ID: rwth0382

EMILIANO IPPOLITI
Institute for Advanced Simulation and Institute of Neuroscience and Medicine (IAS-5 /INM-9), Computational Biomedicine, Forschungszentrum Jülich, Germany

MARIAROSARIA FERRARO
Istituto di Chimica del Riconoscimento Molecolare (ICRM), Consiglio Nazionale delle Ricerche (CNR), Italy

ELISABETTA MORONI
IRCCS Multimedica, Italy

Project Report

A ML approach was used to explore the existence of local dynamic patterns featuring inhibitor-free (A) and inhibitor-bound (I) TRAP1 states in a comparative MD ensemble including 66 systems, wherein 11 new allosteric modulators were used to train and validate Naïve Bayesian (NB) and Radial Basis Function SVM (GDF-SVM) models. Generative NB and discriminative SVM models were employed to learn from MD trajectories and compare performances of the two different approaches to the classification tasks. In synergy with MD simulations, we explored the ability of ML to explain allosteric perturbation as a function of combinations of localized dynamic patterns developed on the ns-µs time scale. Features selection was driven by experimentally demonstrated roles in modulating TRAP1 ATPase activity and in responding to nucleotide-binding (Figure 1).

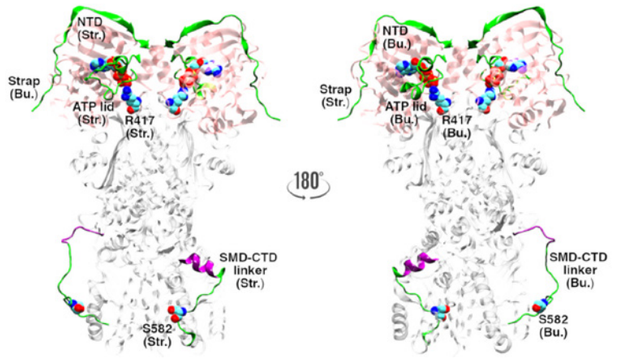

Figure 1.

In virtue of the established hierarchy of timescales in protein motions, we hypothesized that allosteric perturbations could reverberate in dynamic changes at inherently dynamic segments, since the latter were known to drive the onset of slower functionally oriented conformational changes. Two training sets from shorter and longer simulation sets were built based on retrospective data on the three most active ligands (% inhibition: 73-75%). Previous analyses on internal dynamics, long-range signaling and dynamic domains motions established the effects of ligand-induced perturbation in these trajectories. The models were tested to predict up to 8 or 11 out-of-model ligands with lower or equal inhibitory efficacy (% inhibition: 27-65%).

One of the hypotheses we tested was that the most active compounds would have been representative of local patterns inducing the maximum impact on local dynamics and that the less active ligands could have less optimal profiles because of a non-optimal perturbation of a give set of features. Generative models trained on extended dataset validated this hypothesis. Linear regression analyses based on predicted TPR% for individual sets of inhibitor-bound systems returned models explaining from 64% to 71% of the observed variance in TRAP1 inhibition range (red dots in Figure 2d, h). Discriminative models did not reach similar correlations (r2 values < 0.60) but generated qualitative boundaries between states (Figure 2c, f, i). These differences in performance suggested that predictions took advantages from the assumption of features independence. Even if allosteric motions act cooperatively on long timescales, such dependence could not be readily established on the simulated ones, but the local dynamic equilibrium of each feature can still independently respond to ligand perturbation to a different extent, depending on specific allosteric mechanisms and communication propensity of distal sites.

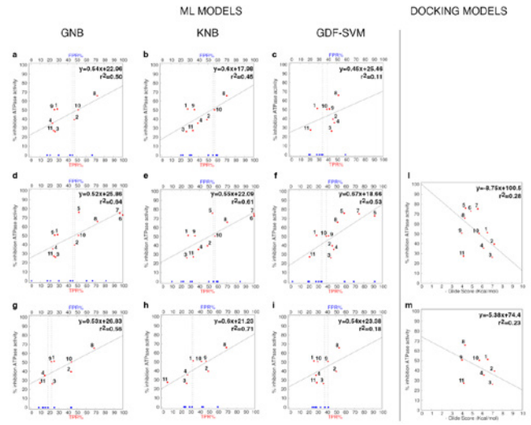

Figure 2.

Discriminative models, simply trying to separate the states based on the input n-dimensional space, do not take into account the probability that connects members of a class to the ensemble of visited features. This aspect probably induced the less active compounds to segregate from the unbound replicates by sampling specific regions which, however, were less representative of patterns that are actually relevant to explain the reasons for activity of the best inhibitors.
By comparing predicted TPR% and FPR% in the 2D plots we showed that, in absence of ligands, the unperturbed systems sample both patterns A and I, with the majority of systems exhibiting preference for state A (blue dots in Figure 2).

As for the global dynamic equilibrium regulating active/inactive pre-existing configurations, we did not exclude that states A and I might co-exist and be interpreted through nanosecond dynamics on a local scale. Consistent with the hierarchy of timescales in protein motions and the extended conformational selection model for allostery, the co-existence of opposite local patterns at responsive TRAP1 elements in a near-native energy minimum may locally initiate a dynamic change that results in a global population shift in a more efficient way. Alternatively, one of them could be simply stabilized or destabilized as a consequence of allosteric perturbation and as a function of the ligand mechanism of action. In this respect, NB models are built so that conditional probabilities of features in a given class could be extracted and the weight of a feature quantified in each state. This property enables the identification of individual or combined contribution of the features to each classified MD frame and could assist further integrative biology studies to rationalize the diverse nature of allosteric modulations or, more widely, perturbing mechanisms.

From the drug discovery standpoint, we showed that, building and validating balanced NB models on the most active ligands of a known series, the models could learn patterns which generalize on the behavior of a much larger ensemble of completely “unseen” trajectories. Comparably, docking models showed no correlation to ligand functional properties (Figure 2l-m). The NB model based on Kernel distributions (KNB) and trained on the extended training set outperformed the one built through normal distributions (GNB) in the prediction of inhibitor-bound states, while the latter showed the greater specificity for the inhibitor-unbound states, possibly approximating the harmonic sampling in near-native unperturbed energy basins. This strategy provided useful interpretation of the way the eight tested inhibitors affect the local functional dynamics and was retrospectively validated by achievement of meaningful correlation between TPR% and percentages of TRAP1 inhibition. Relying on this model, compounds showing weaker inhibition of chaperone function could have been filtered out from the set, without losing the most promising hits and avoiding experimental testing.

Selected national and international cooperations

· Luca Pavarino, Dipartimento di Chimica, Università di Pavia, Pavia, Italy

Natural Sciences

Astronomy and Astrophysics | DFG 311

Cosmic-Ray Physics with the AMS Experiment on the International Space Station

Project ID: jara0052

HENNING GAST
STEFAN SCHAEL
KLAUS LÜBELSMEYER
LEILA ALI CAVASONZA
SOFIA CHOURIDOU
CHAN HOON CHUNG
THOMAS KIRN
NIKOLAY NIKONOV
GEORG SCHWERING
THORSTEN SIEDENBURG
VALERY ZHUKOV
ANDREAS BACHLECHNER
MANBING LI, SICHEN LI
FABIAN MACHATE
ROBIN SONNABEND
Department of Physics
Institute I B
RWTH Aachen University

Project Report

© NASA

Figure 1

AMS is a detector designed for precision spectroscopy of cosmic rays that was installed on the International Space Station in May 2011. With dimensions of 5x4x3 m³ and a weight of 7.5 tons, AMS is the largest cosmic-ray spectrometer ever built. Its construction began in 1995, and a successful prototype flight aboard the Space Shuttle Discovery proved the feasibility of the detector concept in 1998. Led by Nobel laureate Professor Samuel Ting from MIT, AMS has been constructed and is now operated by an international collaboration of more than 200 scientists and engineers, from Europe, America and Asia. The overall construction costs, including the flight of AMS to the Space Station aboard Space Shuttle Endeavour, have amounted to 1.5 billion US dollars. In Germany, RWTH Aachen has been strongly involved in the AMS project since its inception. One of the main components of AMS, the transition radiation detector (TRD), has been designed and constructed by the I. Physikalisches Institut B under the direction of Professor Stefan Schael. Today, the Aachen group, comprising 20 scientists and students, plays a major role in the analysis of the data gathered by AMS and in the operation and calibration of the instrument.

Since their discovery in 1912, cosmic rays have held many surprises in stock for us, from the discovery of new elementary particles to the most violent processes taking place in the Universe and accelerating cosmic rays to enormous energies. As a multi-purpose instrument for the precision spectroscopy of cosmic rays, AMS was conceived to answer fundamental questions about our Universe: What is the nature of Dark Matter? What happened to the antimatter that must have been produced in the Big Bang? Where are cosmic rays accelerated and how do they propagate through the Milky Way? Answers to these questions will have a profound impact on our understanding about the inner workings of our Universe and help advance fundamental science. In particular, the search for dark matter complements the endeavour to search for new elementary particles at the Large Hadron Collider (LHC) at CERN, Geneva.

AMS so far has recorded more than 150 billion individual particle crossings (so called “events“). The raw data volume collected is on the order of 40 TB per year. AMS employs five different sub-detectors for particle identification and for energy or momentum measurements (the TRD, an electromagnetic calorimeter, a ring-imaging Cherenkov counter, a silicon tracker and a time-of-flight system). Before any physics analysis of the data can be performed, the information from all these subdetectors has to be pieced together and complicated reconstruction algorithms have to be run for each of them. The resulting high-level data serves as the input for physics analyses and occupies a volume of 160 TB per year of AMS flight on disk. Several processing runs of AMS data have already been conducted successfully on the JUROPA and JUAMS clusters at JSC as the result of the cooperation within JARA.

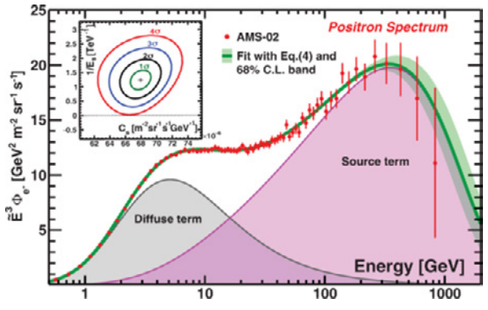

Figure 2: Positron flux measured by AMS (red points), together with a fit of generic model consisting of a diffuse term and a source term with an exponential cutoff (green curve, with 68% uncertainty band). The inset illustrates that the existence of the cutoff is established with 4 standard deviations.

So far, seventeen publications from the AMS collaboration have appeared in the renowned Physical Review Letters. The findings have received considerable attention among astrophysicists and triggered an enormous amount of theoretical work.

Selected conference participations

- H. GAST, “Auf der Suche nach Dunkler Materie und Antimaterie im Weltraum - Das AMS Experiment auf der Internationalen Raumstation”, Public Evening Lecture, DPG Spring Meeting, Aachen, Germany, March 26, 2019
- S. SCHAEL, “AMS-100, the next generation magnetic spectrometer in space”, Next-GAPES - 2019 Konference, Lomonosov Moscow State University, Russia, June 21, 2019
- S. SCHAEL, “AMS-100, the next generation magnetic spectrometer in space” , The 2019 Symposium on Applications of Superconductivity and Cryogenics, University Twente, Netherlands, November 22, 2019
- S. SCHAEL, “AMS-100, the next generation magnetic spectrometer in space”, Kolloquium DLR Bonn, Germany, November 29, 2019
- S. SCHAEL, “New results from the AMS-02 Experiment on the ISS”, Physikalisches Kolloquium der Universität Bonn, Germany, December 13, 2019

Selected national and international cooperations

- SAMUEL C. C. TING, Massachusetts Institute of Technology, USA
- BRUNA BERTUCCI, INFN and University of Perugia, Italy
- BERND HEBER, Christian-Albrechts-Universität zu Kiel, Germany
- IRIS GEBAUER, Karlsruhe Insitute of Technology, Germany

Selected publications

- AGUILAR M ET AL. (AMS Collaboration), Towards Understanding the Origin of Cosmic-Ray Electrons, Physical Review Letters, 2019; 122:041102.
- AGUILAR M ET AL. (AMS Collaboration), Towards Understanding the Origin of Cosmic-Ray Positrons, Physical Review Letters, 2019; 122:101101.
- AGUILAR M ET AL. (AMS Collaboration), Properties of Cosmic Helium Isotopes Measured by the Alpha Magnetic Spectrometer, Physical Review Letters, 2019; 123:181102.

Engineering Sciences

Picture: Freepik

Engineering Sciences

Chemical and Thermal Process Engineering | DFG 403

Flexible Simulation of Fuel cells with OpenFOAM /FlexSim

Project ID: jara0070

WERNER LEHNERT
DIETER FRONING
STEVEN B. BEALE
UWE REIMER
SHIDONG ZHANG
Institute of Energy and Climate Research,
Electrochemical Process Engineering (IEK-14),
Forschungszentrum Jülich, Germany

MARTIN ANDERSSON
Lund University, Sweden

BEDII ÖZDEMIR
Istanbul Teknik Universitesi, Turkey

Project Report

1. Polymer electrolyte fuel cell

The polymer electrolyte fuel cell (PEFC) is a promising device that converts chemical energy directly into electricity. It has attracted significant attention, particularly in the application of electric vehicles. Analysis of the performance of a PEFC using numerical simulations is an important subject. Computational fluid dynamics (CFD) is one of the most widely used tools to perform calculations in fuel cells on the continuum scale. Heat and mass transfer in PEFCs represent critical aspects that need to be addressed during the design process. These physical processes are coupled so their simulation is greatly determined by the fuel cell operating conditions.

A new PEFC model was developed and implemented into the open source package, OpenFOAM. This model enables simulations concerning two-phase (liquid-gas) flow, heat and mass transfer, charge transport, and electrochemical reactions in a PEFC. Among these processes, the dynamics of two-phase flow is the step that consumes most of the computational resources.

The model was verified with analytical results and validated by comparing with experimental data. The comparison can be found in the PhD thesis of Dr. S. Zhang. Additional calculations were conducted on an in-house designed PEFC prototype.

2. CFD in complex geometries

In collaboration with the Lund University, volume-of-fluid (VOF) studies in porous transport layers (PTLs) and gas channels of fuel cells (conjugate problem) were investigated using OpenFOAM. Obtaining numerical convergence required substantial tuning of the code, the problem being not so much the size of the mesh, but rather the time stepping. The rate-limiting factor here is the Courant number, which cannot exceed 1 as well as the related Capillary Courant number.

The geometry considered is in the form of a 'T-shape' with the porous transport layer (PTL) in the form of a thin rectangular prism of size 0.5×0.5×0.1 mm^3 located at the base of the 'T', and the gas flowing across the top in the channel, in the x-direction. The PTL is reproduced by digital reconstruction of nano-computer tomography images of a Freudenberg H2315 PTL in the form of an STL file.

In the PTL, counter-flow of liquid water and gaseous air correspond to product-creation and reactant-destruction by the oxygen reduction reaction at the electrode. In the gas channel the liquid water is entrained by the flowing gas an advected downstream. The flow is reasonably periodic with some randomness.

A special interest group (SIG) was established by Profs. Beale and Lehnert, specifically around the use of OpenFOAM for electrochemical applications. The SIG includes ESI/OpenCFD (France/UK), SerEnergy (Denmark), Cenaero (Belgium).

Selected conference participations

- STEVEN BEALE
  Mathematical Models of Fuel Cells and Electrolyzers: A review,
  4th International Hydrogen Technologies Conference,
  keynote lecture, Edirne, Turkey, June 20-23, 2019
- DIETER FRONING, UWE REIMER, STEVEN BEALE, WERNER LEHNERT
  Modelling of Electrochemical Hydrogen Purification and Compression,
  f-cell, Stuttgart, Germany, September 10-11, 2019
- UWE REIMER, DIETER FRONING, SHIDONG ZHANG,
  STEVEN BEALE, WERNER LEHNERT,
  An Engineering Toolbox for the Evaluation of Metallic Flow Field Plates,
  Hypothesis XIV, Foz do Iguacu, Brazil, April 24-26, 2019
- LASSE BRAMS VINTHER, SØREN JUHL ANDREASEN,
  SHIDONG ZHANG, STEVEN BEALE
  Modeling HTPEM fuel cell and stack using OpenFOAM.
  6th CARISMA International Conference on Medium and High Temperature Proton Exchange Membrane Fuel Cells, Duisburg, Germany, August 27-29, 2019
- DIETER FRONING
  Two-phase flow in gas diffusion layers of a PEFC
  and analysis of the GDL/channel interface.
  Internationl Energy Agency Advanced Fuel Cells Technology Collaboration Program,
  Annex 37, Modelling Meeting. Brunswick, Germany, March 14, 2019
- UWE REIMER
  Evaluation of metallic flow field plates
  for electrochemical hydrogen purification and compression cells.
  International Energy Agency Advanced Fuel Cells Technology Collaboration Program,
  Annex 37, Modelling Meeting. Brunswick, Germany, March 14, 2019

Selected national and international cooperations

- PROF. MARTIN ANDERSSON, Lund University, Sweden
- PROF. BEDII ÖZDEMIR, Istanbul Teknik Universitesi, Turkey
- PROF. HRVOJE JASAK, University of Zagreb, Croatia
- Lasse Brams Vinther, Søren Juhl Andreasen, SerEnergy A/S, Aalborg, Denmark
- Dr. Norbert Weber, Institut für Fluiddynamik,
  Helmholtz-Zentrum Dresden-Rossendorf e.V., Germany

Selected publications

[1] ANDERSSON M, BEALE SB, LEHNERT W.
Dynamic Contact Angle Modeling of Droplet Reattachment at the Gas Channel Wall in Polymer Electrolyte Fuel Cells. eTransportation 1, 100003, 2019, DOI: 10.1016/j.etran.2019.100003.

[2] ANDERSSON M, VUKČEVI V, ZHANG S, QI Y, BEALE SB, JASAK H, LEHNERT W.
Modeling of Droplet Detachment using Dynamic Contact Angles in Polymer Electrolyte Fuel Cell Gas Channels. International Journal of Hydrogen Energy. 44 11088-11096. 2019 DOI: 10.1016/j.ijhydene.2019.02.166.

[3] ZHANG S.
Modeling and Simulation of Polymer Electrolyte Fuel Cells. PhD thesis,
Fakultät für Maschinenwesen der Rheinisch-Westfälischen Technischen Hochschule Aachen. 2019.

Engineering Sciences

Heat Energy Technology, Thermal Machines, Fluid Mechanics | DFG 404

Parallel Stabilized Finite Element Methods for Aero-, Hemo-, and Hydrodynamics

Project ID: jara0185

MAREK BEHR
STEFANIE ELGETI
NORBERT HOSTERS
MAX VON DANWITZ
SEBASTIAN EUSTERHOLZ
LINDA GESENHUES
FELIPE GONZALEZ
STEFAN HASSLER
JAN HELMIG
DANIEL HILGER
VIOLETA KARYOFYLLI
FABIAN KEY
KONSTANTIN KEY
MICHEL MAKE
ANNA RANNO
JAYGHOSH RAO
EUGEN SALZMANN
MAXIMILIAN SCHUSTER
THOMAS SPENKE
LOIC WENDLING
STEFAN WITTSCHIEBER
FLORIAN ZWICKE

Chair for Computational Analysis of Technical Systems (CATS), RWTH Aachen University

Project Report

Among the various advances in parallel stabilized finite element methods for flow simulation, we highlight the development of a physiological model for quantifying the blood damage in biomedical devices. For details, see the article by Stefan Haßler, Lutz Pauli, and Marek Behr "The variational multiscale formulation for the fully-implicit log-morphology equation as a tensor-based blood damage model" which appeared in the International Journal for Numerical Methods in Biomedical Engineering, Vol. 35, pages e3262-1–19 (2019).

Numerical modeling and simulation is an increasingly important tool used during the development of blood-handling medical devices. Computational fluid dynamics (CFD) helps reduce the number of expensive and time-consuming experiments during prototype development. CFD has long been able to predict the hydraulic performance and even the flow field details within such devices and can therefore give useful information towards improvements of their design. This information is very valuable, since adverse event rates for hemolysis, strokes, and renal dysfunction have in fact increased for patients with a ventricular assist device (VAD), possibly due to more widespread use.

Accurate numerical prediction of blood damage such as hemolysis remains a challenge. An purely empirical power law model is widely used to estimate the generation of harmful plasma-free hemoglobin in medical devices. In such a model, the amount of released hemoglobin is proportional to the shear stress and the duration over which the red blood cells (RBCs) are exposed to that stress. The power law parameters are normally determined by a fitting to experimental data obtained in simplified experimental configurations using human or animal blood samples. This modeling approach, the so-called stress-based hemolysis model, always computes a scalar measure of the shear stress from the flow field, which assumes an instantaneous deformation of the RBCs. Since such a model is not taking the viscoelastic behavior of RBCs into account, our group, among others, have worked over the last decade on a strain-based model that estimates the droplet-like deformation of RBCs in blood flow. This so-called morphology equation is able to account for the relaxation, elongation, and rotation of the droplets in the flow. The model has been first used in a Lagrangian reference frame, and later in a more efficient Eulerian reference frame. Although more physiologically sound, the strain-based model is highly non-linear – not unlike material models governing flows of viscoelastic liquids – and suffers from several convergence and stability issues when coupled even with advanced numerical discretization schemes.

In the latest development in 2019, the tensor-based RBC deformation model was reformulated to guarantee the positive definiteness of the morphology variable. We used a logarithmic transformation of the shape tensor in the underlying morphology equation, resulting in so-called log-morph formulation. This introduces highly non-trivial terms in the resulting governing equation. The variational multiscale (VMS) method was used as a general framework for stabilization of partial differential equations. Its resulting terms for the log-morph equation are derived with a Fréchet derivative approach for the linearization of the nonlinear terms. To our best knowledge, this is the first application of the VMS formulation to such a highly nonlinear tensor model.

For a simple two-dimensional stirrer test case, in which both traditional morphology model and the new log-morph model are applicable, we found good agreement between the untransformed morphology equation and the log-morph equation with SUPG and VMS stabilization. The enhanced numerical stability of the log-morph equation is clearly observed for this simple test case. Furthermore, we successfully applied the log-morph-VMS method to a state-of-the-art VAD for which the untransformed morphology equation is not able to converge. Our studies showed that the VMS stabilization method leads to an improved numerical stability for complex test cases compared with an SUPG stabilization scheme.

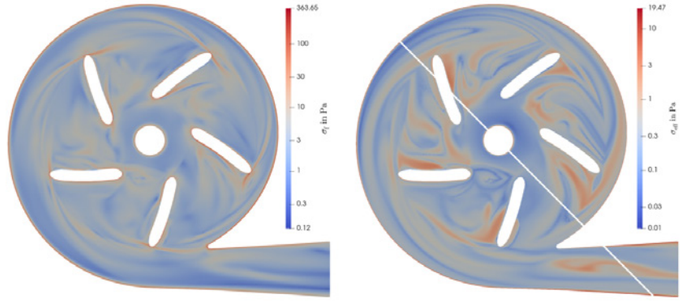

Figure 1: Fluid stress (left) and effective stress (right) in a planar cross-section through a flow chamber of a centrifugal VAD pump. Visible are the impeller axis, five impeller blades, and the outflow cannula at bottom right. The fluid stress is the basis for hemolysis estimation in commonly used stress-based models. Effective stress is computed from the estimated RBC deformation and is the basis for the more physiologically sound strain-based models. The comparison shows the different areas of blood damage predicted by the two models. Note that the strain-based prediction (right) was only possible to obtain numerically after the log-morph transformation proposed in this work.

Ten selected honors, prizes, awards

- Elected (ELGETI) as officer of the Female Researchers Chapter of International Association for Computational Mechanics

Selected conference participations:

- Keynote, Finite Elements in Flow Problems 2019, Chicago, IL, USA, March 31-Apr 3, 2019
- US National Congress on Computational Mechanics, Austin, TX, USA, Jul 29-Aug 1, 2019
- Japan Society of Civil Engineers Seminar, Tokyo, Japan, Oct 8, 2019
- Keynote, Asian Pacific Congress on Comp. Mechanics, Taipei, Taiwan, Dec 17-20, 2019

Five selected national and international cooperations:

- LESZEK DEMKOWICZ, University of Texas at Austin, Austin, TX, USA
- NIKOS CHRISOCHOIDES, Old Dominion University, Norfolk, VA, USA
- KAZUO KASHIYAMA, Chuo University, Tokyo, Japan
- LUCA BIFERALE, University of Rome Tor Vergata, Italy
- WOLFGANG WALL, Technical University of Munich, Germany

Selected publications

- BRÜDERLIN MP, HOSTERS NM, BEHR M.
  Reduced-order model for robust aeroelastic control
  CEAS Aeronautical Journal 10(2), 367-384 (2019) [10.1007/s13272-018-0322-3]
- KARYOFYLLI V, WENDLING L, MAKE MKP, HOSTERS NM, BEHR M.
  Simplex space-time meshes in thermally coupled two-phase flow simulations of mold filling, Computers & fluids 192, 104261 (2019) [10.1016/j.compfluid.2019.104261]
- VON DANWITZ M, KARYOFYLL V, HOSTERS NM, BEHR M.
  Simplex space-time meshes in compressible flow simulations
  International journal for numerical methods in fluids 91(1), 29-48 (2019) [10.1002/fld.4743]
- HASSLER ST, PAULI LH, BEHR M.
  The variational multiscale formulation for the fully-implicit log-morphology equation as a tensor-based blood damage model, International journal for numerical methods in biomedical engineering 35(12), 1-19 (2019) [10.1002/cnm.3262]

Engineering Sciences

Multiphase Simulations of Oil-Jet Cooling Applied to Pistons for Internal Combustion Engines

Project ID: jara0196
MAREK BEHR
NORBERT HOSTERS
MAX VON DANWITZ
VIOLETA KARYOFYLLI
LOIC WENDLING
Chair for Computational Analysis of Technical Systems (CATS), RWTH Aachen University

Project Report

A new CFD simulation model and methodology for oil jet piston cooling have been developed using the modern level set approach. This method has been proven to be robust and versatile for complex oil motion. Various methods have been exploited, such as the level set method, mesh movement, and volume of fluid method, to capture as much of the physics as possible. During this project, the heat equation was implemented and tested for multiphase flows to obtain the heat transfer across the piston surface. The complex atomization behaviors have been investigated for the free oil jet test case (Bontaz experiment). Simulating atomization requires a well-chosen mesh size, especially near the nozzle, to capture the complex physics of an atomization onset and to keep the mass loss to a minimum. The different setups have been successfully compared to experiments. With the highest mesh resolution, the obtained jets were rich in detail. The number and position of the small droplets can be used to statistically characterize the atomization profile for a set of design parameters.

The second test case involved an oil jet impinging a standard gasoline piston without a cooling gallery. Both a static and moving piston were considered. The simulation results exhibit realistic behaviors when spreading underneath the piston surface and are in agreement with the existing impingement theory. For the static piston, a compelling comparison between the photographs of the experiment and the simulation result for both a laminar (T = 30C) and an atomized (T = 100C) jets were provided. The other outcome of this comparison is that the simulation shows further details, e.g., that the oil does not reach the entirety of the piston surface for a static, non-moving piston. Once qualitative results were obtained, numerous parameters have been simulated, ranging from laminar to atomized jets. The simulations closely match the experimental data for various scenarios. For laminar jets, the piston wall temperature, the type of nozzle, and the nozzle diameter seem to have a negligible impact on the cooling performance. Furthermore, the height of the elements in the boundary layer on the piston surface has an impact on the cooling performance until the height is small enough (0.02 mm in our case). The empirical equation devised in the initial report is also valid for our simulations. The piston motion has been successfully added to the previous static test case for two oil temperatures (30 and 60C). The results show a significant improvement in cooling performance (2-fold higher). The piston motion, like in the cooling gallery piston test case, improves the oil spreading, and the oil reaches parts of the surface underneath the piston that it did not reach in the static case. There is a need for more simulations of design parameter variations to extend the Nusselt number empirical equation to include the effects of the piston motion.

Finally, a simulation with a laminar jet interacting with a moving piston with a cooling gallery has been investigated. During several piston strokes, the cooling gallery slowly fills up until saturation. Comparing the oil-filling ratio of the cooling gallery with the literature shows good agreement. Results of a VOF model with the CFD software STAR-CCM+ used in the Ford CAE workflow have been compared to the new level set method. The results are similar for laminar jets despite using different computational approaches (level set versus volume of fluid method). For low RPM (2,000 rpm), low volume flow rate (1.25 L/min), the total power and oil filling ratio values obtained with the level set and VOF methods are slightly different because of the assumptions made on the numerical methods (FEM versus FVM).

Further improvements of the wetting model in XNS are necessary. For low RPM, high volume flow rate (1.875 L/min), the values obtained with the level set method are again higher than with the VOF method. When compared with the lower volume flow rate, the current flow rate leads faster to a saturated gallery with a higher effective total power and OFR, which is expected from the comparatively higher amount of oil injected in the gallery. For high RPM (3,000 rpm) and high volume flow rate (1.875 L/min), the cooling remains practically unchanged even though the saturated OFR is lower than the one obtained at lower engine speed. This result highlights the importance of the relative velocity between the oil and the piston.

As a general conclusion, the project tackled various problems related to oil-jet piston cooling. It has been proven that modern CFD tools like the level set method are versatile and give significant insights into the processes involved in piston cooling. New computational capabilities make it possible to simulate such complex flows with an unprecedented amount of details.

Selected honors

- Elected (ELGETI) as officer of the Female Researchers Chapter of International Association for Computational Mechanics.

Selected conference participations

- Keynote, Finite Elements in Flow Problems 2019, Chicago, IL, USA, March 31-Apr 3, 2019
- US National Congress on Computational Mechanics, Austin, TX, USA, Jul 29-Aug 1, 2019
- Japan Society of Civil Engineers Seminar, Tokyo, Japan, Oct 8, 2019
- Keynote, Asian Pacific Congress on Comp. Mechanics, Taipei, Taiwan, Dec 17-20, 2019

Selected national and international cooperations

- ANSELM HOPF, Ford Research Center Aachen, Germany
- KAZUO KASHIYAMA, Chuo University, Tokyo, Japan
- WOLFGANG WALL, Technical University of Munich, Germany

Selected publications

- WENDLING L, BEHR M, HOPF A, KRAEMER F, WEBER C, & TURNER P.
  CFD Simulation of Oil Jets for Piston Cooling Applications Comparing the Level Set and the Volume of Fluid Method
  SAE Int. J. Adv. & Curr. Prac. in Mobility and SAE Technical Paper 2019-01-0155, SAE International, 2019, 1, 550-561 (+ presentation)
- WENDLING L, BEHR M, HOPF A, KRAEMER F, WEBER C, TURNER P.
  CFD Simulation of Oil Jets for Piston Cooling Applications
  Siemens Digital Industries Software 2019 Simcenter Conference, Amsterdam, Netherlands, 2019
- Patent proposal 218-0266: Volcano-shaped inlet of piston oil-cooling gallery
- Patent proposal 218-0275: Flap valve at outlet of piston oil-cooling gallery
- Patent proposal 218-0314: Pockets labyrinth at outlet of piston oil-cooling gallery
- Patent proposal 218-0379: Helix shape of piston oil-cooling gallery

Engineering Sciences

Direct Numerical Simulation of Görtler Vortices in Hypersonic Flow over Compression Ramps

Project ID: jara0181
IGOR KLIOUTCHNIKOV
SHIBIN CAO
Shock Wave Laboratory,
RWTH Aachen University

Project Report

In this project, the Görtler vortices induced by shock wave-boundary layer interaction on the compression ramp were investigated using direct numerical simulation (DNS) for three ramp angles of 15, 20, and 25 deg. The freestream Mach number and the Reynolds number based on the flat-plate length were 7.7 and 8.6·105, respectively. A mesh resolution of 151 million grid points was considered. The results have been proved to be grid-independent. Several validation tests were performed, and good agreement was achieved by comparing with experiments and theories.

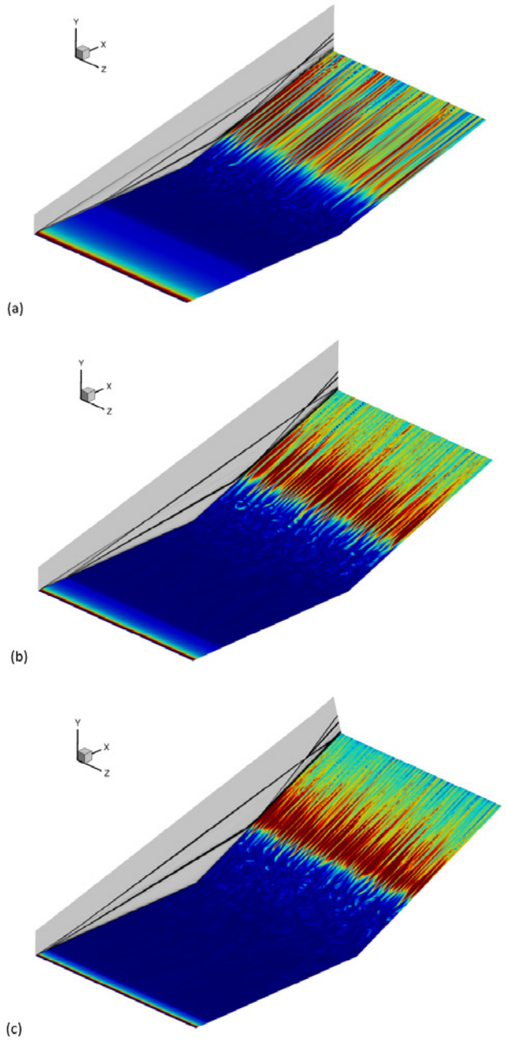

Görtler vortices were observed over the ramp for all three cases and well captured by DNS. For the considered ramp flows, both the flow inside the separation bubble and the Görtler vortices downstream of reattachment show unsteady behaviors. A spanwise variation of the heat flux is present on the ramp surface downstream of reattachment. The Görtler vortices visualized by streamlines in the wall-normal plane indicate wavelengths of 3.1, 2.7, and 2.5 mm for ramp angles of 15, 20, and 25 deg, respectively.

Figure 1: (a), (b), (c): The above figures show the heat flux distribution on the compression ramp surface. The free-stream Mach number and unit Reynolds number are 7.7 and 8.6e6, respectively. The ramp angles are (a) 15°, (b) 20°, (c) 25°. The spanwise (z direction) heat flux variation is induced by the Görtler vortices generated downstream of reattachment position due to the local flow curvature at reattachment. At z = 0, density gradient is shown to indicate the shock system and the extent of the separation bubble. With an increasing ramp angle, the separation bubble size increases, leading to a rise of the flow curvature. Therefore, the Görtler vortices are more unstable and the wavelength becomes smaller. The transition to turbulence also takes place earlier on the ramp.

Three-dimensional structures were found in the separation bubble, leading to a corrugated reattachment with a series of singularities (nodes and saddle points) distributed in spanwise direction. The flow reattachment enhances the downstream evolution of Görtler vortices.

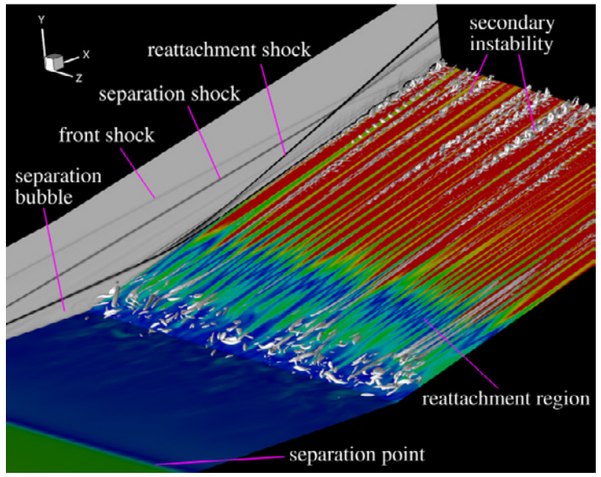

Figure 2: Hypersonic compression ramp flow visualised by density gradient, Mach number, and iso-surface of Q criteria.

Selected conference participations

- Shibin Cao, Igor Klioutchnikov, and Herbert Olivier, Influence of the separation bubble flow at a compression ramp on Görtler-type vortices, 32nd International Symposium on Shock Waves / ISSW32, Singapore, July 14-19, 2019.

Selected publications

- CAO S, KLIOUTCHNIKOV I, OLIVIER H.
Görtler Vortices in Hypersonic Flow on Compression Ramps.
AIAA Journal. 2019;Vol. 57, No. 9

- CAO S, KLIOUTCHNIKOV I, OLIVIER H.
Influence of the separation bubble flow at a compression ramp on Görtler-type vortices.
Proc. 32nd Int. Symposium on Shock Waves. Singapore. July 2019;899-909.

Engineering Sciences

DNS of hydrogen-air self-ignition in supersonic planar shear layer

Project ID: jara0192
IGOR KLIOUTCHNIKOV
Shock Wave Laboratory,
RWTH Aachen University

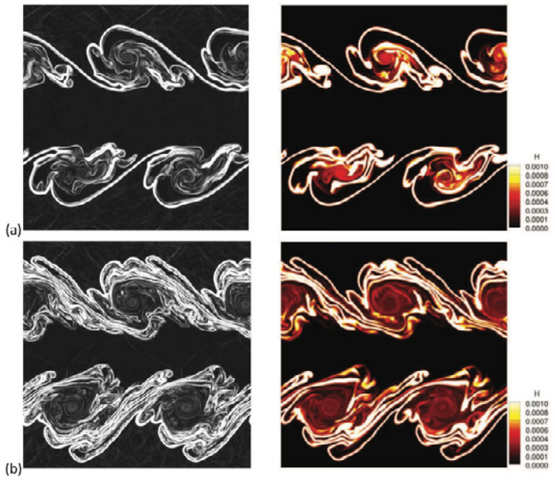

Figure 1:
Temporal evolution of 2D H2-air reacting supersonic shear layer, seven species, eight reactions model, Schlieren (left) and H-radical mass fraction (right):
(a) WENO5,
(b) WENO6o.

Project Report

For DNS (Direct Numerical Simulation) of three-dimensional compressible multicomponent reacting flow, a new in-house solver KICK (Kinetics Computational Kernel) has been developed.

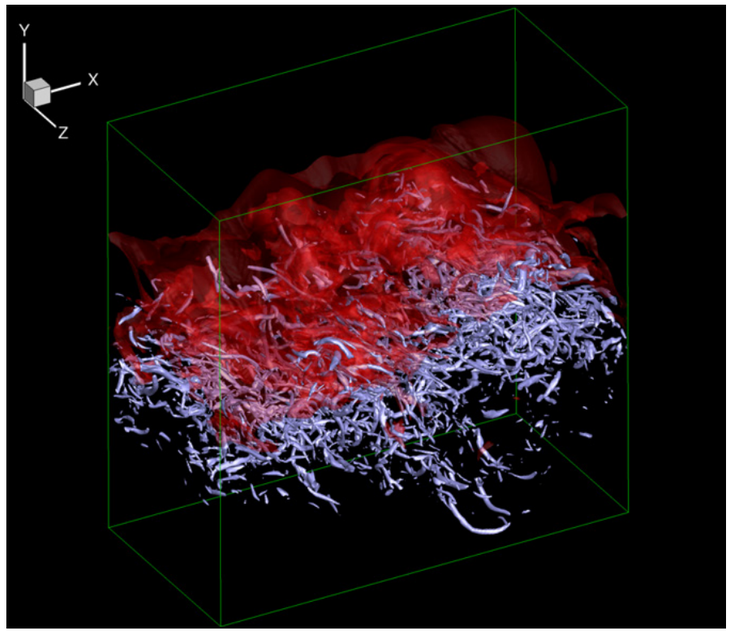

Figure 2: Temporal evolution of supersonic hydrogen-air combustion in a planar shear layer for a convective Mach number of 0.46. The figure shows instantaneous OH and Q iso-surfaces of a H2-air reacting supersonic shear layer, WENO6o scheme and seven species, eight reactions model.

The KICK solver allows the simulation of flows with chemical kinetics, like for combustion processes and high enthalpy flows.

A comprehensive study of a planar shear layer flow for one constant convective Mach number and various density and velocity ratios across the shear layer was carried out. The effects of vortical structures and hydrogen/air self-ignition on the stability of the supersonic planar shear layers was also analyzed.

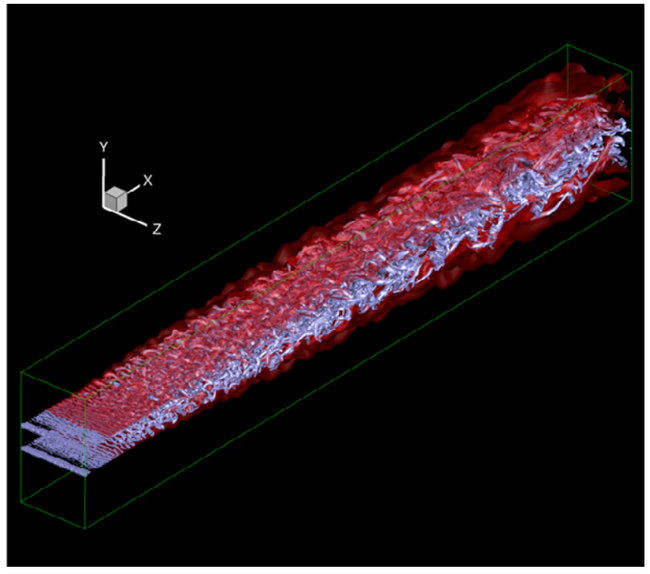

Figure 3: Spatial evolution of a supersonic 3D H2-air mixing layer with self-ignition. The figure shows instantaneous OH and Q iso-surfaces, WENO5 scheme, seven species, eight reactions model.

Selected conference participations

- IGOR KLIOUTCHNIKOV AND HERBERT OLIVIER
  DNS of Hydrogen-air Self-ignition in Supersonic Planar Shear Layers,
  32nd International Symposium on Shock Waves / ISSW32, Singapore, July 14-19, 2019.

Selected publications

- KLIOUTCHNIKOV I, OLIVIER H.
  DNS of Hydrogen-air Self-ignition in Supersonic Planar Shear Layers.
  Proc. 32nd Int. Symposium on Shock Waves. Singapore. July 2019;2687-2723.

Engineering Sciences

CFD Simulations Ecurie Aix

Project ID: rwth0213
UWE NAUMANN
Software and Tools
for Computational Enginering, i12,
RWTH Aachen University

MORITZ MUMM
MARCO FRANZREB
ENES ÖKSÜZ
BADIH TABET
BEN SPOEK
SIMON KINKEL
JOSHUA KONSTANTINOS BOLTEN
MIGUEL CIPRIANO GARCES
JAVIER MANCHEÑO DEVIS
JOHANNES LOSACKER
JAN KLINGENSTEIN
RICHARD WULF
FELIX DIEPERS
Ecurie Aix - Formula Student Team,
RWTH Aachen e.V., Germany

Project Report

Introduction

Every year we, as the Formula Student Team of RWTH Aachen University, develop a completely new electric race car and revise a previous car to be able to drive autonomously. For our Aerodynamics team, the electric vehicle is the main focus. We try to find the best geometries for our car within the regulatory constraints and while keeping performance compromises with other design areas in mind. To help us design and improve our aerodynamic package, we carry out extensive CFD simulations, using Siemens Star-CCM+.

Project Details

Over the years, our simulations have been developed further and further to improve accuracy, resulting in several simulation approaches being used currently, depending on the desired information about the different aerodynamic phenomena and influences on the racetrack. These include a straight-line half car simulation using a symmetry plane which consists of around 50 million cells, a full car simulation with a yawed car and turned front tires as well as a cornering simulation, the latter two both using around 100 million cells. In our development process, we mainly use the straight-line and yaw-angle simulations as they provide much quicker turnaround times and yield enough information. The yawed car is used to include the influence of various driving states on our aerodynamic performance. This is especially important because the purpose of our high-downforce vehicle concept is to increase performance in grip-limited driving conditions, which means those are also the situations in which the car state differs most from the neutral state. This is also the reason for the development of the cornering simulation. Here, the car can be fully transformed to represent real driving situations in corners, including a curved wind tunnel which makes sure that the air flow relative to the vehicle matches the real air flow during cornering. For these simulations we currently use a segregated flow solver for incompressible flow with the realizable k-epsilon turbulence model while pursuing a low wall-y+ treatment.

Apart from the external aerodynamics, we also use CFD simulations for the design of our cooling systems. These include a water cooling circuit for our four electric motors and the corresponding inverters as well as an air- cooled battery. Apart from system simulation in MATLAB Simulink and Siemens Amesim, we use thermal CFD simulations to analyze their behaviour.

Achievements

Over the course of 2019, we put a lot of effort in developing our car, but also in developing our simulations. Especially the cornering simulation and thermal cooling simulations were a point of focus. We were able to set up our cornering simulation based on the best practices advised by Siemens and then to start adjusting refinement regions so they alter their shape with varying cornering radii. We also looked at different initialization settings like turbulence initialization and seeding to reduce computation time.

To reduce the effort for our developers, we developed scripts which automatically run mesh, simulation and post- processing jobs on the CLAIX18 with interdependencies. After the process ends, our developers can download a folder which contains scenes and post-processing pictures. These are used to analyze the flow field and to identify areas that can be improved.

0n the side of the thermal simulations, we formed a cooperation with Siemens to develop a co-simulation of Star-CCM+ and Amesim. This unsteady simulation is able to calculate the temperatures in our battery over the course of a whole Endurance run, the longest discipline at our competitions. The simulation uses a battery model based on cell test data which enables it to compute the transient behaviour of the battery pack. This helps us to find a better design for our battery cooling. At the same time, it gives us the opportunity to predict our battery temperatures at the competition in the prevailing ambient conditions and thus makes it possible to adjust our driving strategy to extract the maximum overall performance from our vehicle.

In addition to the development in the core simulations, we also conducted some tests with tools that could potentially become valuable in the future and could provide the opportunity to quicker converge to a beneficial design and find even more optimized solutions. The most promising tools we tested and partially started to use already are design manager studies and the adjoint solver method. The design manager automatically executes several simulations with varying parameters at the same time while the adjoint solver coupled with mesh morphing makes it possible to automatically 0 tiMIZP a part s geometry.

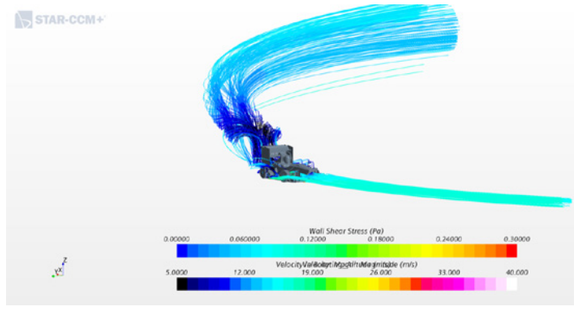

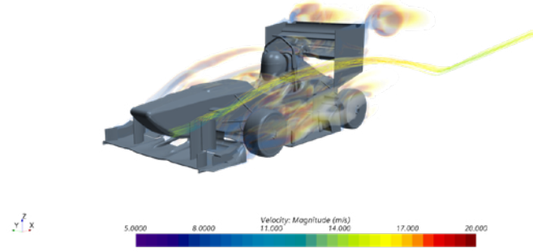

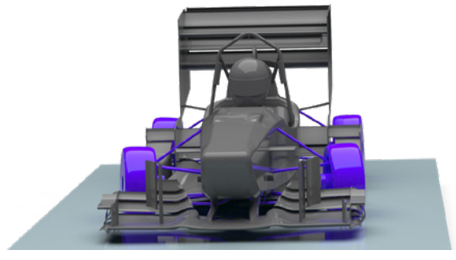

Even though improvements in our simulations can help us find better solutions and reduce development effort in the future, the main goal for our aerodynamics group, as for the whole team, is always to improve our current race car. For this season, we constrained ourselves to reusing old wing profiles and geometries, but we still managed to increase our downforce by three percent while keeping the same aerodynamic efficiency.

Furthermore, we improved our water cooling system by 46 % in terms of flow resistance resulting in a much greater water mass flow and higher heat transfers. This means we are able to run at higher power and recuperation values, allowing a quicker race time.

Large-Eddy Simulations of fuel injection, combustion, and pollutant formation in compression ignition engines

Project ID: jara0188
MARCO DAVIDOVIC
MATHIS BODE
HEINZ PITSCH
Institute for Combustion Technology (ITV),
RWTH Aachen University

Project Report

Two simulation cases have been targeted within this project. First, a high-pressure vessel fuel injection has been computed. Inert spray simulations have been used for parameter calibration in order to reduce the computational effort assuming that the chemical reactions do not strongly affect the spray penetration prior to ignition. Afterwards, the identified parameter set has been applied to the reactive simulation and validated against the experimental data. Both liquid and gas penetration lengths are in reasonable agreement with the experimental results.

Figure 1a) shows a quantitative comparison of the oxygen species fields, which have been obtained by the simulation and by laser-optical measurements. The experimental results have been ensemble averaged over multiple injection events. In order to avoid the computation of multiple LES realizations, the simulation results have been temporally averaged after the spray reached a quasi-steady state. The effect of the temporal averaging procedure and the location of the laser sheet can be seen in Figure 1b. Full engine simulations have been performed for DnBE after the calibration of the spray model. The compression until start of injection (SOI) has been computed using the in-house RANS solver ACFlux.

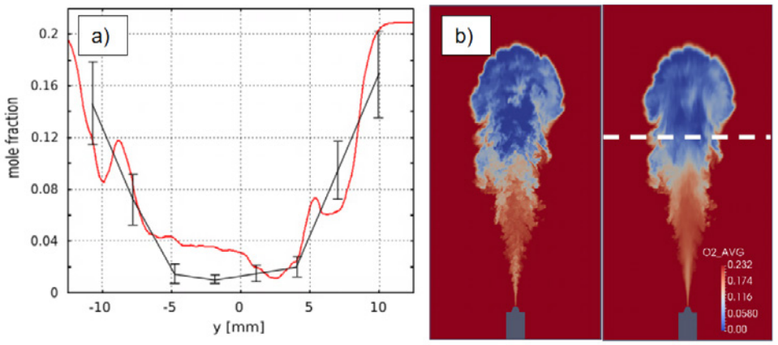

Figure 1: (a) Comparison of experimentally and numerically obtained oxygen fields 50 mm downstream the injector orifice (Ensemble averaged experimental results in black / Temporally averaged simulation results in red)
(b) Simulated oxygen mass fraction field.
Left: Instantaneous field / Right: Temporally averaged field

The velocity and energy field have been interpolated onto the LES grid. Zero-flux boundary condition has been applied for internal energy due to stability issues arising from the Dirichlet boundary condition at the moving piston. The spray model parameters of the calibrated spray chamber simulations have also been applied in the engine case. The numerical grid consists of 30E6 cells at SOI. During the simulation, a maximum number of 600E3 Lagrangian parcels have been present in the computational domain. The flamelet discretization and chemical mechanism have been chosen according to the high-pressure spray chamber setup.

A comparison of the simulated pressure trace and the experimental data is shown in Figure 2a. It can be seen that the ignition delay and early combustion phase are in very good agreement with the experimental results. However, at roughly 4° a TDC, the LES begins overpredicting the in-cylinder pressure. In Figure 2b, the instantaneous temperature and mixture fraction fields are shown for several crank angles. Starting at 4° a TDC, high temperatures can be observed close to the piston wall and hence, high wall heat losses can be expected. Since adiabatic walls are enforced in the simulation, it can be concluded that deviation between experiments and simulation is caused by wall heat losses.

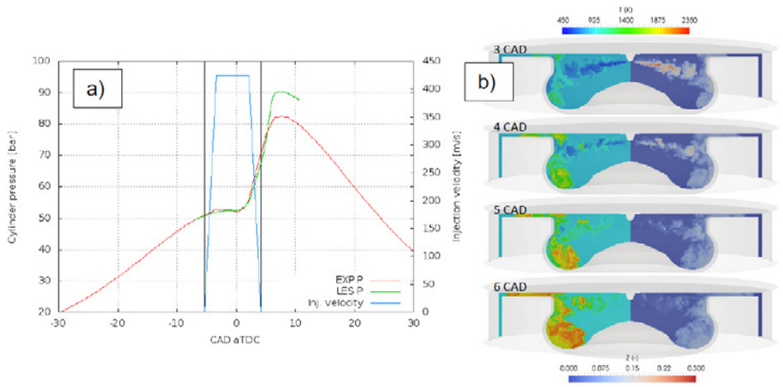

Figure 2: (a) In-cylinder pressure over crank angle (after top dead center) and modeled injection rate.
(b) Instantaneous flow fields at different crank angles.
Left: temperature / Right: mixture fraction.

Selected conference participations

- M. BODE, M. DAVIDOVIC, J.H. GÖBBERT, B. DICK, P. OFFENHÄUSER, C. TERBOVEN, M.S. MÜLLER, T. LIPPERT, M.M. RESCH AND H. PITSCH.
  Towards clean propulsion with synthetic fuels: A cluster-modularized approach employing hierarchies of simulations and deep learning.
  In ISC High Performance, Frankfurt, Germany, June 16–20, 2019

Engineering Sciences

Spray Combustion LES of OMEX and OMEX/Diesel Blends

Project ID: rwth0381

HEINZ PITSCH
DOMINIK GOEB
Institute for Combustion Technology (ITV),
RWTH Aachen University

Project Report

Coupling the power sector with its growing share of renewables to the transportation sector is an essential pathway to decrease road traffic well-to-wheel CO_2 emissions. By using electrolysis to produce hydrogen, followed by a conversion into tailor-made liquid e-fuels, the advantages of liquid fuels in terms of energy density, storage, existing infrastructure, and mature engine technology can be retained. Additional emission reduction potentials can be realized by tailoring the synthetic fuel's properties. Oxymethylene ethers (OME_X) with the molecular structure $CH_3O(CH_2O)xCH_3$ have been proposed as a renewable replacement fuel or blend component for compression ignition engines. The formation of soot during combustion of OME_X is suppressed. Hence, the soot-NO_X tradeoff of classical diesel engines is eliminated, and a sizeable reduction in NO_X emissions can be achieved by raising exhaust gas recirculation significantly. More so, even blends of conventional diesel fuel with OME_X exhibit super-linear reduction of soot production, with soot emissions remaining negligible for up to 65 vol-% diesel in a blend.

Within this project,which was conducted in parallel and complementary to the computing project jara0200, the spray and ignition properties of neat OME_1 and n-dodecane as reference fuels, and a blend of these two fuels with 35 vol-% OME_1, as suggested in the literature as best compromise between soot reduction and deviation from diesel fuel properties, were investigated. Large-eddy simulations (LES) of spray formation and ignition were performed for the three fuels, validated against experimental results, and then used to analyze auto-ignition and soot precursor formation.

In this project, the calibration of the spray parameters and validation of the numerical models was performed, before the production runs of multiple LES realizations were computed in jara0200. Additionally, the super-linear soot reduction of soot precursors in the gas phase, which was found for the fuel blend, was investigated in more detail using a combination of LES and 1D flamelet computations.

In Table 1, the total mass of the most prominent soot precursors acetylene (C2H2) and polycyclic aromatic hydrocarbons (PAH) are shown for the different fuels. Even though the blend contains only 35 vol-% OME_1, the soot precursor mass reduces by a factor of around 7 and 27, respectively.

	n-dodecane	Blend	OME_1
C_2H_2	1.7E-8	2.5E-9	2.2E-11
PAH	1.6E-10	5.9E-12	4.2E-16

Table 1: Total acetylene (C_2H_2) and PAH mass in kg in the computational domain at 0.4 ms for n-dodecane and the blend, and 0.8 ms for OME_1, respectively

Using the information about the mixture distribution in the LES in form of the probability distribution function (PDF) of the mixture fraction and 1D flamelets under the same conditions, the reason for this superlinear reduction was investigated, see Figure 1.

The solid lines display the PDF of filtered mixture fraction Z in the LES, i.e. how likely it is to encounter a specific mixture of fuel and air. It can be seen that the differences between n-dodecane and the fuel blend are negligible except for very lean mixtures which are not

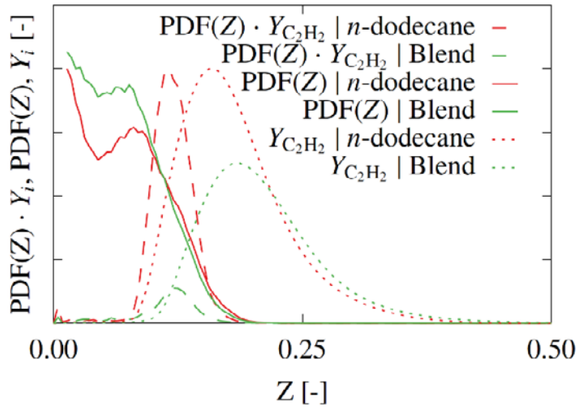

Figure 1: Normalized mass fractions of C_2H_2 for n-dodecane and the blend in mixture fraction space averaged overall realizations and flamelets together with the PDFs of mixture fractionin the LES at 0.4 ms and the resulting normalized convolutions.

relevant for soot formation. The LES was coupled to a chemistry solver, which solves the unsteady laminar flamelet equations in mixture fraction space, representing a locally laminar flame. The dashed lines correspond to the resulting distributions of the acetylene mass fraction in mixture fraction space. It can be clearly seen that the concentration of this soot precursor peaks in a rich mixture. Going from n-dodecane to the fuel blend, the maximum peak of acetylene mass fraction both reduces and shifts towards richer mixture fractions. The reduction of the peak alone accounts for about a factor of two in reduction of acetylene, however it is the small shift towards higher mixtures which results in a much smaller amount of acetylene in the flame. The dotted line shows the convolution of the PDF(Z) with the mass fraction distribution, with the integral of this function corresponding to the total mass in the physical LES domain.

It can be concluded that the significant reduction of soot precursor production with OME_1 is not only rooted in chemistry effects, represented by the reduction of the peak, but mainly also in the shift of the stoichiometry of the fuel. The oxygen content in the fuel blend leads to a higher most reactive mixture fraction, as less air is required for optimal combustion, and thereby also to a higher mixture fraction of maximum soot precursor production, which is less present in the mixing field of the spray. This is a valuable conclusion, at it is likely also applicable to other oxygenated fuels in fuel blends.

Selected publications

· GOEB D, DAVIDOVIC M, CAI L, PANCHARIA P, BODE M, JACOBS S, BEECKMANN J, WILLEMS W, HEUFER KA, PITSCH H.
Oxymethylene Ether-n-Dodecane Blend Spray Combustion: Experimental Study and Large-Eddy Simulations. Proceedings of the Combustion Institute. Accepted. 2020

Numerical Characterization of the Nozzle Internal Flow in the SpraySyn Dispersion Gas Nozzle using Large-Eddy Simulations

Project ID: rwth0419

HEINZ PITSCH
FABIAN FRÖDE
TEMISTOCLE GRENGA
Institute for Combustion Technology (ITV),
RWTH Aachen University

Project Report

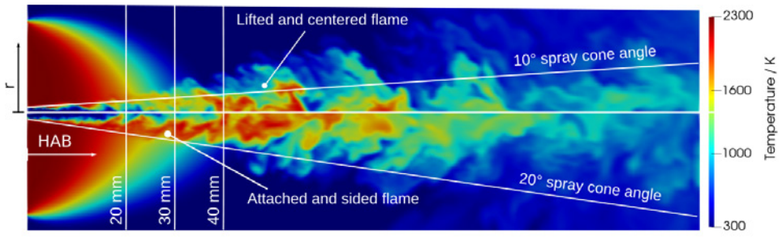

Figure 1

Two reactive Euler-Lagrange Large Eddy Simulations were performed with a controlled penetration of the droplets in order to investigate how spray characteristics influence local reaction conditions in a steady and stable operating burner for the coaxial nozzle configuration. The droplet penetration is controlled in the simulations by prescribing a maximum initial radial velocity for the droplets through the definition of a spray cone angle. The standard pure ethanol spray-flame was computed as no reaction mechanisms are available for ethylhexanoic acid. Two spray cone angles, 10 and 20 degrees, were studied with all other parameters constant. The two computed spray-flames show large qualitative and quantitative differences,which are illustrated by the instantaneous temperature fields on a cut plane reported here.

While for the 10 degrees case (top half in the first panel), a more lifted and centered spray-flame on the tip of the jet can be observed, the 20 degrees spray cone angle leads to a spray-flame which is attached to the pilot flame and is oriented towards the sides. Even though, the used combustion model is capable of capturing local extinction and re-ignition phenomena, no spray-flame pulsations could be identified on long time-scales in the simulations, thus it can be assumed that a steady spray formation with respect to spray cone angle and mass flow rate prevents spray-flame pulsations.

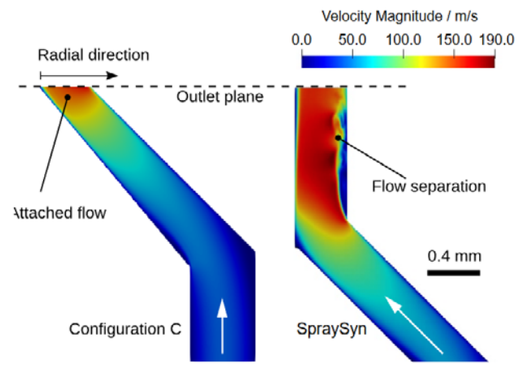

Figure 2

Aiming for a fundamental understanding of the impact of nozzle design variation on the resulting spray and spray-flame interaction, state-of-the-art predictive LESs were performed for“Configuration C”and “SpraySyn” nozzles. A strong acceleration of the oxygen along the axial direction of the nozzle (bottom to top) is clearly visible for both cases. Contrary to the SpraySyn nozzle, which shows a flow separation after the sharp edge at the outer wall and a recirculation zone, the new nozzle design leads to an attached flow at all times. The velocity statistics show significant differences.While the standard SpraySyn geometry leads to a shift of the average velocity profile to the inner wall,the other nozzle shifts the profile to the outer wall. The flow separation of the SpraySyn nozzle leads to large fluctuations at the outer wall of the nozzle while Configuration C shows almost no fluctuations.

One fundamental difference between both nozzle designs is, that the gas at the outlet of nozzle Configuration Con average has a radial momentum. The investigation of how those flow characteristics impact spray formation in detail will be conducted in the next project. Similarly to the experiments, simulations of the SpraySyn case showed a nozzle tip wetting. However, it was found that the interface capturing method proposed by LeChenadec and Pitsch (Journal of Computational Physics, 2013) leads to significant mass conservation errors close to the wall and in particular if the interface is in the vicinity to the gas inlet. This issue has been addressed during this project by a correction of the fluxes inspired by Owkes and Desjardins (Journal of Computational Physics, 2014). The new numerical algorithm is fully mass conserving and consistent boundary conditions can be formulated making the improved method suitable for the aimed DNS study. It is planned to complete the DNS study in the next project.

Selected conference participations

- F. FRÖDE,T. GRENGA, H. PITSCH, M. BIEBER, M. A. REDDEMANN, R. KNEER, R. TISCHENDORF, H.-J. SCHMID,
  Influence of Atomization on Particle Formation in Spray Flames,
  SPP1980-Spraysyn Meeting, Duisburg, Germany, September 23-24, 2019.

Five selected national and international cooperations

- RICARDO TISCHENDORF, HANS-JOACHIM SCHMID,
  PTV, Paderborn University
- MALTE BIEBER, MANUEL A. REDDEMANN, REINHOLD KNEER,
  WSA, RWTH Aachen University

Engineering Sciences

Materials Engineering | DFG 405

Numerical simulation of powder filling and pre-consolidation procedures in the PM HIP

Project ID: jara0195/rwth0492

CHRISTOPH BROECKMANN
YUANBIN DENG
Institute for Materials Applications in Mechanical Engineering (IWM), RWTH Aachen University

Project Report

Hot Isostatic Pressing (HIP) is a process to densify powder or cast and sintered parts of metals or ceramics in a furnace at relatively high pressure (100-200 MPa) and high temperatures. Although Powder Metallurgy HIP (PM HIP) technology has already been developed for decades, its application in industry is still limited due to the high cost, low rate of final products, and the long delivery time. Nevertheless, its advantages in producing 100% dense and/or near-net-shape (NNS) components is obvious, as it can reach high cost efficiency through the reduction in machining costs. In this perspective, the prediction of the final shape of the HIPed components is very important, however, the accuracy of the prediction is influenced by numerous factors, such as shape of the capsule, size of the powder particle, initial powder distribution after filling, material properties, and HIP processing parameters. Among these factors, the filling density is strongly influenced by the powder encapsulation process (Figure 1). The conventional powder encapsulation process prior to HIP generally consists of three steps: capsule manufacturing, powder filling and pre-consolidation, and capsule evacuation and sealing. The inter-particle friction increases following the increase of the surface area of the powder particles, which is dependent on their morphology and size. The higher the inter-particle friction is, the lower is the flow of the powders and the filling density. This results in a powder density distribution in the capsule.

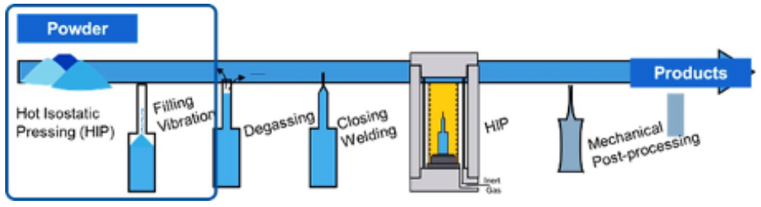

Figure 1: PM HIP production chain.

With the improved simulation capabilities, the Discrete Element Method (DEM) was developed and applied to simulate the powder technological process. The time-driven DEM is employed to describe the motion of an ensemble of particles by time integration of the Newton's equations of motion. The particles interact via explicitly defined force laws, which can be affected by external forces such as gravity. Nowadays, the powder filling and subsequent pre-consolidation process (vibration and tapping) are also possible to be simulated by DEM. In this way, it is possible to numerically predict the density distribution in the HIP capsules, which can then be mapped into a Finite-Element (FE) Model to simulate the subsequent powder densification process during HIP.

The scheme of a virtual HIP simulation loop of the PM HIP production chain is shown in Figure 2. To predict the anisotropic shrinkage and to provide instructions for achieving NNS components by HIP, an integrated simulation tool based on DEM and FEM was developed. The initial powder relative density distribution inside a capsule after filling is first obtained by DEM calculations. This in turn generates an initial density field of the powder distribution, which can be implemented in the FEM model by assigning the density distribution to each spatially corresponding meshed element using a MATLAB code. In this way, the anisotropic shrinkage of the HIPed capsules can be predicted precisely by the HIP simulation tool. The densification model, which integrates primary and secondary creep deformation mechanisms in the whole temperature and pressure range, is implemented using UMAT subroutines (Fortran code) in the commercial FE-software ABAQUS. The deformation and the density distribution are simulated in macro-scale after the implementation of the properties of the powder and capsule materials.

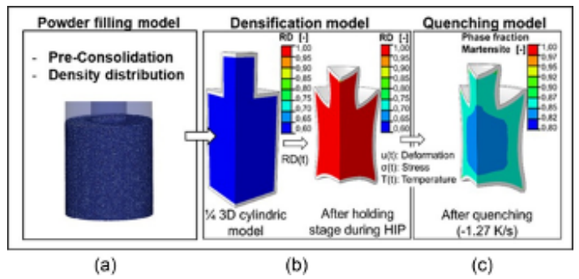

Figure 2: Virtual HIP simulation loop of PM HIP production.

In the HPC-Project, the coarse-grain method was developed and successful applied to build the DEM-model of the powder. In this method, the powder particles are scaled-up instead of being generated in the one-to-one grain level. However, during the scaling-up, the new built particle system should keep the same physical performances of the powders by adjusting the powder properties (e.g. friction coefficient and cohesion energy density). Through this adjustment, the new particle system can achieve the same packing density and repose angle as the original sized powder. After iterations of the adjustments, a coarse-grain system with a scaling-up factor of 15 was chosen for further simulations, to also save the costs of the computing resources.

Figure 2(a) shows the results of an example of the particle filling simulation, in which the density distribution was calculated using Voronoi method by MATLAB. The relative density distribution on the cross section of the capsule is shown in Figure 3(b), from which a high-density region in the middle of the capsule can be clearly observed. In contrast, the corners close to the filling tube show a relatively lower filling density. Experimental results also revealed the same phenomenon that the corner regions (red rectangle marked areas in Figure 3(a)) show a poor filling density. The agreement of the simulated and experimental results confirms that the powder filling process can be simulated by the particle system with the coarse-grain method.

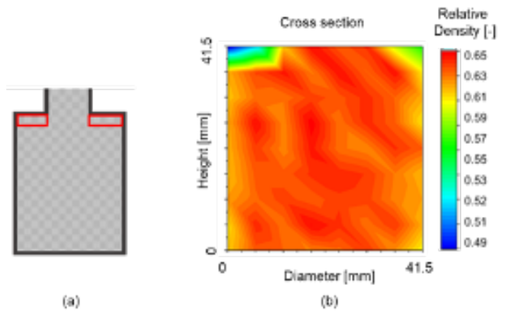

Figure 3: Powder density distribution in the capsule.

In this project, many numerical studies have been conducted based on Discrete Element Method. With the help of these numerical methods, the HIP process chain from powder to component could be modelled as a basis for the virtual product development. The application of these models would significantly reduce the needs for the often-costly prototypes and the trial-and-error processes that are nowadays inherent to the capsule design and final shape prediction.

Engineering Sciences

Materials Science | DFG 406

Quantum mechanically guided materials design

Project ID: jara0131
JOCHEN M. SCHNEIDER
DENIS MUSIC
PAVEL ONDRAČKA
SIMON EVERTZ
APARNA SAKSENA
DIMITRI BOGDANOVSKI
LOAY ELALFY
SIDA LIU
MARSHAL AMALRAJ
Materials Chemistry,
RWTH Aachen University

Project Report

At Materials Chemistry, our goal is to contribute towards the basic understanding required to realize the synthesis of tailor-made structural and functional materials. Computational tools based on quantum-mechanical methods provide a description of phase stabilities of materials, their electronic structure and macroscopic materials properties (such as elastic moduli or thermal conductivity). An array of analysis tools including atom probe tomography, scanning tunneling electron microscopy, X-ray diffraction, energy-dispersive X-ray spectroscopy and X-ray photospectroscopy, among others, enable full-spectrum characterization of experimentally synthesized materials, resulting in our core approach of quantum-mechanically guided materials design. Many novel materials classes, ranging from nitrides and high entropy alloys to nanolaminates and thermoelectric devices were explored in this JARA project based on several projects funded by the DFG. The results have been communicated in peer-reviewed, international scientific journals.

We investigated the anomalous thermoelastic behavior of bcc V, Nb, Ta as well as fcc Pd and Pt. A density functional theory (DFT) based correlative investigation between V, Nb, Ta, Pd and Pt with anomalous thermoelastic properties and Mo and Cu with ordinary behavior revealed a high density of states (DOS) at the Fermi level to be a necessary but not sufficient condition for anomalous thermoelastic behavior. In addition, anomalous metals in contrast to ordinary metals reallocate electronic states in the vicinity of the Fermi level upon lattice distortion, causing an increase in bond strength as identified by crystal orbital Hamilton population analysis. Hence, the combination of high DOS and electronic reallocation upon lattice distortion was identified to be the physical origin for anomalous thermoelastic behavior in metals.

In another, purely computational, study of thermoelectrics, we explored their potential application as biomedically relevant materials via investigation of the adsorption energy and analysis of the atomistic process upon adsorption of aspartic acid, a common amino acid in mammals that, as part of the cell membrane is relevant for cell adsorption, and thus for biocompatibility. A range of room-temperature thermoelectric materials were modeled in this study. A combination of ab initio molecular dynamics runs modeling the aspartic acid molecule in close vicinity of a thermoelectric surface, and subsequent static density functional theory calculations performed after adsorption was used. Based on the results, MgAgSb and TiO2:V are suggested to be biocompatible, opening the pathway to further studies and possible applications.

The $CuInSe_2$ (001)/GaAs(001) interface was studied using DFT, where GaAs is a common substrate to grow semiconductive $CuInSe_2$. The Se/Ga interfacial stacking is preferred, caused by the strong Se-Ga. Furthermore, the interaction of intrinsic (Cu and In vacancies and antisites) and extrinsic (Ga, O, H, and C) point defects in $CuInSe_2$ with the interface was evaluated. They segregate at the interface except from the In antisite and Ga, being a frequent dopant. $CuInSe_2$ on GaAs exhibits a compressive strain of 1.2 % so that large atoms, such as In, are not favored at the interface, minimizing the strain energy. Moreover, Ga forms stronger bonds in the bulk region than at the interface, while the opposite occurs for residual gas impurities O, H, and C. These results are relevant for the transport properties of photovoltaic and thermoelectric $CuInSe_2$ based devices.

Further calculational efforts done in this project period included calculations of elastic properties of MoAlB, surface binding potential of sputtered species of Mo_2BC, phase stability, magnetic moments of the corresponding stable states and the spin polarized DOS calculations on the FeMnCoCrAl-based system for various Al concentrations, and prediction of the metastable phase formation of TiAlN based on combinatorial magnetron sputtering experiment.

It is not possible to list here all of the important results obtained in the framework of this project, however we stress again, that, as highlighted in the introduction, the quantum mechanical calculations are crucial for both the design and understanding of novel coatings and materials and would not be possible without HPC resources.

Selected honors, prizes, awards

- Jochen M. Schneider, Appointed member of the Henry Royce Institute Strategic Facilities Advisory Board, University of Manchester, Manchester, UK, https://www.royce.ac.uk/about-the-royce/
- Jochen M. Schneider, Faculty 5 teaching award, RWTH Aachen University; For outstanding didactics and exemplary implementation of modern teaching methods.
- S. Evertz, Design of thin film metallic glasses with superior fracture toughness, Best poster award at 26th International Symposium on Metastable, Amorphous and Nanostructured Materials (ISMANAM-2019), Chennai, India

Selected conference participations

- J.M. SCHNEIDER
  Tracking phase changes in Cr2AlC by in-situ resistivity measurements, Invited talk at the 43rd International Conference and Exposition on Advanced Ceramics and Composites (ICACC) 2019, Daytona Beach, Florida, USA, January 27- February 01, 2019
- J.M. SCHNEIDER
  Quantum-mechanically guided materials design and experimentally guided quantum mechanical calculations of short range-ordered thin film materials", Invited talk at the International Symposium of Metastable, Amorphous and Nanostructured Materials (ISMANAM), Chennai, India, July 08-12, 2019
- J.M. SCHNEIDER
  Quantum-Mechanically Guided Materials Design and Experimentally Guided Quantum Mechanical Calculations of Short Range-Ordered Thin Film Materials & a Critical Appraisal of High Entropy Ceramics, Invited talk at the International Thin Films Conference (TACT), Taipei, Taiwan, November 17-20, 2019

Selected national and international cooperations

- MICHAEL STUER, Manufactures Cartier Horlogerie, La Chaux-de-Fonds, Switzerland
- KEKE CHANG, Engineering Laboratory of Nuclear Energy Materials, Ningbo Institute of Materials Technology and Engineering, Chinese Academy of Sciences, Ningbo, Zhejiang, People's Republic of China
- RAJIB SAHU, Max-Planck-Institut für Eisenforschung GmbH, Düsseldorf, Germany
- DANIEL PRIMETZHOFER, Department of Physics and Astronomy, Uppsala University, Sweden

Selected publications

- MARSHAL A, PRADEEP KG, MUSIC D, WANG L, PETRACIC O, AND SCHNEIDER JM. Combinatorial evaluation of phase formation and magnetic properties of FeMnCoCrAl high entropy alloy thin film library. Scientific Reports, 9, no. 1, 1–11, 2019
- LIU S, CHANG K, MRÁZ S, CHEN X, HANS M, MUSIC D, PRIMETZHOFER D, AND SCHNEIDER JM. Modeling of metastable phase formation for sputtered Ti1-xAlxN thin films. Acta Materialia, 165, 615–625, 2019
- KEUTER P, MUSIC D, SCHNABEL V, STUER M, AND SCHNEIDER JM, From qualitative to quantitative description of the anomalous thermoelastic behavior of V, Nb, Ta, Pd and Pt. Journal of Physics: Condensed Matter, 31, no. 22, 225402, 2019
- MUSIC D AND STELZER B.
  Intrinsic thermal shock behavior of common rutile oxides Physics 1, 290, 2019
- ACHENBACH JO, SAHU R, VÖLKER B, HANS M, PRIMETZHOFER D, MILJANOVIC DJ, SCHEU C AND SCHNEIDER JM. Synthesis and Properties of Orthorhombic MoAlB Coatings. Coatings 9, 510, 2019

Quantum mechanically guided design of wear-protective coatings for polymer forming tools

Project ID: jara0151
JOCHEN M. SCHNEIDER
DENIS MUSIC
MARCUS HANS
PAVEL ONDRAČKA
DAMIAN M. HOLZAPFEL
HOLGER RUESS
LENA PATTERER,
Materials Chemistry,
RWTH Aachen University

Project Report

Within the framework of the Collaborative Research Center SFB-TR 87, we have investigated the interaction of amorphous TiO_2 and Al_2O_3 as well as mixed-phase Ti-Al-O substrates with adjoining polycarbonate monomers using ab initio molecular dynamics simulations during the current project period. Furthermore, the dependence of the mechanical properties of VAlN and TiAlN on residual stress was studied.

During production, polymers such as polycarbonate (PC) often adhere to metal surfaces of machines, leading to thermal and shear-induced degradation of the polymer and production losses. This degradation can be prevented via usage of protective coatings such as Ti-Al-O-N, significantly reducing PC adhesion, but an in-depth understanding of polymer-surface interactions is essential to optimize these coatings. Metal oxides such as TiO_2 and Al_2O_3, found in the top layer of Ti-Al-O-N-based coatings, can catalyze PC degradation, depending on crystal structure. To understand the role of this destructive effect counteracting the intended anti-adhesive properties, a combined experimental and theoretical study, using density functional theory simulations, of TiO_2, Al_2O_3 and mixed-phase Ti-Al-O was performed.
Ab initio molecular dynamics (MD) runs using the established liquid-quench algorithm were applied to ordered structural models of TiO_2, Al_2O_3 and Ti-Al-O, yielding amorphous structures. In these, a vacuum region was introduced and polycarbonate monomers placed next to the resulting surface. Subsequent MD simulations showed PC interaction with all three amorphous substrates, with bonds forming between surface metal atoms and O atoms in the PC molecule, in agreement with XPS measurements. This is illustrated in the snapshots of the simulation cells in Figure 1.

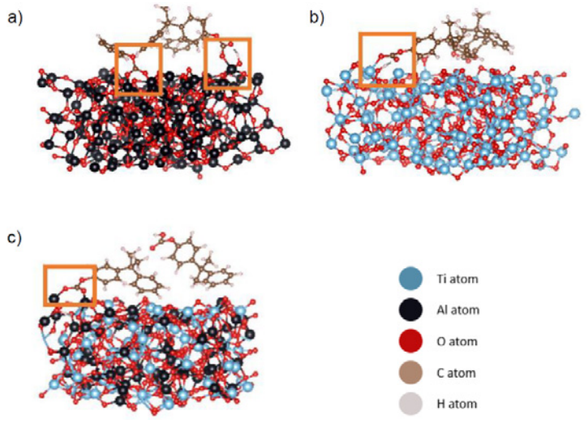

Figure 1: Snapshots of the final state of amorphous Al_2O_3 (a), TiO_2 (b) and Ti-Al-O (c) surfaces with two PC monomers after ab initio MD runs at 623 K.

For the Ti-Al-O surface, oxygen in PC binds to surface Al atoms only, indicating an energetic preference of the Al-O bond compared to Ti-O. In the case of two PC monomers, both form Al-O bonds at an amorphous Al_2O_3 surface, even at higher simulated temperatures (623 K and 1200 K), while for both amorphous TiO_2 and Ti-Al-O, only one of the monomers binds to the substrate at higher temperatures. Thus, amorphous Al_2O_3 exerts a stronger attraction upon polycarbonate than the other phases. Simultaneously, formation of hydroxides via adsorption of monomer H atoms at the surface and subsequent O-H bond formation occurs for all substrates, in good agreement with experimental results, and is most pronounced in TiO_2. Thus, in the framework of the SFB-TR 87, the basis for an understanding of surface-polymer interactions and classification of the substrate's adsorbent strength has been laid.

Another topic of investigation was the influence of residual stress on the elastic properties of TiAlN and VAlN. These materials are long-known hard protective coatings with parameters tunable by point defects and applying compressive residual stress. During their synthesis by physical vapor deposition (PVD), the deposition geometry modulates their chemical composition due to variation in the plasma flux. We investigated this relationship by means of evaluating the elasticity and residual stress of PVD-synthesized Ti-Al-N for stationary and rotating geometries in a combined experimental/DFT approach, employing 128-atom supercells of $Ti_{0.5}Al_{0.5}N$ with different configurations for the latter. The bulk modulus as a function of temperature and stress state was obtained by applying the Debye-Grüneisen model and fitting to the Birch-Murnaghan equation of state, yielding DFT-derived elastic moduli and linear coefficients of thermal expansion. This data was compared to nanoindentation results and was shown to be in excellent qualitative agreement. The experimental deposition regime directly affects the residual stress, in turn controlling the elastic modulus.

For the VAlN system, an extensive and theoretically unexplained spread in elastic moduli from experiments, ranging from 254 to 599 GPa, is reported in literature. To identify its origin, we studied the effect of chemical composition, non-metal to metal ratio and stress state on the elastic modulus at room temperature via DFT. Higher Al content results in an increase in elastic moduli from 388 to 488 GPa, and both V/N ratio and stress affect the moduli by 6% and 13%, respectively, enabling direct prediction from the residual stress state for these metastable materials.

Selected honors, prizes, awards

- J. M. Schneider, Faculty 5 teaching award, RWTH Aachen University; For outstanding didactics and exemplary implementation of modern teaching methods.
- J. M. Schneider, Appointed member of the Henry Royce Institute Strategic Facilities Advisory Board University of Manchester, Manchester, U.K., https://www.royce.ac.uk/about-the-royce/

Selected conference participations

- M. Hans, Chemical composition-dependent phase stability of TiAlN, invited talk at International Thin Film Conference 2019, Taipei, Taiwan, November 18, 2019

Selected national and international cooperations

- Peter Awakowicz, Department of Electrical Engineering and Information Technology, Ruhr-Universität Bochum, Germany
- Guido Grundmeier, Technical Chemistry, Paderborn University, Germany
- David Holec, Department of Physical Metallurgy and Metallic Materials, University of Leoben, Austria

Selected publications

- HANS M, PATTERER L, MUSIC D, HOLZAPFEL DM, EVERTZ S, SCHNABEL V, STELZER B, PRIMETZHOFER D, VÖLKER B, WIDRIG B, ERIKSSON AO, RAMM J, ARNDT M, RUDIGIER H, SCHNEIDER JM.
  Stress-Dependent Elasticity of TiAlN Coatings. Coatings, 2019, 9(1), 24:1–24:12.
- RUESS H.
  Effect of target power density on the chemical composition, phase formation, and-mechanical properties of MAX-phase Cr2AlC coatings and prediction of mechanical properties of VAlN, Ph.D. thesis, RWTH Aachen University, 2019
- PATTERER L.
  Interaction of polycarbonate with amorphous metal oxide coatings at elevated temperatures. Master thesis, RWTH Aachen University, March 2019

Engineering Sciences

Quantum mechanically guided design of medium and high manganese steels

Project ID: JARA0152

JOCHEN M. SCHNEIDER
PHD, DENIS MUSIC
MARCUS HANS
FRIEDERIKE HERRIG,
Materials Chemistry,
RWTH Aachen University

Project Report

The present project was performed within the framework of the Collaborative Research Center SFB761 “Steel ab initio”, which was in its final year in 2019, with the role of interfaces in high-Mn steels, in particular between the main austenitic matrix and κ-carbide precipitates, being one of the central questions. It is known from other material systems that alloying elements frequently segregate towards interfacial regions, which may adversely affect phase stability and macroscopic properties such as corrosion resistance or plasticity, rendering the understanding of interfacial effects application-relevant.

We have employed density functional theory simulations on an atomistic level to contribute to a mechanistic understanding of interfaces by investigating segregation of Mn and C on (001) surfaces of a model Fe2.0Mn1.1Al0.9C0.6 κ-carbide slab, approximating experimental compositions. These surfaces were terminated either by Al and Fe/Mn (“Al-termination”) or by Fe/Mn and C/vacancies on the C site (“Fe-termination”), with random distribution of Fe and Mn on the corresponding 3c Wyckoff position generated via the special quasirandom structures (SQS) ansatz. The constructed models are schematically shown in Figure 1.

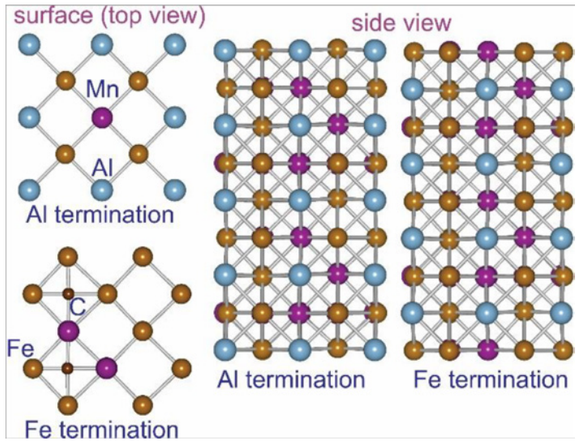

Figure 1: Surface models for the $Fe_{2.0}Mn_{1.1}Al_{0.9}C_{0.6}$ κ-carbide, with surfaces terminated either by Al and Fe/Mn (“Al-termination”) or by Fe/Mn and C/vacancies (“Fe-termination”), shown in top and side views. Al atoms are blue, Fe atoms brown, Mn atoms purple (large radius), C atoms brownish-purple (small radius).

Upon subtraction of the ground-state energy of a given surface slab with segregated atoms from that of the same system without segregated atoms, we obtained segregation energies. Those generally increased with a higher degree of coverage, ranging from ca. –270 mJ m^{-2} (20% Mn at available sites on the Al-terminated surface) to ca. –630 mJ m^{-2} (full Mn coverage of available sites at the Al-terminated surface) and were substantially higher for C, with approx. –1500 mJ m^{-2} at full C coverage of the Fe-terminated surface. While the energetic trend for Mn segregation on the Fe-terminated surface was less clearly pronounced, with a slight increase at maximum coverage after preceding decrease, and oscillating between approx. –300 and –550 mJ m^{-2}, the energy values remained negative throughout for all cases. This implies that both Mn and C segregateon all termination variants of the (001) κ-carbide surfaces, potentially inducing similar macroscopic effects,-described previously, as in other alloys.

We further explained the segregation energy trends as a function of the electronic structure, a unique possibility of ab initio atomistic simulations. While the very strong bonding between C and neighboring transition metal atoms was already known from literature, also reflected in the large segregation energy value mentioned above and explaining the difficulty of removal of C from the (001) κ-carbide surface, there was no such explanation for Mn. Analysis of the density of states (DOS) for the Al-terminated carbide with full Mn coverage, as the energetically most favored system for Mn segregations, revealed a strong asymmetry in the spin-up and spin-down components of the local DOS of Mn, significantly higher than that of Fe, suggesting a stronger polarization and an enhanced magnetic moment. Said moment indeed increases from an average value of 2.35 μB for Mn atoms in the bulk to 3.86 μB for Mn atoms at the surface, while no comparably significant increase is seen for Fe. Thus, the increased polarization of the Mn surface states implies electronic structure relaxation and stabilization, and is an argument for energetically favored segregation of Mn at the (001)surface.

The usage of such electronic structure analysis techniques, complemented with trends of the total energy, for model systems with minute, precisely controlled variations in composition or atomic arrangement/local chemical environment, can reveal causal relationships at an atomistic level. This capability is a unique selling point of computational approaches, not available via experimental means, and complements large-scale empirical findings from experiments. The resulting synergy from both approaches has long been utilized fruitfully at MCh.

Selected honors, prizes, awards

- JOCHEN M. SCHNEIDER: Appointment as member of the Strategic Facilities Advisory Board of the Henry Royce Institute, University of Manchester, UK
- JOCHEN M. SCHNEIDER: teaching award for outstanding didactics and exemplary implementation of modern teaching methods, Faculty 5, RWTH Aachen University

Selected conference participations

- JOCHEN M. SCHNEIDER, Quantum-mechanically guided materials design and experimentally guided quantum mechanical calculations of short range-ordered thin film materials, International Symposium of Metastable, Amorphous and Nanostructured Materials (ISMANAM), Chennai, India, July 08-12, 2019
- DENIS MUSIC ET AL., κ-carbide microstructures and the role of interfaces in high-Mn lightweight steels, HMnS 2019: The 4th International Conference on Medium and High Manganese Steels, Aachen, Germany, April 01-03, 2019
- FRIEDERIKE HERRIG, Elastic properties of austenitic Fe-Mn-X (X = C, Al, Si, Cr, Co, Ni, Cu), HMnS 2019: The 4th International Conference on Medium and High Manganese Steels, Aachen, Germany, April 01-03, 2019

Selected national and international cooperations

- RICHARD DRONSKOWSKI, Institute of Inorganic Chemistry, RWTH Aachen University
- WOLFGANG BECK, IEHK Steel Institute, RWTH Aachen University
- JÖRG NEUGEBAUER, Max-Planck-Institut für Eisenforschung, Düsseldorf, Germany
- TILMAN HICKEL, Max-Planck-Institut für Eisenforschung, Düsseldorf, Germany

Selected publications

- HERRIG F.
  Ab initio guided design of thin film model systems for FeMn based steels,
  PhD thesis, Materials Chemistry, RWTH Aachen University, 2019.

Engineering Sciences

Atomistic insight into metallurgical slags: high temperature properties investigation and new model development

Project ID: rwth0355

GUIXUAN WU
Institute of Energy and Climate Research Microstructure and Properties of Materials, (IEK-2), Forschungszentrum Jülich, Germany

MENGYI ZHU
Department of Materials Science and Engineering, Norwegian University of Science and Technology (NTNU), Norway

MICHAEL MÜLLER
Institute of Energy and Climate Research Microstructure and Properties of Materials, (IEK-2), Forschungszentrum Jülich, Germany

Project Report

In pyrometallurgical processes such as iron and steel making, slags are not only used to protect metals from oxidation, prevent heat loss, absorb impurities and inclusions from the metal melts, but also act as lubricant agents in continuous casting. To achieve these functionalities of the slags in different metallurgical processes with an optimum approach, the comprehensive information on specific physical, chemical and transport properties of slag melts is required, for example density, chemical activity, viscosity, and diffusivity. Sufficiently describing the slag properties as function of composition and temperature plays an essential role in process optimization and technology innovation.

The slag is usually a mixture of multi-component oxides like SiO_2, Al_2O_3, B_2O_3, CaO, MgO, Na_2O, K_2O, FeO, Fe_2O_3 etc. In the past decades, considerable attention has been paid to the investigation on composition-property relations. However, the mechanism for the local viscosity maximum around the fayalite composition, taken as an example, is not completely clear. Therefore, it is hard to describe such a local viscosity maximum as function of composition. It is now well known that slag property is strongly dependent on its microscopic structure at atomistic level. Direct observation of slag melt structure still remains an ongoing challenge due to the extreme high temperature (usually around 1500 °C) in metallurgical processes. Therefore, computational simulations as alternative to reveal the atomistic insight into metallurgical slags are promising and the slag melt structure obtained is a robust base to further describe the composition-property relations.

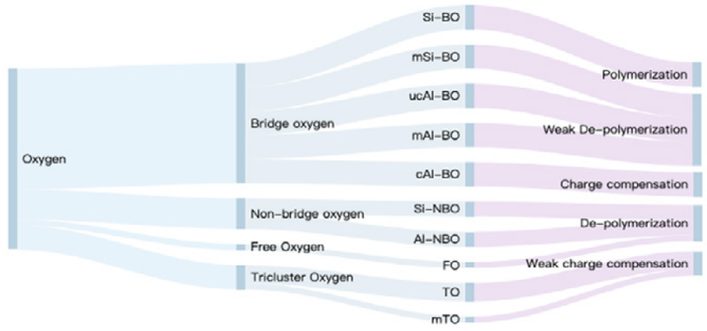

Figure 1: Classification of oxygen-based structural units, where symbol “m” indicates the oxygen is “modified” by at least one network modifier, “c” indicates the oxygen is “charge compensated”, and “uc” indicates the oxygen is charge uncompensated.

In the present work, molecular dynamic (MD) simulations have been performed to obtain the structural information including bond length, coordination number, and oxygen speciation, with which the property such as density, viscosity, and self-diffusion coefficient as function of composition can be well understood and further sufficiently modelled. Fig. 1 shows that the slag melt structure is described as ten novel self-defined oxygen-based units, which are functionally classified into five different groups, i.e. the polymerization, weak de-polymerization, charge compensation, de-polymerization, and weak charge compensation. These new structure units show unique features in describing slag properties especially with respect to the charge compensation effect. The variation in physical properties such as density and self-diffusion coefficient, as shown in Fig. 2, is correlated to the slag structural features.

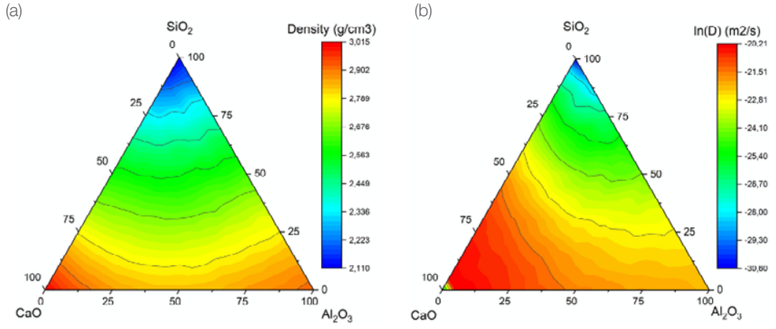

Figure 2: (a) Simulated densities of the slag system SiO2-Al2O3-CaO at 1800 oC;
(b) Simulated oxygen self-diffusion coefficients of the slag system SiO_2-Al_2O_3-CaO at 1800 oC.

A clear trend is noticed in Fig. 2(a) that slag density decreases with increasing SiO_2 content, which reflects the network forming role of the silica tetrahedron in slags (i.e. the formation of the structural unit Si-BO). On the other hand, slag density exhibits a minimum with increasing Al_2O_3 content at constant SiO_2 content. This is attributed to the charge compensation effect (i.e. the formation of the structural unit cAl-BO). A similar strong composition-structure-property relation is seen in Fig. 2(b) that at constant SiO_2 or Al_2O_3 content a higher slag diffusivity occurs due to the network de-polymerization induced by an increase in CaO content. It should be mentioned that the formation of potential solids is suppressed in Fig. 2.

MD simulations have also been performed to investigate the mechanism for the local viscosity maximum around the fayalite composition, the anomalous second lubricant effect in alkaline silicate melts, the super-exponential viscosity variations on mixed alkali aluminosilicate melts, and the shift in position of viscosity maximum induced by charge compensation effect. Furthermore, the reliability of the simulation results is comprehensively assessed by using existing data including chemical and physical properties as well as structural properties. It is shown that the slag composition-property relationship can be better established based on the novel self-defined oxygen-based units obtained via MD simulations and the modelling of different structure-dependent properties can also be better developed. This is a prototype to develop more reliable models by means of MD simulation, and the results obtained provide the guideline to design optimum slag system for specific metallurgical process or other relevant high temperature processes such as the gasification of coal and biomass.

Engineering Sciences

Electrical Engineering and Information Technology | DFG 408

LDA learning using deep neural networks

Project ID: nova0033
ABIN JOSE
CHRISTIAN ROHLFING
Institut für Nachrichtentechnik,
RWTH Aachen University

Project Report

Deep Learning for Feature Space Generation

Currently, deep neural networks are the state-of-the-art in image classification algorithms. In most of the classification algorithms, a feature space is used to distinguish between different image categories. The feature space was hand engineered before the revival of deep learning which is popularly known as feature engineering. With the recent advancement in deep learning, the feature vectors of the images are learned by neural networks which can be used for image classification. One popular classical approach, Linear Discriminant Analysis (LDA), can be learned to generate a discriminant direction, along which the classes can be separated in a low-dimensional space. We propose a method for learning the LDA using a Siamese Neural Network (SNN) architecture.

The novelty of our work is that we learn the LDA projection matrix between the final fully connected layers of an SNN. An SNN architecture is used since the proposed loss maximizes the Kullback-Leibler (KL) divergence between the feature distributions from the two branches of an SNN. The network learns an optimized feature space having inherent properties pertaining to the learning of LDA. The advantage of our approach is that the image descriptors learned are a) low-dimensional, b) has small within-class variance, and c) large between-class variance. Compared to other state-of-the-art LDA learning approaches, the proposed method has the advantages that the LDA learning happens end-to-end and the network learns the trivial solution of LDA generating orthogonal feature vectors. We measured the classification accuracy in three datasets, namely MNIST, CIFAR-10, and STL-10 and compared the performance of our approach to other state-of-the-art LDA learning methods. We also measured the KL divergence between the class pairs and visualized the projection of feature vectors along the learned discriminant directions.

LDA Learning using Siamese Neural Networks

We explored if a Siamese Neural Network could be used for learning the optimum feature space which has LDA properties. Siamese Neural Network (SNN) consists basically of two parallel CNNs with shared weights. Each branch of the SNN acts as a feature extractor for the images. The network is designed such that the final fully connected layer has at most L-1 nodes, equal to the number of discriminant directions, where L is the number of classes in a dataset. Thus, the LDA projection matrix learned between the fully connected layers is the weight of the neural network between these layers. Figure 1 shows the results of projection of feature vectors along the eigenvector directions for epoch 5, epoch 500 and epoch 1000. During training, as the number of epochs increases, the LDA projection is getting learned. The within-class scatter is decreasing, and between-class scatter is increasing as it is shown in the Figure. 1. At the end of epoch 1000, we could clearly observe that the projection of feature vectors along the eigenvector direction shows clear separation between the classes. The classes can be separated easily by linear decision boundaries.

Parameter tuning for fine-tuning the results using ITC cluster

One of the main hyperparameters during training of the neural network is the batch size. It is better to have higher batch sizes during training as the statistics of the feature space can be well captured by a larger batch size than a smaller one. This is because LDA learning requires calculating the KL divergence (Figure 2) between the feature distributions. If the batch size is large, the probability distribution of the feature space is closer to the actual feature space distribution. Hence, it was important to fine tune this hyperparameter. The two other major hyperparameters for fine-tuning the network are dropout and learning rate. We have mainly used the ITC cluster to fine tune these hyperparameters of the neural network by running simulations with different combinations of these parameters. The classification performance of the feature space learned with the LDA metric was also evaluated. For MNIST, CIFAR-10 and STL-10, the classification accuracy is summarized in Table 1 (with the best parameter setting). The results are compared to other state-of-the-art LDA learning approaches [1] and [2].

Method	MNIST	CIFAR-10	STL-10	Dimensionality
TripleNet	99.54%	87.10%	70.61%	128
Stuhlsatz et al. [2]	99.34%	-	-	9
DeepLDA-test1 [1]	99.71%	92.42%	55.92%	9
DeepLDA-test2 [1]	99.68%	**92.71%**	66.97%	9
Ours	**99.73%**	88.17%	**71.62%**	9

Table 1: Comparison of classification accuracy of our method with other state-of-the-art LDA learning approaches.

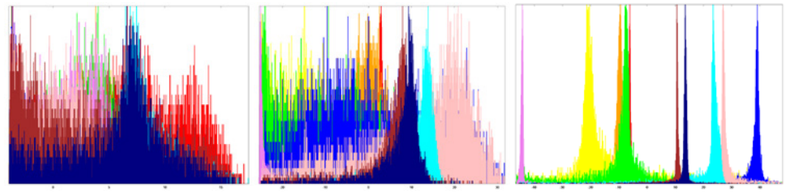

(a) Epoch 5 (b) Epoch 500 (c) Epoch 1000

Figure 1: Linear Discriminant Analysis learning for CIFAR-10 by training a Siamese Neural Network (SNN) architecture. As training epochs proceed, we could observe that the with-in class scatter decreases, and between-class scatter increases clearly showing the LDA projection getting learned during training.

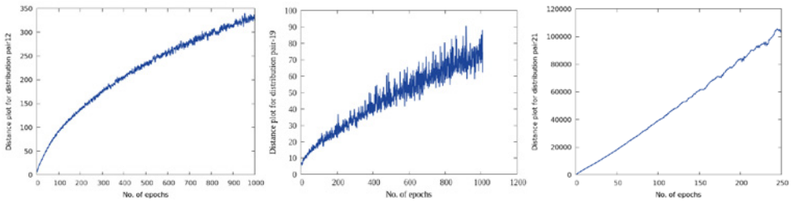

(a) (b) (c)

Figure 2: KL divergence between different class pairs for (a) CIFAR-10 dataset, (b) STL-10 dataset, (c) MNIST dataset.

Selected publications

[1] DORFER M, KELZ R, WIDMER G.
Deep linear discriminant analysis.
In Int. Conf. Learn. Represent., pages 1–13, 2016.

[2] STUHLSATZ A, LIPPEL J, ZIELKE T.
Feature extraction with deep neural networks by a generalized discriminant analysis.
IEEE Trans. Neural Netw. Learn. Syst., 23(4):596–608, 2012

Engineering Sciences

Versatile Video Coding

Project ID: rwth0333
MAX BLÄSER
JOHANNES SAUER
CHRISTIAN ROHLFING
Institut für Nachrichtentechnik,
RWTH Aachen University

Project Report
MPEG Standardization

The Joint Video Experts Team (JVET), a collaborative team formed by MPEG and ITU-T Study Group 16's VCEG started work on a new video compression standard nicknamed as "Versatile Video Coding" (VVC) in April 2018 during the MPEG Meeting in San Diego. The new standard will likely be finished by the year 2020. The design goal of the new standard is to double the compression efficiency compared to previous MPEG standards and thereby making new and emerging applications such as UHD video streaming and immersive video widely available. The Institut für Nachrichtentechnik (IENT) from RWTH Aachen University has participated in the "Joint Call for Proposals on Video Compression with Capability beyond HEVC" (CfP) which was issued by JVET in October 2017 and has contributed to the development of the new standard since then. An essential requirement for being able to contribute to the development of the new standard is the ability to perform a large amount of video encoding and decoding using an experimental, software-based codec called the VTM software (VVC Test Model). Any new algorithm or modification to already existing technology that is presented at JVET must be thoroughly tested and evaluated by coding a pre-defined set of video sequences with different characteristics. Both the software usage and the test set of video sequences are specified by the so called "Common Testing Conditions", which apply for all standardization participants. With the computing power of the HPC, the IENT was able to contribute to the core experiment on inter prediction (CE4), as well as investigate efficient coding of 360° video. Further, cross-checks of experimental results obtained by other standardization participants were performed.

2D Video Coding

In the CE4 contributions by IENT, new algorithms were evaluated that perform non-rectangular block partitioning of the video, which is of particular importance for 2D video coding applications. Non-rectangular partitioning, especially geometry-based partitioning as proposed by IENT, has the prospect of improving coding efficiency by up to 1%, as the partitioning allows better adaption to the local properties of the video. An example of such a state-of-the-art partitioning scheme can be seen in Figure 1. As a result of this effort a geometry-based partitioning scheme is now part of the new video coding standard VVC.

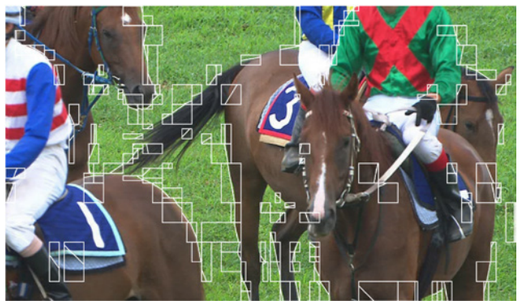

Figure 1: Example of a coded picture using non-rectangular block partitioning.

360° Video Coding

In the contributions of IENT to the coding of 360° video, new tools targeted at better compression of 360° video were investigated. The native format of 360° content is video on the surface of a sphere. However for coding a 2-dimensional representation of the video is necessary. The conversion to such a representation cannot be achieved without the introduction of geo metric distortions. IENT investigated the impact of these distortions in 360° video projected to a cube, which is then unfolded to get a 2-dimensional representation for coding. In particular a improved motion compensation method was developed, which improves the prediction across cube face boundaries, as can be seen in Figure 2. This method has the prospect of improving coding efficiency by up to 2%. Further, IENT developed a method for improved loop filtering across face boundaries. While this method

Figure2: (a) Face A and B. Red: Geometric distortion at face boundary (b) Blue: Corrected geometric distortion.

does not have a large impact the difference can be clearly seen visually. In order to enable a high-level integration of the developed 360° coding tools into the video coding scheme a mechanism for providing "uncoded areas" was developed. These areas do not have to be coded, but are generated and decoder-side and can then be used for inter prediction. Other applications of uncoded areas were explored as well. [1]

Selected publications

[1] GAO H, ESENLIK S, ALSHINA E, KOTRA AM, BLÄSER M, SAUER J.
CE4: CE4-1.1, CE4-1.2 and CE4-1.14: Geometric Merge Mode (GEO),
Doc. JVET-P0068, JVET, Geneva, Switzerland, Oct. 2019.
[2] GAO H, ESENLIK S, ALSHINA E, KOTRA AM, BLÄSER M, SAUER J.
CE4: CE4-1.7, CE4-1.8: GEO and TPM Blending Off for SCC,
Doc. JVET-P0069, JVET, Geneva, Switzerland, Oct. 2019.
[3] GAO H, ESENLIK S, ALSHINA E, KOTRA AM, WANG B, BLÄSER M, SAUER J.
CE4-Related: Geometric Merge Mode (GEO) Simplifications,
Doc. JVET-JVET-P0107, JVET, Geneva, Switzerland, Oct. 2019.
[4] GAO H, ESENLIK S, ALSHINA E, KOTRA AM, BLÄSER M, SAUER J.
Simplified GEO without multiplication and minimum blending mask storage (harmonization of JVET-P0107, JVET-P0264 and JVET-P0304),
Doc. JVET-P0884, JVET, Geneva, Switzerland, Oct. 2019.
[5] SAUER J, BLÄSER M.
Coding of 360o video in non-compact cube layout using uncoded areas,
Doc. JVET-P0316, JVET, Geneva, Switzerland, Oct. 2019.
[6] CHEN CC, REUZE K, CHIEN WJ, KARCZEWICZ M, ZHU W, ZHANG L, XU J, ZHANG K, BLÄSER M, SAUER J.
Non-CE4/8: On disabling blending process in TPM,
Doc. JVET-O1172, JVET, Gothenburg, Sweden, July 2019.
[7] ESENLIK S, GAO H, WANG B, KOTRA AM, ZHAO Z, ALSHINA E, BLÄSER M, SAUER J.
Non-CE4: Adaptive blending filtering for TPM,
Doc. JVET-O0513, JVET, Gothenburg, Sweden, July 2019.
[8] ESENLIK S, GAO H, FILIPPOV A, RUFITSKIY V, KOTRA AM, WANG B, ALSHINA E, BLÄSER M, SAUER J.
Non-CE4: Geometrical partitioning for inter blocks,
Doc. JVET-O0489, JVET, Gothenburg, Sweden, July 2019.
[9] SAUER J, BLÄSER M.
Geometry padding for cube based 360 degree video using uncoded areas,
Doc. JVET-O0487, JVET, Gothenburg, Sweden, July 2019.
[10] SAUER J, BLÄSER M.
Parameterizable cubemap for 360 degree video coding,
Doc. JVET-O0488, JVET, Gothenburg, Sweden, July 2019.

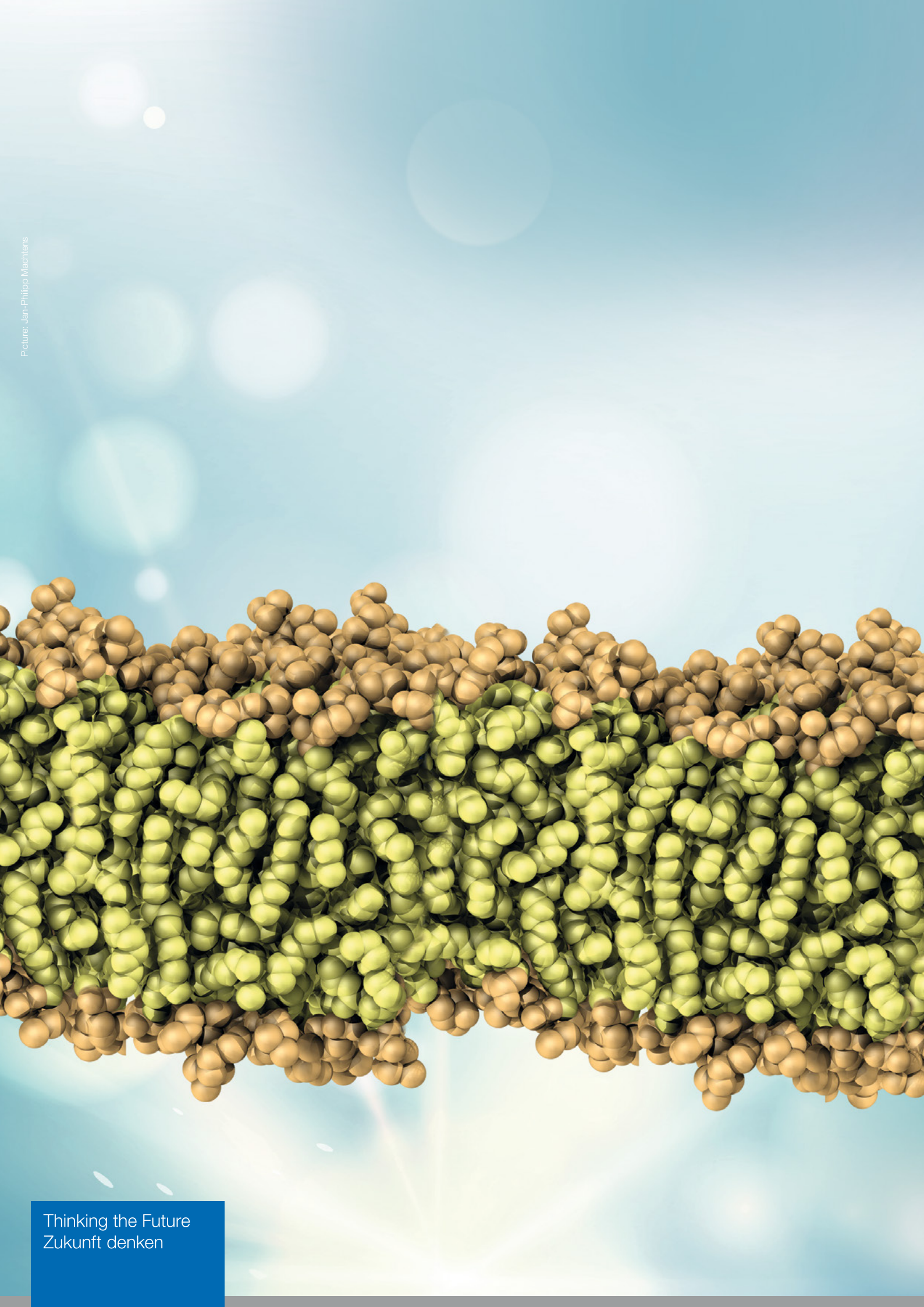

Picture: Jan-Philipp Machtens

Thinking the Future
Zukunft denken